Distinct cortical profiles underlie the common reportability of thought-free experiences

Paradeisios Alexandros Boulakis [†1,2], **Anikó Kusztor** [†3,4], **Naotsugu Tsuchiya** [3,4,5,6,7], **Thomas Andrillon** [*8], **and Athena Demertzi** [*1,2,✉]

[1]Physiology of Cognition Lab, GIGA CRC-Human Imaging, Allée du 6 Août 8 (B30), 4000, University of Liège, Belgium; [2]Psychology and Neuroscience of Cognition Research Unit, Place des Orateurs 3 (B33), 4000, University of Liège, Belgium; [3]School of Psychological Science, Monash University, Melbourne, Victoria 3168, Australia; [4]Turner Institute for Brain and Mental Health, Faculty of Medicine, Nursing and Health Science, Monash University, Victoria, Australia; [5]Center for Information and Neural Networks (CiNet), National Institute of Information and Communications Technology (NICT), Osaka, Japan; [6]Advanced Telecommunications Research Computational Neuroscience Laboratories, Kyoto, Japan; [7]Theoretical Sciences Visiting Program (TSVP), Okinawa Institute of Science and Technology Graduate University, Onna, 904-0495, Japan; [8]Institut du Cerveau—Paris Brain Institute—ICM, Inserm, Sorbonne Université, CNRS, APHP, Hôpital de la Pitié Salpêtrière, 75013 Paris, France

Mind blanking (MB) is a mental state of seemingly no reportable thought content. The question of how we can entertain no thoughts while awake is challenging for the study of spontaneous thinking. By combining EEG–fMRI with experience sampling during task performance, we categorised changes in mental content and self-reported vigilance to map the neurophysiological signatures of MB. We demonstrate that fMRI connectivity around MB reports is characterised by a "rich" pattern of long and short-range signal anticorrelations. At the same time, sleepiness reports are linked to a "simpler" hyperconnected fMRI pattern, characterised by overall positive connectivity. Put together, an interaction appears: when people report being alert, connectomes around MB reports resemble the hyperconnected pattern, indicating that the neuronal correlates of MB depend on self-rated vigilance. The hyperconnected pattern also correlated with EEG slow-wave activity, tying MB's topology to sleep-like electrophysiology during wakefulness. Collectively, we show that distinct cortical events underlie the shared phenomenology of a thought-free mind. We conclude that MB's neurophysiological correlates vary across perceived vigilance levels and that more refined characterisation of the neuronal correlates of thought-less mental states exist. Our findings build on the quest to bridge mental content and its absence with measurable brain activity and provide insights into how ongoing thinking is maintained during wakefulness.

mind blanking |mind wandering |spontaneous thinking |attentional lapses |experience sampling | brain patterns | time-varying functional connectivity | slow waves | local sleeps | canonical correlations | global signal | fMRI | EEG

Correspondence: ***a.demertzi @uliege.be***

Introduction

Wakeful life is experienced as being full of thoughts. The content of these thoughts can reflect either external demands and goal-oriented tasks, such as problem-solving or responding to the environment, or can arise spontaneously in the absence of external cues, as seen in daydreaming, mind-wandering, or internally generated thoughts(Christoff et al., 2016; Smallwood et al., 2021; Stawarczyk et al., 2011). Considering this affluence in mental content people often assume that their mind is perpetually "thought-full", continuously alternating between externally and internally generated contents. Yet, this view is challenged by occasional reports, such as "I have no thoughts", "I am not sure what I was thinking about", and "I forgot what I had in mind", among others. These types of episodes are known as mind blanking (MB) (Andrillon et al., 2025; Boulakis and Demertzi, 2025; Ward and Wegner, 2013).

Our understanding of how MB episodes emerge has only now started to get illuminated (Andrillon et al., 2025). So far, experimental work indicates that MB stands in behavioural and neuronal contrast to mental states associated with reportable thought content (Andrillon et al., 2021; Boulakis et al., 2023, 2025; Kawagoe et al., 2019; Mortaheb et al., 2022). During wakefulness, MB reports occur infrequently (5-10% of the time), both in resting conditions (Boulakis et al., 2025; Mortaheb et al., 2022) and during task-engagement (Andrillon et al., 2021; Robison et al., 2019; Stawarczyk et al., 2020). At the same time, the frequency of MB reports also seems to depend on arousal levels, as they increase after sleep deprivation (Boulakis et al., 2025) and during subjectively felt lower vigilance (Andrillon et al., 2021; Stawarczyk and D'Argembeau, 2016).

The indication that low arousal is linked to the absence of reportable thought content is further supported by neuroimaging and electrophysiological findings. Using fMRI, we previously examined how functional connectivity organises around contentful mental state reports and MB (Mortaheb et al., 2022). We found that, under task-free conditions, MB was associated with a connectivity pattern characterised by a global inter-areal synchronisation. Considering that similar increases in whole-cortex functional connectivity have also been reported during NREM sleep in humans (El-Baba et al., 2019) and under isoflurane anaesthesia in animals (Aedo-Jury et al., 2020), this overall positive connectivity has been

[1†]These authors contributed equally to this work.
[2*]These authors contributed equally to this work.

interpreted as an indication that low cortical arousal underlie MB reports. The low arousal stance was further supported by the finding that the amplitude of the fMRI global signal (GS) was higher around the time of MB reports (Mortaheb et al., 2022). The GS refers to the average signal intensity across all voxels in the grey matter (Power et al., 2018). As the amplitude of the GS was shown to positively correlate with delta oscillations in the EEG frequency band and to decrease after ingestion of caffeine (Wong et al., 2013), it was considered a proxy of cortical arousal. Therefore, with regard to MB, the co-occurrence of fMRI hyperconnectivity and increased GS amplitude points to the possibility of low neurophysiological arousal during MB reports. A direct correlation between fMRI and electrophysiology could strengthen this interpretation.

Indeed, what we know so far about MB's EEG substrate comes from a separate piece of work, where we have shown that MB reports are preceded by the presence of slow-wave-like (SW) activity during wakefulness, known as "local sleeps" (Andrillon et al., 2019, 2021; Vyazovskiy et al., 2011; Vyazovskiy and Harris, 2013). Combining EEG with experience sampling during a sustained attention to response task (SART), we found that attentional lapses were associated with the presence of transient sleep-like SWs, and the properties of these SWs differentiated the two mental reports: steeper SW over posterior electrodes was associated with MB, larger and steeper SW in frontal electrodes was associated with mind-wandering reports (Andrillon et al., 2021). A replication and re-analysis of this paradigm revealed that MB was further associated with higher power in the EEG delta and alpha bands, lower power in beta and gamma, and reduced parietal complexity, all indicative of a reduced cortical arousal mode (Munoz-Musat et al., 2025). It should be noted, though, that the low spatial resolution of EEG limits the identification of the precise networks involved in sleep-like SW and MB.

In the present study, we combined simultaneous fMRI-EEG recordings with experience sampling to determine the spatio-temporal profile of MB, as measured by multimodal brain activity. We hypothesised that MB-related fMRI connectivity would be organised in an overall positive inter-regional pattern and that this hyperconnected pattern would correlate with EEG SW-like activity. By taking reported vigilance levels into account, we were also open to the possibility that distinct MB fingerprints would emerge, in line with our recent theory that different forms of empty-mindedness may exist (Andrillon et al., 2025).

Methods

Participants

Thirty-nine participants were recruited for the study (mean age = 26.4, sd = 4.5, range = [18-32]; females = 24). All participants reported normal or corrected-to-normal vision and no neurological or psychiatric disorders. One participant was excluded due to subsequent changes in the experimental paradigm, resulting in a total sample size of n = 38. Participants received monetary compensation. The project was approved by the Monash University Human Resources Ethics Committee (Project ID 17674).

Experimental design and Stimuli

During a SART (Robertson et al., 1997), participants were asked to pay attention to a series of pictures of human faces (Figure 1). In every trial, face stimuli (one male face, or eight different female faces, extracted from the Radboud Face Database (Langner et al., 2010)) were presented for 500 ms, followed by a blank screen. The trial duration was between 1000–1500 ms (random uniform jitter). Participants were instructed to indicate the presence of a female face (GO trials) by pressing a button on a keypad placed under their dominant hand and to withhold button presses (NOGO trials) for the male face. The order of the face stimuli was randomised before the onset of every session. Participants completed four blocks of the task, with self-paced breaks in between, each block lasting approximately 12-15 minutes and totalling approximately 50 minutes.

Intermittently during the SART, we utilised experience sampling to probe reports of participants' mental states and vigilance levels throughout the session. The mental state options were explained to participants both orally and in writing before the experience-sampling session. Specifically, every 30-70s (uniformly jittered), we interrupted the SART and displayed the word "STOP" on the screen. Following the probe, participants were asked: *"Just before the interruption, where was your attention focused?"* Possible responses were a) On-Task (defined as entirely focused on the task), b) Off-Task (defined as thinking about something other than the task), Blank (defined as not thinking of anything), and d) I cannot recall. If participants selected the Off-Task option, they were additionally presented with the following question: *"Just before the interruption, what distracted your attention from the task?"*. Available options were: b1) Something in the room, b2) Something personal, and b3) Something about the task. After reporting their mental states, participants were asked: *"Over the past few trials: How alert have you been?"* Available levels were: a) Extremely alert, b) Alert, c) Sleepy, and d) Extremely Sleepy. Each block included 10 sets of probes. Each participant responded to 40 probes across four blocks.

Behavioural Analysis

Reaction times were defined as the difference between the onset of the probe screen and the button press, and they were contrasted across mental states and vigilance levels. Reaction times $<.25$ s or >8 s were discarded following our previous analysis protocol (Boulakis et al., 2025). Overall, we removed 8% of the total probes

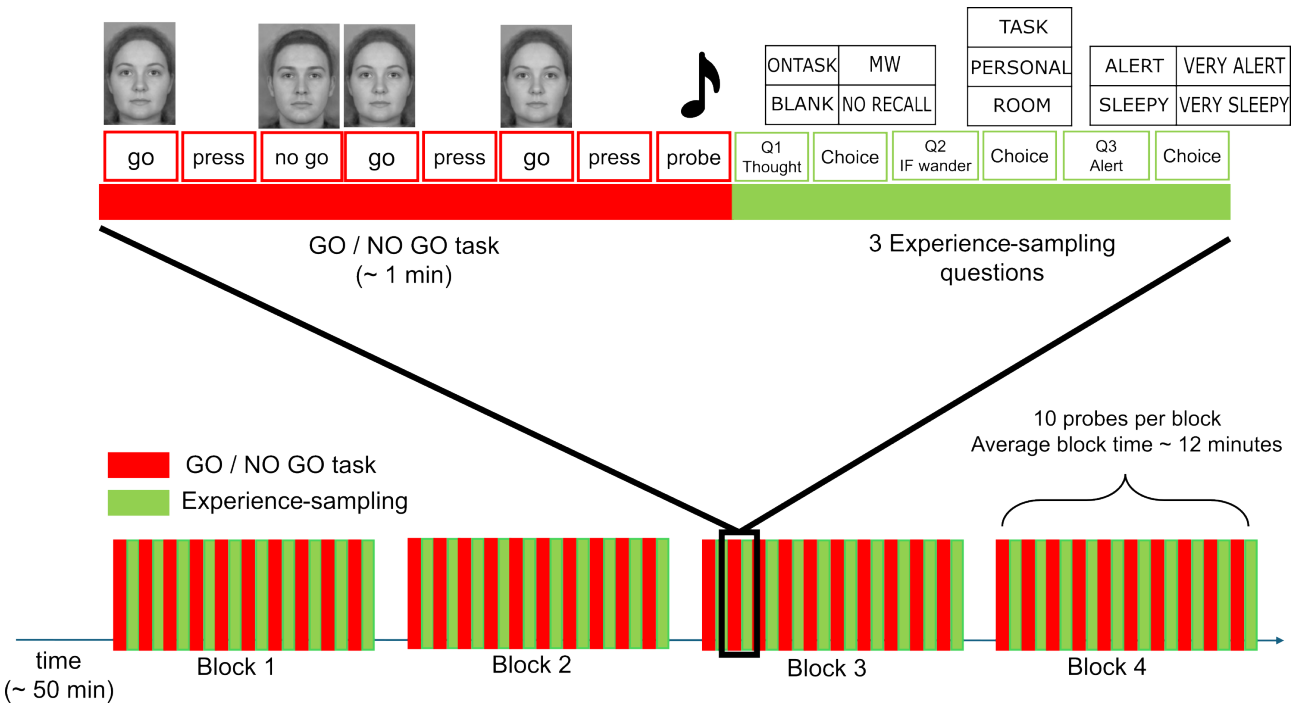

Figure 1. Experimental design of the sustained attention to report task (SART) combined with experience-sampling probes for reporting mental states and vigilance levels. Across four experimental blocks (12 min each), participants were presented with a sequence of female or male faces. Participants were instructed to press a button when a female face was presented (GO stimulus) and to avoid pressing a button when male faces were presented (NOGO stimulus). At random intervals, participants were presented with probes that invited them to report their mental content and their level of vigilance. First, participants indicated their thoughts by choosing amongst a) ONTASK thoughts, b) MW thoughts, c) BLANK, or d) I cannot recall my thoughts. If participants selected the MW thought option, they were further probed to report whether this related to the task, the experimental room or personal content. Finally, participants indicated their vigilance levels by choosing amongst a) Very Alert, b) Alert, c) Sleepy or d) Very Sleepy. In every block, 10 probes were presented, leading to a total of 40 probes per participant. Images of male and female faces were extracted from the Radboud Face Database (Langner et al., 2010).

(118/1515).

EEG

EEG acquisition parameters. EEG data were acquired using the BrainAmp MR plus system (Brain Products, Munich, Germany), equipped with a 64-channel EEG Cap (64Ch Standard BrainCap-MR with multitrodes). Electrode placement followed the international 10-20 system. The ground electrode was positioned in the location of AFz, and the reference was in the location of FCz. The electrodes were prepared with conductive gel to reduce impedance levels to $<$5 kΩ. The data were recorded with the BrainAmp MR plus DC and bipolar BrainAmp ExG MR amplifiers and the BrainVision Recorder (Version 2.2) software with a resolution of 0.5 µV/bit at 5000 Hz and with a hardware bandpass filter (0.01-250 Hz). The EEG and fMRI data acquisition were synchronised using the Brain Products SyncBox.

EEG preprocessing. Gradient artifacts were removed via subtraction of a mean template in each channel, according to the average artifact subtraction (AAS) methodology, utilising the software BrainVision Analyzer 2 (Version 2.2, Brain Products GmbH, Gilching, Germany). A sliding moving-average window implementation of 21 epochs of a full gradient artifact (1.56 s time window) was used for the construction of the average artifact template. The reason for using 21 epochs was based upon the default settings of the BrainVision Analyzer. After this step, the data were downsampled to 500 Hz. Cardioballistic artifacts were also removed using the AAS method: R-peaks were identified via a semi-automated pipeline, then they were visually inspected and corrected when necessary. Further preprocessing was done using the EEGLAB MATLAB toolbox (v2021.1). Data were split into 25 s pre-probe epochs and filtered using a 100 Hz high-cut-off Hamming filter. Next, the data were visually inspected for bad electrodes and epochs. Eye- and cardiac-related artifacts were detected and removed using ICA. At that stage, as we noticed that residual cardioballistic artifacts were still present in the frontal and temporal channels, we applied denoising source separation (DSS) on heartbeat-evoked potentials and removed the time-locked activity from every channel (de Cheveigne et al., 2008).

Extraction of slow waves. We followed a previously validated method to detect slow-wave activity (Andrillon et al., 2021). First, data were re-referenced to the average of mastoid electrodes and band-pass filtered within a [1,10] Hz range with a Chebyshev filter. Then, slow waves were defined in each electrode separately by identifying two consecutive zero-crossings (start and end of the slow waves). For each wave, we extracted its peak-to-peak amplitude, that is, the amplitude between the positive and negative peaks of the slow wave. Waves with extreme amplitudes ($>$75 µV positive peak, and $>$150 µV peak-to-peak differences) and with dura-

tion corresponding to larger than 7 Hz activity were excluded. Finally, we selected the top 10% of the largest waves in each electrode and extracted their timings, as well as their downward and upward slopes. Slow wave markers were eventually extracted from a 10 s window before each probe.

fMRI

fMRI acquisition parameters. Participants were instructed to lie still in the MRI scanner with their eyes closed, minimizing eye movements and muscle artifacts. Data were collected using a Siemens Skyra 3T MRI system, equipped with a Siemens 20-channel Head/Neck coil, allowing for simultaneous EEG and ECG recordings. The participants' heads were stabilized with foam pillows placed between the cap and the MR coil. Anatomical images were acquired using a T1-weighted MPRAGE sequence with a voxel size of 1.00 mm^3, repetition time (TR) = 2.3 s, echo time (TE) = 2.07 ms, and a slice thickness of 1.00 mm. Functional images were obtained using an Echo Planar Imaging (EPI) sequence with the following parameters: TR = 1.56 s, TE = 30 ms, slice thickness = 3 mm, and flip angle = 70°.

fMRI preprocessing. Before preprocessing, fMRI data were converted to BIDS (Gorgolewski et al., 2016). Preprocessing was performed using fMRIPrep 23.2.1 (Esteban et al. (2018, 2019), RRID:SCR 016216), based on Nipype 1.8.6 (Gorgolewski et al. (2011, 2018), RRID:SCR 002502) and the AFNI software 24.3.00 (Cox and Hyde, 1997). We are reporting the preprocessing output text of the fMRIPrep software as provided.

Anatomical data preprocessing. A total of 1 T1-weighted (T1w) images were found within the input BIDS dataset. The T1w image was corrected for intensity non-uniformity (INU) with N4BiasFieldCorrection (Tustison et al., 2010), distributed with ANTs 2.5.0 (Avants et al. (2008), RRID:SCR 004757), and used as T1w-reference throughout the workflow. The T1w-reference was then skull-stripped with the antsBrainExtraction.sh workflow (from ANTs), using OASIS30ANTs as target template. Brain tissue segmentation of cerebrospinal fluid (CSF), white-matter (WM) and gray-matter (GM) was performed on the brain-extracted T1w using fast (FSL (6.0.7.14), RRID:SCR 002823, Zhang et al. (2001)). Volume-based spatial normalisation to one standard space (MNI152NLin2009cAsym) was performed through nonlinear registration with antsRegistration (ANTs 2.5.0),using brain-extracted versions of both T1w reference and the T1w template. The following template was selected for spatial normalisation and accessed with TemplateFlow (23.1.0, Ciric et al. (2017) : ICBM 152 Nonlinear Asymmetrical template version 2009c [Fonov et al. (2009), RRID:SCR 008796; TemplateFlowID: NI152NLin2009cAsym].

Functional data preprocessing. For each of the 4 BOLD runs per participant (across all tasks and sessions), the following preprocessing was performed. First, a reference volume was generated, using a custom methodology of fMRIPrep, for use in head motion correction. Head-motion parameters with respect to the BOLD reference (transformation matrices, and six corresponding rotation and translation parameters) are estimated before any spatiotemporal filtering using mcflirt (FSL, Jenkinson et al. (2002)). The BOLD reference was then co-registered to the T1w reference using mri coreg (FreeSurfer) followed by flirt (FSL, Jenkinson and Smith (2001)) with the boundary-based registration (Greve and Fischl, 2009) cost-function. Co-registration was done using conFig.d with six degrees of freedom. Several confounding time series were calculated based on the preprocessed BOLD: framewise displacement (FD), DVARS and three region-wise global signals. FD was computed using two formulations following Power (absolute sum of relative motions, Power et al. (2014) and Jenkinson (relative root mean square displacement between affines, Power et al. (2014)). FD and DVARS are calculated for each functional run, both using their implementations in Nipype (following the definitions by Power et al. (2014)). The three global signals are extracted within the CSF, the WM, and the whole-brain masks. Additionally, a set of physiological regressors were extracted to allow for component-based noise correction (CompCor, Behzadi et al. (2007)). Principal components are estimated after high-pass filtering the preprocessed BOLD time series (using a discrete cosine filter with 128s cut-off) for the two CompCor variants: temporal (tCompCor) and anatomical (aCompCor). tCompCor components are then calculated from the top 2% variable voxels within the brain mask. For aCompCor, three probabilistic masks (CSF, WM and combined CSF+WM) are generated in anatomical space. The implementation differs from that of Behzadi et al. (2007) in that instead of eroding the masks by 2 pixels on BOLD space, a mask of pixels that likely contain a volume fraction of GM is subtracted from the aCompCor masks. This mask is obtained by thresholding the corresponding partial volume map at 0.05, and it ensures components are not extracted from voxels containing a minimal fraction of GM. Finally, these masks are resampled into BOLD space and binarised by thresholding at 0.99 (as in the original implementation). Components are also calculated separately within the WM and CSF masks. For each CompCor decomposition, the k components with the largest singular values are retained, such that the retained components' time series are sufficient to explain 50 percent of variance across the nuisance mask (CSF, WM, combined, or temporal). The remaining components are dropped from consideration. The head-motion estimates calculated in the correction step were also placed within the corresponding confounds file. The confound time series derived from head motion estimates and global signals were expanded with the inclusion of temporal deriva-

tives and quadratic terms for each (Satterthwaite et al., 2013). Frames that exceeded a threshold of 0.5 mm FD or 1.5 standardised DVARS were annotated as motion outliers. Additional nuisance time series are calculated by means of principal components analysis of the signal found within a thin band (crown) of voxels around the edge of the brain, as proposed by Patriat et al. (2017). All resamplings can be performed with a single interpolation step by composing all the pertinent transformations (i.e. head-motion transform matrices, susceptibility distortion correction when available, and coregistrations to anatomical and output spaces). Gridded (volumetric) resamplings were performed using nitransforms, conFig.d with cubic B-spline interpolation.

Apart from the fMRIPrep pipeline, we additionally applied a Gaussian kernel of 6 mm full width at half-maximum using the 3dmerge function from AFNI. Following smoothing, denoising was performed using a locally developed Nipype pipeline. In this pipeline, we fitted a GLM to the fMRI BOLD voxel time series. The GLM modelled a) the effect of six movement parameters (translation in x, y, and z directions, and rotation in yaw, roll, and pitch directions) and their first derivative, b) constant and linear trends using zero-th-order and first-order Legendre polynomials, c) principal components of signals in the WM and CSF masks, and d) outlier data points. Then, a bandpass filter in the range of 0.008 - 0.09 Hz was applied on the residuals of the model to extract low-frequency fluctuations of the BOLD signal. Finally, we utilised the Schafer 100 ROI parcellation (Schaefer et al., 2018)and 19 subcortical ROIs to extract the averaged BOLD signals inside each ROI (Supplementary Figure S1a,b). To ensure generalizability and robustness of the pipeline, we varied the regression of the global signal and the regression of task events (Supplementary Material).

Global signal amplitude analysis. We extracted the instantaneous global signal amplitude by applying the Hilbert transformation at each ROI timepoint as:

$$\widehat{x}_{i,r}(t) = \left(\frac{1}{\pi t}\right) * x_{i,r}(t)$$

where $*$ indicates a convolution operator. Using this transformation, we produced an analytical signal for each regional time series as:

$$x^a_{i,r}(t) = x_{i,r}(t) + j\widehat{x}_{i,r}(t)$$

where $j = \sqrt{-1}$. For each mental report and vigilance level, we extracted the last 6 TR ($\sim$10s) preceding the probes of the real component of the analytical signal. To account for the potential lag of the BOLD response, we also reanalysed the shifted global signal amplitude time series by 1 and 2 TR (Supplementary Material).

Functional connectivity estimation. We used phase-based coherence analysis to extract ROI-ROI functional connectivity (FC) at each TR of the scanning session. For every participant i, we z-scored each of the ROI r time series and applied a band-pass filter of 0.1-0.4 Hz to isolate the low-oscillatory BOLD signal of interest. Then, we calculated the Hilbert transformation. From the Hilbert analytical signal, the instantaneous phase of each time series can be estimated as:

$$\phi_{i,r}(t) = \frac{\widehat{x_{l,r}}(t)}{x_{l,r}(t)}$$

To ensure that the phase time series were accurately represented and free from artefacts, we applied Empirical Mode Decomposition (EMD) to each voxel phase time series. EMD is a signal processing technique that decomposes a signal into its underlying frequency components, known as intrinsic mode functions (IMFs). At each iteration of the algorithm, EMD identifies the local extrema of the original signal, from which upper and lower envelopes are constructed using spline interpolation. The mean of these envelopes is calculated and subtracted from the original signal to extract the first intrinsic mode function (IMF). This procedure is iterated until the extracted signal meets the criteria for being an IMF. Therefore, at each iteration, the algorithm produces an IMF and the residual trend of the signal after the IMF is subtracted. As such, we kept the first oscillation and discarded the remaining IMFs.

Then, we warped the denoised phase signal $\phi_{i,r}(t)$ to the $[-\pi, \pi]$ interval and, naming the obtained signal as $\theta_{i,r}(t)$, we calculated a connectivity measure for each pair of regions as the cosine of their phase difference. For example, the connectivity measure between regions r and s in subject i was defined as:

$$conn_{i,r,s}(t) \triangleq \cos\left(\theta_{i,r}(t) - \theta_{i,s}(t)\right)$$

By this definition, completely synchronised time series lead to a connectivity value of 1, completely desynchronised time series produce a connectivity value of zero, and anticorrelated time series produce a connectivity measure of -1. Using this approach, we created a connectivity matrix of 119 x 119 (Supplementary Figure S1c), representing the sum of cortical and subcortical parcels, at each time point t for each subject i yjay we called $C_i(t)$:

$$C_i(t) \triangleq \left[conn_{i,r,s}(t)\right]_{r,s}$$

Functional connectivity estimation. We applied clustering to identify representative connectivity patterns that summarise the dominant modes of variation in time-varying functional connectivity. First, given that the connectivity matrices described above are symmetrical, we extracted the upper triangular part of the matrix for every participant at every TR. By aggregating all connectivity vectors, we created a new matrix where each row represents the phase-based connectivity at a single time point (TR) for a participant, and each column represents the phase-based connectivity values between

different ROIs (Supplementary Figure S1d). We applied k-means clustering to the resulting connectivity matrix, using the Manhattan distance as the distance metric (Supplementary Figure S1e). To assess the generalizability of the connectivity patterns to the distance choice, we also clustered the data using cosine and Euclidean distance (Supplementary Material). Clustering produced k distinct centroids that represented brain connectivity matrices, along with the occurrence frequency of each configuration for every participant. To ensure the generalizability of the centroids, we varied the number of centroids from $k = 3$ to $k = 8$. We initialised clusters using the "K-means++" method and applied clustering 200 times (Arthur and Vassilvitskii, 2007). Finally, we ordered the patterns by their standard deviation and estimated the frequency of each centroid by counting the number of matrices assigned to each centroid for each participant.

Then, we estimated the optimal number of centroids by calculating the inter-pattern correlation variance across all k. We further assessed centroid similarity across k by correlating all patterns with the first and last centroid obtained at $k = 5$. If the centroids were stable when ordered, the first centroid at $k = 5$ is expected to exhibit the strongest correlation with the first centroid across $k = 3 - 8$. Similarly, the last centroid at $k = 5$ should have shown the strongest correlation with the last centroid across the same range of k.

Coupling between connectivity patterns and experience sampling. To assess the relationship between each of the connectivity patterns created by our clustering approach and the experience-sampling reports, we extracted the upper triangular parts of the connectivity matrices 6 TR (∼10s) preceding each report. As the goal of this study is to eventually link electrophysiology with time-varying connectivity, the choice of the window (10 s) was motivated by previous results showing that mental states correlated with distinct neuronal and electrophysiological activity from that window (Andrillon et al., 2021; Boulakis et al., 2023; Mortaheb et al., 2022). For every distance metric used during k-means clustering (Euclidean, Manhattan or cosine), we estimated the distance of the extracted connectivity vectors with each of the k centroids (Supplementary Figure S1f-g). Higher values suggest that, during that TR, the connectome is organised into a configuration dissimilar (or more distant) to the examined connectivity pattern. Inversely, lower values indicate larger similarity (or proximity) to the examined connectivity pattern. In the main text, we present results originating from $k = 5$, as that number of clusters showed the highest inter-pattern correlation covariance. To ensure generalizability, we replicated our analysis across all clustering k (3-8) (Supplementary Material). Additionally, to account for a potential effect of the hemodynamic response, we re-analysed our data using the shifted versions of the connectivity matrices with time lags ranging from zero (four TRs before the probe) to two (two TRs pre-probe and two TRs post-probe matrices) (Supplementary Material). Across all analyses, model significance was corrected for the total number of k clusters examined using the Bonferroni correction.

Coupling between connectivity patterns and SW-like activity. To understand how SW-like activity would correlate with connectivity patterns, we utilised Canonical Correlations Analysis (CCA). CCA is a multivariate statistical technique used to identify the relationships between two sets of variables (hae, 2007; Wang et al., 2020; Zhuang et al., 2020). CCA reduces two sets of variables, X and Y, into lower-dimensional representations called canonical components. These components are created as linear combinations of the original variables. The method then selects the combinations in such a way that the canonical components from X and Y are maximally correlated with each other. To put it simply, CCA uncovers correlations in latent representations of sets of variables.

In our dataset, one set of variables refers to the SW markers per EEG channel (X_N^M, where M represents SW activity at every EEG channel, averaged over 10 s preceding probes, and N represents the total number of experience-sampling reports across participants), and the other set refers to the distances of the connectivity matrix of the underlying fMRI patterns (Y_N^P, where P represents the average distance of a connectivity matrix from each of the k identified patterns and N represents the total number of experience-sampling reports across participants) (Figure 6a-b).

A regularisation penalty cap L1 and cap L2 were added to each set of variables, respectively, to ensure numerical stability and avoid multicollinearity. To assess the significance of each canonical component, a permutation approach was adopted (Zhuang et al., 2020). We permuted the EEG variable 5,000 times and refitted the CCA model, extracting an empirical null distribution for the correlations. The resulting empirical p-values were FDR-corrected for the number of centroids tested per model. Finally, to assess the contribution of each variable to the canonical component, we estimated the correlations between the canonical components and each variable.

Statistical analysis

Statistical analysis was performed using generalised mixed-effects models and non-parametric tests. For the mixed-effects models, the family used to model the dependent variable varied depending on the distribution of the dependent variable. For a binary variable, the data were modelled using a Binomial distribution with a logit link function. In case of positive variables, data were modelled using a Gamma distribution. Finally, the remaining tests were conducted using a Gaussian distribution with an identity function. We allowed intercepts and slopes to vary freely, using subject ID as a random effect. In the case of a singular fit, we first iteratively

removed slopes and subsequently intercepts. Models containing main effects of mental states and vigilance levels, as well as their interactions, were contrasted with null models that included only random intercepts. Model comparison was conducted using a chi-square difference test, with model evidence further quantified via Bayes factors (relative evidence based on Bayesian Information Criterion). Pairwise multiple contrasts of significant models were corrected using FDR correction. Since confidence limits are not estimated using the FDR correction, we provide the Bonferroni-corrected confidence limits. For all analyses, descriptive statistics of all fixed parameters are included to ensure transparency and facilitate replication based on our own distribution parameters.

Results

The frequency of MB reports increases along with reports about sleepiness

Following our previous analysis (Andrillon et al., 2021), we aggregated Blank and No Recall reports, as well as reports about sleepiness (Sleepy and Very Sleepy) and vigilance (Alert and Very Alert). For transparency, the pre-aggregation descriptive statistics for all vigilance reports and mental states are also provided (Supplementary Table S1).

Overall, participants were engaged with the task (Mean proportions of reports ±SD: On-Task=.49±.25, MW=.39±.21, MB=.13±.14) and reported an alert state of vigilance (Mean proportions ±SD: Alert=.57±.3, Sleepy=.43±.3). Participants reported MB (Kruskal chi=43.81, df=2, p=3.1e-10, eta squared=.38, C.I.=[0.28,1]) and sleepiness (Kruskal chi=4.1, df=1, p=4.2e-2, eta squared=.04, C.I.=[0,1]) significantly less frequently (Figure 2a-b; Supplementary Table S2 for all pairwise contrasts across reports).

To examine whether mental state reports were associated with vigilance, we fitted a binomial mixed-effects model for each mental state, with vigilance levels as the predictor. Our results showed that On-Task reports increased when participants reported being generally alert (very alert + alert), while MW and MB reports increased when participants reported being generally sleepy (very sleepy + sleepy; Figure 2c; Supplementary Table S3 for detailed pairwise contrasts).

Finally, we examined whether mental states and vigilance levels affected reaction times to probes (Chi squared=50.47, df=5, p=1.11e-09, BF10=1245.62). A contrast analysis of the main effects of mental states showed that MB tended to be reported slower compared to the other mental states. Yet, there were no statistically significant differences across vigilance levels. (Figure 2d-e; Supplementary Table S4 for descriptive statistics of reaction times across mental states and alertness levels; Supplementary Table S5 for all main and interaction pairwise contrasts).

MB and sleepiness reports are associated with higher GS amplitude

We estimated the global signal amplitude as the real part of the Hilbert transform of the BOLD global signal. A gamma mixed-effects model using global signal amplitude as the dependent variable and containing both main effects (mental states, vigilance levels) and their interactions showed greater evidence compared to a null model of random intercepts (Chi squared=106.32, df=5, p=2.45e-21, BF10=1.85e13): Both MB reports and sleepiness were associated with increased global signal amplitude (Figure 3; Supplementary Table S6 for descriptive statistics of global signal amplitude across mental states and vigilance levels; Supplementary Table S7 for all main and interaction pairwise contrasts). When participants reported feeling alert, both MB and MW showed an increased global signal amplitude compared to On-Task thoughts; at the same time, during sleepiness, MB scans showed higher global signal amplitude only compared to MW thoughts (Figure 3). These results were replicated across various analysis lags (Supplementary Figure S2). When we regressed out task effects, the relationship between MB and global signal amplitude did not reach statistical significance (Supplementary Figure S3). For the sake of comparability with our past works (Mortaheb et al., 2022), we also performed the analysis by regressing out the GS. We found that after GS regression, the relationship between sleepiness and global signal amplitude did not reach statistical significance, but MB was associated with significantly lower global signal amplitude, inverting the relationship (Supplementary Figures S4 and S5).

Time-varying functional connectivity self-organises in distinct and replicable brain patterns

We estimated how functional connectivity self-organises into distinct connectivity patterns during task engagement. Specifically, we estimated time-varying phase-based connectivity matrices using coherence as the connectivity measure. We then aggregated the matrices at every TR and every subject and applied K-means clustering (Manhattan distance) to generate k representative patterns. The number of k centroids varied from 3 to 8. Here, we focus on $k = 6$, as it showed the largest inter-pattern covariance. Effectively, this suggests that at lower k, clusters were not that well defined, while at higher k, clusters contained redundant information (Supplementary Figure S6).

Overall, we found that functional connectivity during task decomposed into a) a pattern of complex inter-areal interactions, containing positive and negative phase coherence values, with higher coherence between the DMN and the limbic network (P1), b) a pattern of anticorrelations primarily between the visual network and the other networks (P2), c) a pattern of complex inter-areal interactions, containing positive and negative phase coherence values, with higher coherence between the DMN and the visual, control and limbic net-

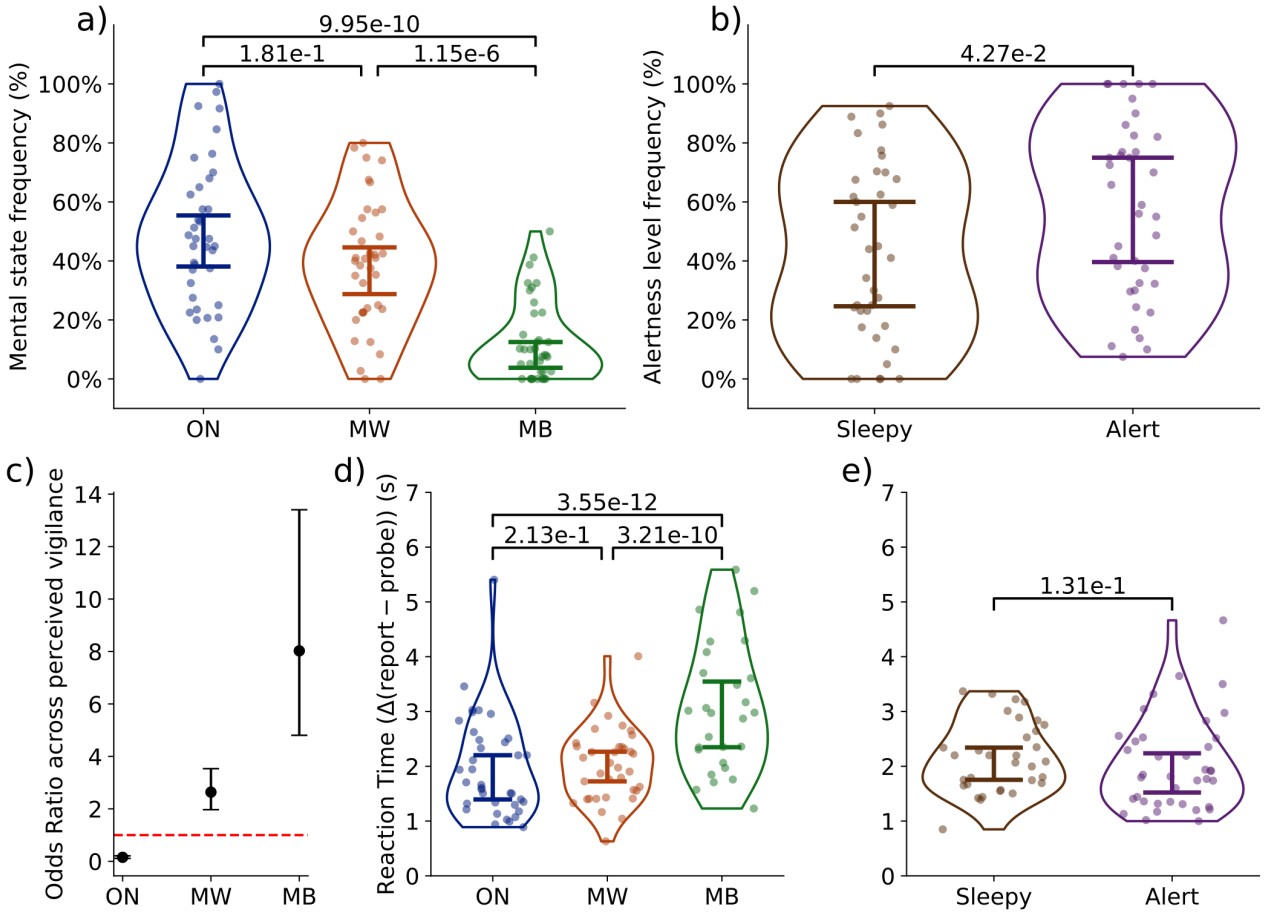

Figure 2. Characteristics of experience-sampling reports during the SART. a) Across the whole task, participants reported MB statistically less frequently compared to On-Task and MW. There was no significant difference between On-Task and MW reports. **b)** Across the whole task, participants tended to report being Alert more often than Sleepy. **c)** Perceived vigilance levels affected how frequently people experienced different mental states. When participants reported sleepiness, they were more likely to report MW and MB. When participants reported feeling alert, they were more likely to report On-Task thoughts. Black dots indicate logistic regression odds ratio beta estimates. Error bars indicate the confidence limits around the odds-ratio estimates. The red, dotted line indicates equal probability between sleepiness and alertness (no effect). **d)** When probed to report their thoughts, MB was reported the slowest.**e)** There was no statistically significant difference in report times across vigilance levels. Notes: Violin plots indicate data dispersion. Point plots indicate single-subject mean estimates. Whisker plots indicate 95% confidence intervals around the median estimate. All contrasts were FDR-corrected for multiple comparisons. Mixed-effects models included subject ID as a random effects intercept. ON = On-Task thoughts, MW = mind wandering thoughts, MB = mind blanking.

works (P3), d) a pattern of primarily low inter-areal coherence, but between the visual and the somatosensory networks (P4), and e) a pattern of overall high inter-areal coherence (P5) (Figure 4a). Critically, patterns P1, P2 and P5 were reproduced irrespective of clustering algorithm (Euclidean or cosine distance) or denoising parameters (task regression, global signal regression), while P3 and P4 showed variations across clustering schemes (Supplementary Figures S6 to S9 for Manhattan distance; Figures S10 to S13 for cosine distance; Figures S14 to S17 for Euclidean distance).

The examination of pattern occurrence frequency suggested that P5 was the most frequent, followed by P1 (Figure 4b; Supplementary Table S8 for descriptive statistics of connectivity pattern occurrence frequencies; Supplementary Table S9 for pairwise contrasts). Importantly, regressing out the global signal led P5 to be one of the least frequently occurring patterns (Supplementary Figures S8 and S9). This trend was also present in the clusters generated by cosine distance (Supplementary Figures S10 to S13). However, using Euclidean distance, a low-connectivity pattern tended to dominate the frequency space, instead of the high-connectivity one (Supplementary Figures S14 to S17). This potentially indicates algorithm-specific effects on the identified clusters. Finally, it should be noted that for Euclidean distance at $k = 7$, the algorithm did not assign any time points to one connectivity pattern when both global signal and task information were regressed out.

Neurobehavioral coupling associates MB and vigilance reports with distinct brain configurations

Overall, mental states and vigilance levels were associated with different connectivity patterns. P1 had a higher proximity (lower distance values) to MB reports as well as reports about being alert (Figure 5; Manhattan distance from P1). Simple effects analysis further indicated that the link between P1 and MB was present only when participants reported being alert. Proximity to P2 differentiated both attentional lapses (MW thoughts

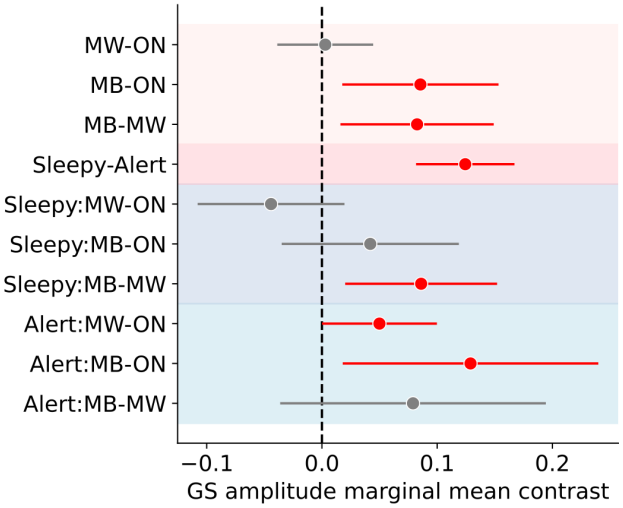

Figure 3. MB and sleepiness are accompanied by increased global signal (GS) amplitude (main effects - red shade and interactions - blue shade). Specifically, MB was characterised by higher GS amplitude relative to On-Task and MW (light red shade), and sleepiness was associated with increased GS amplitude compared to alertness (dark red shade). Simple-effect analyses indicated that during sleepiness, MB showed higher GS amplitude than MW (dark blue shade). In contrast, during alertness, both MB and MW were accompanied by increased GS amplitude compared to On-Task reports (light blue shade). **Notes:** Red points and error bars indicate statistically significant contrasts. Point plots and error bars indicate contrast means and 95% confidence limits. The x-axis represents marginal mean contrast estimates of global signal amplitude. All contrasts were FDR-corrected for multiple comparisons. Mixed-effects models included subject ID as a random effects intercept. All statistical models were compared with null models containing only random intercepts. ON = on-task thoughts, MW = mind wandering thoughts, MB = mind blanking. For the complete list of descriptive statistics and model parameters, see Supplementary Tables S6 and S7.

and MB reports) from On-Task reports (Supplementary Figure S18); MW thoughts further differed from On-Task only during sleepiness, yet MB differed from both On-Task and MW thoughts during alertness. Proximity to P3 was associated with MB reports (Supplementary Figure S18), and this was consistent across vigilance levels. P4 correlated with sleepiness (Supplementary Figure S18), with no statistically significant relationship between mental states, either in terms of main effects or the simple effects.

Importantly, there was a higher proximity of the hyperconnected P5 to sleepiness reports (Figure 5; Manhattan distance from P5). However, no mental state showed a statistically significant relationship with P5. By stratifying mental states by vigilance levels, though, we showed that, during alertness, MB reports were indeed associated with higher proximity to P5, compared to On-Task and MW thoughts. No significant relationship was observed for self-reported sleepiness (See Supplementary Table S10 for descriptive statistics of the relationship between mental states, vigilance, and connectivity patterns, and Supplementary Table S11 for pairwise contrasts). Taken together, our initial hypothesis that the overconnected pattern would be linked to MB holds true, but only when participants report being alert.

To validate our analysis, we systematically varied the number of k clusters, GS regression, task regression, clustering algorithm and the lag of the BOLD signal (216 distinct permutations of analysis parameters) across all k clusters (Supplementary Figures S18 to S21 for Manhattan distance, $k = 5$; Dataverse: https://doi.org/10.58119/ULG/4LEK9M for all results dataframes across parameterisation). Overall, we demonstrate that our analysis is replicated across task regression and different BOLD lags. Regarding GS regression, we found that it abolished or inverted the relationship of vigilance reports across P1 and P5. Finally, different clustering algorithms produced similar main effects, with MB being related to the anticorrelations pattern (94/108 parameter permutations when excluding global signal regression), while sleepiness was associated with hyperconnectivity (106/108 parameter permutations when excluding global signal regression). Critically, the relationship between MB and hyperconnectivity during alertness was statistically significant only when using Manhattan distance as the clustering algorithm. For cosine and Euclidean distance, we note that MB's proximity to P5 was consistently but non-significantly lower compared to on-task and MW thoughts (54/72 parameter permutations when excluding global signal regression and results from Manhattan distance).

EEG SW-like activity and fMRI hyperconnectivity are linked to one another

Having validated that the hyperconnected pattern is related to decreased vigilance and MB reports during alertness, we investigated whether we could link the fMRI brain patterns and EEG SW-like activity, by means of Canonical Correlation Analysis (CCA; see Methods for details, Figure 6a,b).

Overall, we observed that proximity to the hyperconnected pattern correlated with the amplitude and the downslope of the SWs in a subset of 25 participants containing complete EEG and fMRI sessions. For the SW amplitude, the fMRI component positively correlated with distance from hyperconnectivity, while the EEG component negatively correlated with SW amplitude. These results suggest that, as SW amplitude decreases, functional connectivity moves further away from the high-coherence pattern (P5) (Figure 6c; SW Amplitude). Regarding the SW downslope, a frontal-temporal-central SW component showed anticorrelation with proximity to P5. Similarly to SW amplitude, as the downslope of the SW increased, functional connectivity organised in a manner more similar to the fMRI hyperconnectivity (Figure 6c; SW Downslope). No statistically significant relationship was observed between SW density and upslope and the brain patterns.

A replication of our analysis by varying task regression, GS regression, and clustering algorithm showed that frontal-central-temporal SW amplitude, upslope and downslope were consistently related to the hyperconnectivity brain pattern. Visual inspection showed similar canonical components across clustering algorithms (Supplementary Figures S22 to S25 for Manhattan dis-

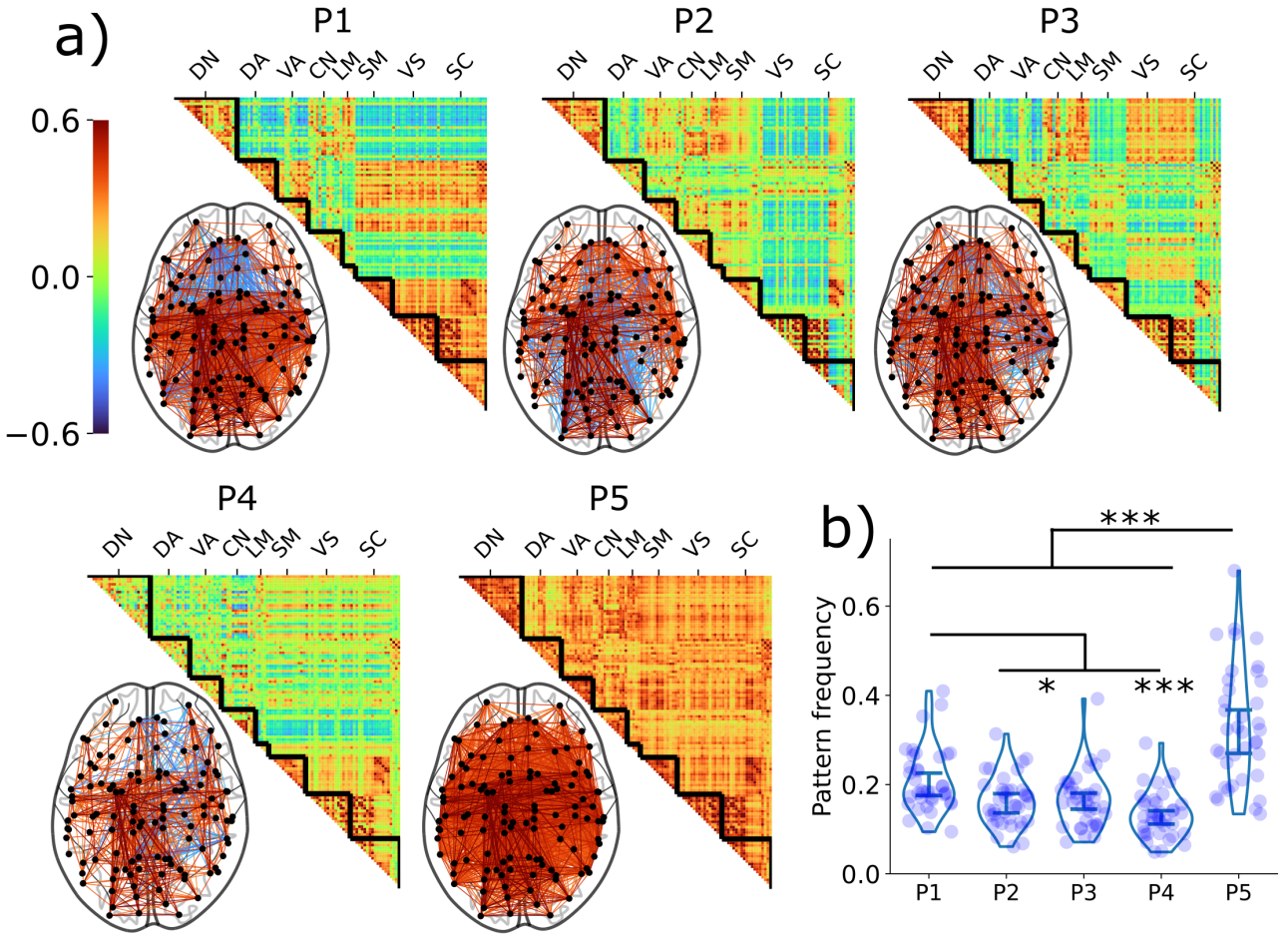

Figure 4. Time-varying functional connectivity during task engagement self-organises into five connectivity patterns. a) Data-driven clustering identified a pattern dominated by anticorrelations, with higher coherence between the DMN and the limbic network (P1), visual network anticorrelations pattern (P2), a pattern dominated by anticorrelations, with higher coherence between the DMN and the visual, control, limbic networks (P3), a lower overall coherence pattern (P4), and a cortex-wide high coherence pattern (P5). **b)** Patterns occurred at different frequencies, with P5 being the most frequent, followed by P1. The remaining patterns did not show a statistically significant difference in frequencies. **Notes:** Patterns are ordered based on decreasing standard deviation of the connectivity within a connectivity pattern. Colour bars and brain renders indicate the strength of coherence. Positive values indicate higher phase synchronisation. Values approaching zero indicate the absence of a systematic phase relationship. To facilitate visualisation onto brain renders, a 0.3 coherence edge threshold was applied. DN = default network, DA = dorsal attentional network, VA = ventral attentional network, CN = control network, LM = limbic network, SM = somatosensory network, VS = visual network, SC = subcortical network, *p<.05, **p<.01, ***p<.001.

tance; Dataverse: https://doi.org/10.58119/ULG/4LEK9M for all canonical correlations across parametrisation).

Discussion

We combined simultaneous fMRI-EEG during experience sampling to uncover nuanced modes of MB reports. We specifically sought to understand how MB relates to levels of perceived vigilance and how multimodal imaging helps unravel associated neural profiles. The underlying hypothesis was that MB's overall positive fMRI functional connectivity would be mediated by EEG slow-wave (SW) like activity, hence shedding light on the role of reduced arousal in the reportability of seemingly content-less experiences.

Behaviourally, we show a link between MB reports and experienced low arousal. First, MB was reported less frequently compared to mental states with thought content (i.e., On-Task, MW), in accordance with past findings about the sparse prevalence of MB reports (Andrillon et al., 2021; Mortaheb et al., 2022). At the same time, MB report frequency increased as participants became sleepy. These results replicate previous work showing that lower vigilance levels accompany MB (Andrillon et al., 2021; Stawarczyk and D'Argembeau, 2016) and align with recent findings showing more frequent MB reports at lower arousal states, such as after sleep deprivation (Boulakis et al., 2025). The additional finding that MB had the slowest report time further corroborates the reduced vigilance scope (Philip et al., 2003; Włodarczyk et al., 2002).

At the brain level, we replicated that MB is differentiated from content-oriented mental states based on a higher amplitude of the fMRI GS (Mortaheb et al., 2022). At the same time, we show, for the first time, that GS amplitude increased as participants became sleepier. Although the interpretation of the GS and what it represents remains an open question (Uddin, 2017), it is generally assumed that the variance it introduces can

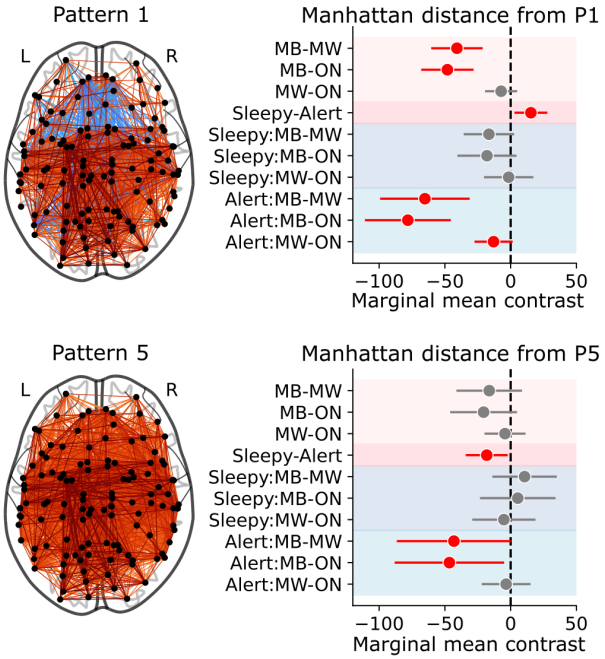

Figure 5. The link between brain patterns around thought reports and MB varies based on the levels of self-reported vigilance (main effects - red shade and interactions - blue shade). P1 had higher proximity (lower distance values) to MB reports and to reports about being alert. Simple effects analysis further indicated that the relationship between P1 and MB was present only when participants reported being alert. Consistent with our hypothesis, proximity to P5 was higher during self-reports of sleepiness; importantly, when we stratified mental states across vigilance levels, we observed that connectomes around MB reports were closer to P5 during alertness compared to On-Task and MW thoughts, suggestive of the presence of two distinct modes of MB. Notes: Areas shaded in light red indicate the main effects of mental states. Areas shaded in dark red indicate the main effects of self-reported vigilance. Areas shaded in dark blue indicate simple effects when people reported being alert. Areas shaded in light blue indicate simple effects when people reported being sleepy. The x-axis represents marginal mean contrast estimates of distance to the accompanying pattern. Point plots in bold and error bars indicate contrast means and 95% confidence limits. Red points indicate statistical significance. All contrasts were FDR-corrected for multiple comparisons. Mixed-effects models included subject ID as a random effects intercept. All statistical models were compared with null models containing only random intercepts. ON = on-task thoughts, MW = mind wandering thoughts, MB = mind blanking. For the full list of descriptive statistics and model parameters, see Supplementary Tables S10 and S11.

be accounted for by artifacts, such as motion and physiology, like heart rate and respiration (Bolt et al., 2025; Power et al., 2017). However, GS was also shown to covary with electrophysiological (Schölvinck et al., 2010) and metabolic markers (Turchi et al., 2018) of ongoing neuronal activity, implying that it reflects neurophysiological activity as well. Pertinently to this study, arousal fluctuations during wakefulness (Bolt et al., 2025; Wong et al., 2013; Zhang and Northoff, 2022) and sleep (Bolt et al., 2025; Özbay et al., 2019) were shown to modulate the amplitude of the GS, leading to the formulation that arousal propagation across the cortex elicits cortical synchronisation and subsequent GS amplitude increases. Our results build upon this literature and show that fluctuations in the GS amplitude not only track physiological arousal and sleepiness but could also carry information about experiential mental states.

Having shown that the amplitude of the GS is linked to MB and subjective levels of sleepiness, we then set out to examine how ongoing mental states and vigilance reports related to whole-brain activity. As thinking is inherently a dynamic process, an approach that describes how thoughts evolve might be better situated when considering their underlying brain dynamics (Christoff et al., 2016). The biological and theoretical motivation behind such a dynamics approach is that functional connectivity varies over time, organising itself across consistent and robust connectivity patterns that show generalizability across species (Barttfeld et al., 2015; Hudetz et al., 2015; Uhrig et al., 2018), suggesting that they represent a fundamental mode of cortical organisation (Castro et al., 2024; Demertzi et al., 2019; Mortaheb et al., 2022). Pertinently to ongoing thinking, the repertoire of dynamic brain states appears to vary with consciousness level (Castro et al., 2024; Demertzi et al., 2019) and task engagement (Türker et al., 2023), providing a time-resolved approach of mapping brain states to subjective phenomenology (Mortaheb et al., 2022, 2024). Following this rationale, we examined how time-varying functional connectivity organises itself during task engagement. We found that functional connectivity can be optimally summarised into five patterns, ranging from complex inter-areal anticorrelations to globally synchronised modes. The patterns elicited during the task bear resemblance to those previously reported during rest (Mortaheb et al., 2022; Türker et al., 2024) and at different levels of consciousness (Demertzi et al., 2019), suggesting that across various conscious states and cognitive demands, the brain explores a similar space.

We consistently replicated three previously observed patterns (Demertzi et al., 2019; Mortaheb et al., 2022, 2024; Türker et al., 2023, 2024), namely the complex anticorrelations pattern (P1), the pattern driven by the visual network (P2), and the pattern with an overall high positive coherence (P5). The overall positive coherence pattern was further found to be the most frequent, followed by the complex anticorrelations pattern. A significant deviation from previous works is that the low-coherence pattern, marked by reduced functional connectivity was here clearly defined only at higher k clusters ($>$6). During rest, the low-coherence pattern appears to dominate the clustering space (Demertzi et al., 2019). We believe these results can be accounted for by the fact that we directly estimated connectivity patterns from task time-varying FC. Indeed, while rest and task connectivity produce similar whole-brain network structure (Cole et al., 2014), the functional properties of rest and task connectivity differ, with task producing weaker connectivity and less variable neuronal dynamics (Cole et al., 2021; Ito et al., 2020). Despite similar network organisation, task connectivity, compared to rest, also shows altered within-network (Betti et al., 2013) and between-network interactions (Shine et al., 2016; Spadone et al., 2015), and increased connectivity across task-relevant cortical sites (Shine et al., 2016; Spadone et al., 2015). Overall, our results support the

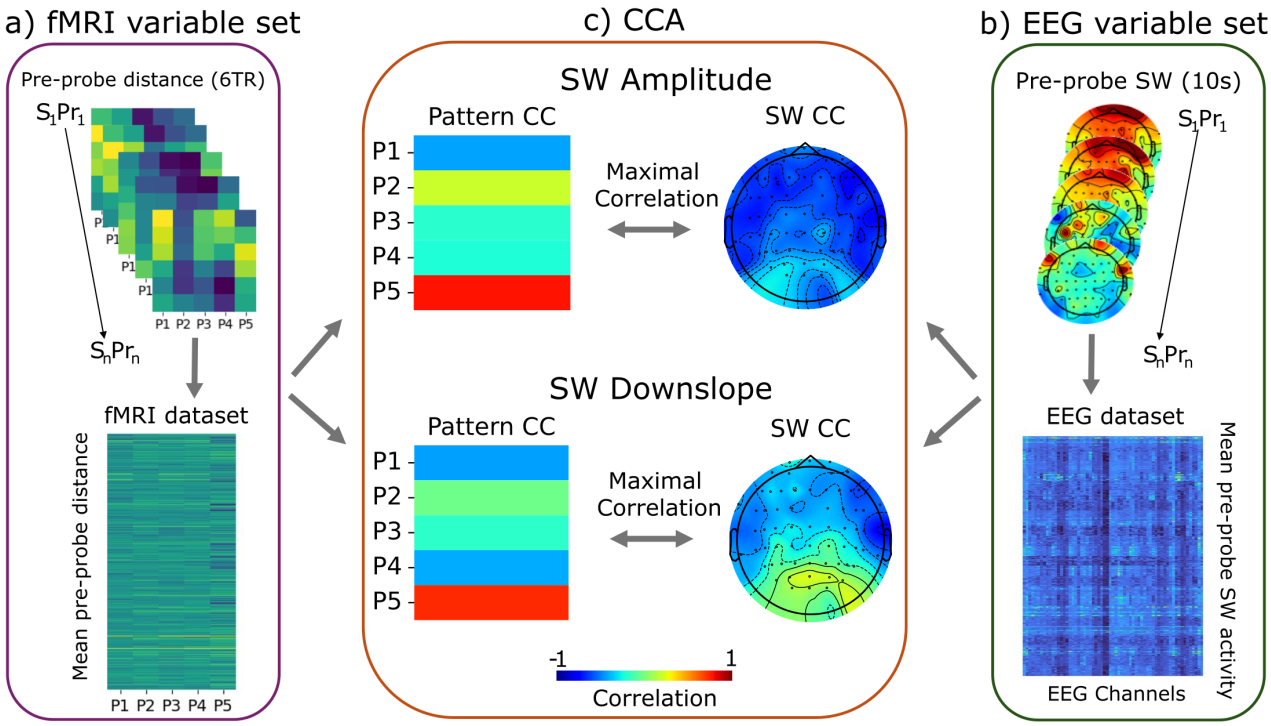

Figure 6. fMRI hyperconnectivity is linked to slow-wave-like (SW) activity. CCA is a multivariate statistical technique designed to identify latent relationships between two sets of multivariate variables. In this study, it was used to uncover shared variance between time-varying fMRI connectivity patterns and EEG-derived slow-wave-like (SW) markers. **a)** For each probe, we first extracted the functional connectivity profile from the six TRs (approximately 10 s) immediately preceding the probe. Then, we computed the Manhattan distance of functional connectivity at each TR relative to the five canonical brain connectivity patterns identified through clustering. These pre-probe distances were then averaged to yield a single distance measure per connectivity pattern, for each probe. By concatenating these measures across all subjects and probes, we constructed an fMRI dataset of size $(N_{subj} * N_{probes})$ x 5, where each row represents the pre-probe connectivity profile expressed in terms of similarity to the five patterns. **b)** In parallel, SW activity was quantified for the same pre-probe period. From the 10 seconds of EEG preceding each probe, we extracted markers of SW activity. These features were likewise concatenated across all subjects and probes, yielding an EEG dataset of size $(N_{subj} * N_{probes})$ x 63. CCA was then applied to these paired datasets to identify canonical components (linear combinations of EEG and fMRI variables) that maximally correlate across the two modalities. **c)** SW Amplitude: The distance to brain patterns P1,3,4 showed a negative correlation with the first fMRI canonical component, while the distance to brain pattern P5 showed a positive correlation to the component, indicating that fMRI hyperconnectivity is linked to EEG slow-wave like activity. SW Downslope: The first canonical component was correlated with time-varying functional connectivity that was more similar to brain pattern P5 and less similar to P1, 3, and 4. The SW upslope EEG component showed a fronto-centro-temporal orientation, suggesting that a stronger SW upslope is linked to fMRI hyperconnectivity. **Notes:** Heatmaps illustrate the correlation between the fMRI canonical components and the Manhattan distance of the connectivity matrices from brain patterns (P1-5). EEG topomaps depict the correlation between the EEG canonical components and SW activity in each brain channel. Colour bars represent correlation values ([-1,1]) for both the fMRI and the EEG canonical components. Statistical significance of each canonical correlation was evaluated by estimating an empirical null distribution of canonical correlations using permutations of one of the datasets. CCA = canonical correlation analysis, CC = canonical component, Corr = correlation, SW = slow-wave-like

idea that, while the brain explores similar connectivity repertoires during rest and task engagement, the dynamics of this exploration are determined by the task demands.

To relate the brain patterns with the ongoing vigilance and mental states, we estimated the distance of all connectivity matrices to each of the brain patterns produced, as in our previous work (Mortaheb et al., 2022). Overall, different patterns captured nuanced interactions with mental states. Analysing the complex anticorrelations patterns P1 and P3, we found that they bore a greater relationship to how the connectome around MB reports was organised. These results were contrary to our original hypothesis, i.e. that MB would be linked to fMRI hyperconnectivity. Similar anti-correlated patterns were previously associated with enhanced stimulus perception at threshold levels (Türker et al., 2024). We recently proposed that probes during MB might capture moments of transitioning (either successful or unsuccessful) between different content, and this phenomenologically translates as “no thought” as content is not yet (Boulakis and Demertzi, 2025). As such, a potential interpretation is that the predominantly anti-correlated brain pattern might reflect moments where reportable content is not yet established. This interpretation is supported by the fact that spontaneous thought initiation is accompanied by increased connectivity between the default mode network, the limbic and the control network, regions with positive correlations in both P1 and P3 (Bartoli et al., 2024; Girn et al., 2017; Kim et al., 2022). However, since the connectivity patterns in the study here were generated from task-BOLD measurements, pre-probe periods inherently contain a mixture of overlapping cognitive processes associated with the task, such as perceptual discrimination, inhibition and motor processing. Therefore, this interpretation about thought transitions remains to be further explored.

Following our main line of inquiry, we set out to examine how the hyperconnected P5 relates to different electrophysiological and experiential events. Although

the main effects did not provide evidence for a relationship between MB and the hyperconnected pattern, an interesting interaction emerged when vigilance levels were taken into account: by comparison to other mental states, MB-related connectivity were more similar to P5 when participants reported being alert. This finding offers partial support for our hypothesis that MB is linked to the hyperconnected brain pattern as previously shown during a task-free fMRI investigation of MB (Mortaheb et al., 2022). To gain some insights about this interaction, we can turn to our recently proposed physio-cognitive model of thought reportability, which hypothesises that mental content results from the interplay between cognitive mechanisms and physiological arousal (Andrillon et al., 2025). In that model, arousal changes shape cortical activity patterns, which in turn influence how MB can be reported. In other words, we hypothesised that arousal functions as a neuronal background (Boly et al., 2017; Koch et al., 2016). By modulating the strength of dynamic neural assemblies, it alters our capacity to introspect and report our thoughts (Andrillon et al., 2025; Boulakis and Demertzi, 2025). This account permits different types of MB to emerge, associated with discrete functions and neuronal correlates. Indeed, the idea of a unified blank has been criticised (Boulakis et al., 2023; Kaufmann et al., 2024). As proximity to patterns is not necessarily mutually exclusive, every connectome retains a modicum of similarity to every identified connectivity pattern. Therefore, a potential reconciliatory approach would be that, across vigilance levels, MB approaches P1, as it potentially reflects cortical mechanisms associated with thought transition. However, during alertness, this might also be accompanied by overall changes to cortical arousal (as indicated by the proximity to P5).

When looking into the properties of the hyperconnected P5, we identified a correlation with increased amplitude in the EEG in the form of SWs. Particularly, SW markers during wakefulness (amplitude, downslope) correlated with functional connectomes more proximal to the hyperconnected P5 and were more distant to the anticorrelated patterns P1-4, hence directly relating MB whole-brain topology with sleep-like electrophysiological activity. The notion about the link between the fMRI hyperconnectivity and sleep is consistent with previous works (El-Baba et al., 2019; Li et al., 2020). We recently hypothesised that such globally high synchronisation may also result from the presence of SW-like activity during wakefulness (Andrillon et al., 2025; Mortaheb et al., 2022). Indeed, SW activity originates from alternating patterns of neuronal firing (up states) and neuronal silencing (down states) at a slow scale (1-4 Hz) in both sleep (Steriade et al., 1993) and wakefulness (Sheybani et al., 2023). While SWs represent localized cortical events, they are not static and propagate across the cortex as a travelling wave (Massimini et al., 2004; Menicucci et al., 2009). Subsequently, propagation may elicit long and short-range neuronal synchrony (Tononi and Cirelli, 2014), taking the form of cortex-wide increases in functional connectivity (Aedo-Jury et al., 2020; Schwalm et al., 2017).

Our study is not without limitations. To improve statistical power, we aggregated different blank reports (blank and no recall). While these reports point to the same phenomenology of MB, it should be noted that they propose different cognitive mechanisms (metacognitive awareness of empty moments vs memory failure). As such, it remains to be further evaluated whether they share commonalities in their underlying cognitive mechanisms. Another limitation is that functional connectivity cluster estimates rely on a series of methodological choices, including preprocessing parameters, the selection of connectivity metrics, and the details of algorithmic implementation. To address the combinatorial issue of our different decision-making processes, we opted for a systematic characterisation of our clustering approach across global signal regression, task regression, clustering algorithm, analysis lag, and clustering k. While this aims to ameliorate the issue of multiple potential pipelines, we noted some discrepancies in pattern frequency across the clustering metric. When Euclidean distance was used, the low-connectivity pattern emerged as the most frequent one. Therefore, our analysis could also capture effects elicited by clustering parameters, rather than properties of time-varying cortical organisation.

Overall, we show that the previously reported hyperconnected brain pattern and sleep-like intrusions that correlate with MB reports might represent two sides of the same coin. We show that, while MB and sleepiness both relate to fMRI hyperconnectivity, their interaction uncovers dissociable cortical correlates of MB, based on how participants evaluate their vigilance level. Our work builds on the quest to bridge mental content and its absence with measurable brain activity, and provides insights into how ongoing thinking is maintained during wakefulness. In conclusion, our findings elaborate on how experienced and cortical arousal lead to subjective mental content, providing a more refined characterisation of the neuronal correlates of “thought-less” mental states.

Data availability

All behavioural dataframes, ROI time courses, global signal dataframes, k-means models, connectome distance dataframes and Canonical Correlations models across all our analysis parameters can be found in https://doi.org/10.58119/ULG/4LEK9M.

Code availability

All analysis was conducted in Python and R. An archived version of the code at the time of submission can be found at https://gitlab.uliege.be/poc/mind-blanking-monash-collab.

Acknowledgments

Analysis was conducted at the GIGA-CRC-Human Imaging platform of ULiège, Belgium. We would like to thank Dr. Sepehr Mortaheb and Nikolaos-Ioannis Simos for their insightful comments during analysis. The authors acknowledge the facilities and scientific and technical assistance of the National Imaging Facility (NIF), a National Collaborative Research Infrastructure Strategy (NCRIS) capability at Monash Biomedical Imaging (MBI), a Technology Research Platform at Monash University. The authors acknowledge the facilities and scientific and technical assistance of Monash Biomedical Imaging (MBI), a Technology Research Platform at Monash University.

Funding

At the time of the research, PAB was an FNRS Research Fellow. AD is an FNRS Research Associate. This work was supported by the Belgian Fund for Scientific Research (FRS-FNRS), the European Union's Horizon 2020 Research and Innovation Marie Skłodowska-Curie RISE programme NeuronsXnets (grant agreement 101007926), the European Cooperation in Science and Technology COST Action (CA18106), the Léon Fredericq Foundation, and the University Hospital of Liège. TA, NT, and AK were supported by Australian Research Council (DP240102680) and National Health Medical Research Council (GNT1183280, GNT2037172). NT and AK were supported by Japan Society for the Promotion of Science Grant-in-Aid for Transformative Research Areas (A) (23H04829, 23H04830) and Japan Science and Technology (JST) Moonshot R&D Grant (JPMJMS2295-14). NT was supported by Theoretical Sciences Visiting Program, Okinawa Institute of Science and Technology. The funders had no role in study design, data collection and analysis, decision to publish, or preparation of the manuscript.

Author Contributions

Paradeisios Alexandros Boulakis: Conceptualisation, Data Curation, Formal Analysis, Methodology, Project Administration, Software, Validation, Visualisation, Writing – original draft. Anikó Kusztor: Data Curation, Formal Analysis, Methodology, Formal Analysis, Software, Resources, Writing - review & editing. Naotsugu Tsuchiya: Methodology, Writing - review & editing. Thomas Andrillon: Formal Analysis, Funding Acquisition, Methodology, Software, Supervision, Writing - review & editing. Athena Demertzi: Conceptualisation, Methodology, Supervision, Writing – original draft, Writing – review & editing.

Bibliography

Canonical Correlation Analysis, pages 321–330. Springer Berlin Heidelberg, Berlin, Heidelberg, (2007). ISBN 978-3-540-72244-1. doi: 10.1007/978-3-540-72244-1_14. URL https://doi.org/10.1007/978-3-540-72244-1_14.

Aedo-Jury, F., Schwalm, M., Hamzehpour, L., and Stroh, A. (2020). Brain states govern the spatio-temporal dynamics of resting-state functional connectivity. *eLife*, 9:53186. doi: 10.7554/eLife.53186.

Andrillon, T., Windt, J., Silk, T., Drummond, S., Bellgrove, M., and Tsuchiya, N. (2019). Does the mind wander when the brain takes a break? local sleep in wakefulness, attentional lapses and mind-wandering. *Frontiers in Neuroscience*, 13:949. doi: 10.3389/fnins.2019.00949.

Andrillon, T., Burns, A., Mackay, T., Windt, J., and Tsuchiya, N. (2021). Predicting lapses of attention with sleep-like slow waves. *Nature Communications*, 12(1):3657–12.

Andrillon, T., Lutz, A., Windt, J., and Demertzi, A. (2025). Where is my mind? a neurocognitive investigation of mind blanking. *Trends in Cognitive Sciences*, 29(7):600–613.

Arthur, D. and Vassilvitskii, S. k-means++: the advantages of careful seeding. In *Proceedings of the Eighteenth Annual ACM-SIAM Symposium on Discrete Algorithms*, SODA '07, page 1027–1035, USA, (2007). Society for Industrial and Applied Mathematics. ISBN 9780898716245.

Avants, B., Epstein, C., Grossman, M., and Gee, J. (2008). Symmetric diffeomorphic image registration with cross-correlation: Evaluating automated labeling of elderly and neurodegenerative brain. *Medical Image Analysis*, 12(1):26–41. doi: 10.1016/j.media.2007.06.004.

Bartoli, E., Devara, E., Dang, H., Rabinovich, R., Mathura, R., Anand, A., Pascuzzi, B., Adkinson, J., Kenett, Y., Bijanki, K., Sheth, S., and Shofty, B. (2024). Default mode network electrophysiological dynamics and causal role in creative thinking. *Brain*, 147 (10):3409–3425. doi: 10.1093/brain/awae199.

Barttfeld, P., Uhrig, L., Sitt, J., Sigman, M., Jarraya, B., and Dehaene, S. (2015). Signature of consciousness in the dynamics of resting-state brain activity. *Proceedings of the National Academy of Sciences*, 112(3):887–892. doi: 10.1073/pnas.1418031112.

Behzadi, Y., Restom, K., Liau, J., and Liu, T. (2007). A component based noise correction method (compcor) for bold and perfusion based fmri. *NeuroImage*, 37(1):90–101. doi: 10.1016/j.neuroimage.2007.04.042.

Betti, V., Della Penna, S., Pasquale, F., Mantini, D., Marzetti, L., Romani, G., and Corbetta, M. (2013). Natural scenes viewing alters the dynamics of functional connectivity in the human brain. *Neuron*, 79(4):782–797. doi: 10.1016/j.neuron.2013.06.022.

Bolt, T., Wang, S., Nomi, J., Setton, R., Gold, B., Frederick, B., Yeo, B., Chen, J., Picchioni, D., Duyn, J., Spreng, R., Keilholz, S., Uddin, L., and Chang, C. (2025). Autonomic physiological coupling of the global fmri signal. *Nature Neuroscience*, 28(6):1327–1335. doi: 10.1038/s41593-025-01945-y.

Boly, M., Massimini, M., Tsuchiya, N., Postle, B., Koch, C., and Tononi, G. (2017). Are the neural correlates of consciousness in the front or in the back of the cerebral cortex? *Clinical and Neuroimaging Evidence. Journal of Neuroscience*, 37(40):9603–9613. doi: 10.1523/JNEUROSCI.3218-16.2017.

Boulakis, P. and Demertzi, A. (2025). Relating mind-blanking to the content and dynamics of spontaneous thinking. *Current Opinion in Behavioral Sciences*, 61:101481. doi: 10.1016/j.cobeha.2024.101481.

Boulakis, P., Mortaheb, S., Calster, L., Majerus, S., and Demertzi, A. (2023). Whole-brain deactivations precede uninduced mind-blanking reports. *The Journal of Neuroscience*, 43(40):6807–6815.

Boulakis, P., Simos, N., Zoi, S., Mortaheb, S., Schmidt, C., Raimondo, F., and Demertzi, A. (2025). Variations of autonomic arousal mediate the reportability of mind blanking occurrences. *Scientific Reports*, 15(1):4956–19.

Castro, P., Luppi, A., Tagliazucchi, E., Perl, Y., Naci, L., Owen, A., Sitt, J., Destexhe, A., and Cofré, R. (2024). Dynamical structure-function correlations provide robust and generalizable signatures of consciousness in humans. *Communications Biology*, 7(1):1–12. doi: 10.1038/s42003-024-06858-3.

Christoff, K., Irving, Z., Fox, K., Spreng, R., and Andrews-Hanna, J. (2016). Mind-wandering as spontaneous thought: A dynamic framework. *Nature Reviews Neuroscience*, 17(11). doi: 10.1038/nrn.2016.113.

Ciric, R., Wolf, D. H., Power, J. D., Roalf, D. R., Baum, G. L., Ruparel, K., Shinohara, R. T., Elliott, M. A., Eickhoff, S. B., Davatzikos, C., Gur, R. C., Gur, R. E., Bassett, D. S., and Satterthwaite, T. D. (2017). Benchmarking of participant-level confound regression strategies for the control of motion artifact in studies of functional connectivity. *NeuroImage*, 154: 174–187. doi: https://doi.org/10.1016/j.neuroimage.2017.03.020. Cleaning up the fMRI time series: Mitigating noise with advanced acquisition and correction strategies.

Cole, M., Bassett, D., Power, J., Braver, T., and Petersen, S. (2014). Intrinsic and task-evoked network architectures of the human brain. *Neuron*, 83(1):238–251. doi: 10.1016/j.neuron.2014.05.014.

Cole, M., Ito, T., Cocuzza, C., and Sanchez-Romero, R. (2021). The functional relevance of task-state functional connectivity. *Journal of Neuroscience*, 41(12):2684–2702. doi: 10.1523/JNEUROSCI.1713-20.2021.

Cox, R. and Hyde, J. (1997). Software tools for analysis and visualization of fmri data. *NMR in Biomedicine*, 10(4–5):171–178. doi: 10.1002/(SICI)1099-1492(199706/08)10:4/5.

de Cheveigne, Alain, and Simon, J. Z. (2008). Denoising based on spatial filtering. *Journal of Neuroscience Methods*, 171(2):331–339. doi: 10.1016/j.jneumeth.2008.03.015.

Demertzi, A., Tagliazucchi, E., Dehaene, S., Deco, G., Barttfeld, P., Raimondo, F., Martial, C., Fernández-Espejo, D., Rohaut, B., Voss, H., Schiff, N., Owen, A., Laureys, S., Naccache, L., and Sitt, J. (2019). Human consciousness is supported by dynamic complex patterns of brain signal coordination. *Science Advances*, 5(2):7603. doi: 10.1126/sciadv.aat7603.

El-Baba, M., Lewis, D., Fang, Z., Owen, A., Fogel, S., and Morton, J. (2019). Functional connectivity dynamics slow with descent from wakefulness to sleep. *PLOS ONE*, 14(12): 0224669. doi: 10.1371/journal.pone.0224669.

Esteban, O., Blair, R., Markiewicz, C., Berleant, S., Moodie, C., Ma, F., Isik, A., Erramuzpe, A., Kent, M., andGoncalves, J. D., DuPre, E., Sitek, K., Gomez, D., Lurie, D., Ye, Z., Poldrack, R., and Gorgolewski, K., (2018). URL https://doi.org/10.5281/zenodo.852659. fMRIPrep 23.2.1. Software.

Esteban, O., Markiewicz, C., Blair, R., Moodie, C., Isik, A., Erramuzpe, A., Kent, J., Goncalves, M., DuPre, E., Snyder, M., Oya, H., Ghosh, S., Wright, J., Durnez, J., Poldrack, R., and Gorgolewski, K. (2019). fmriprep: A robust preprocessing pipeline for functional mri. *Nature Methods*, 16(1):111–116. doi: 10.1038/s41592-018-0235-4.

Fonov, V., Evans, A., McKinstry, R., Almli, C., and Collins, D. (2009). Unbiased nonlinear average age-appropriate brain templates from birth to adulthood. *NeuroImage*, 47, Supplement 1:102. doi: 10.1016/S1053-8119(09)70884-5.

Girn, M., Mills, C., Laycock, E., Ellamil, M., Ward, L., and Christoff, K. Neural dynamics of spontaneous thought: An electroencephalographic study. In Schmorrow, D. and Fidopiastis, C., editors, *Augmented Cognition. Neurocognition and Machine Learning*, page 28–44. Springer International Publishing, (2017). doi: 10.1007/978-3-319-58628-1_3. URL https://doi.org/10.1007/978-3-319-58628-1_3.

Gorgolewski, K., Burns, C., Madison, C., Clark, D., Halchenko, Y., Waskom, M., and Ghosh, S. (2011). Nipype: A flexible, lightweight and extensible neuroimaging data processing framework in python. *Frontiers in Neuroinformatics*, 5:13. doi: 10.3389/fninf.2011.00013.

Gorgolewski, K., Esteban, O., Markiewicz, C., Ziegler, E., Ellis, D., Notter, M., Jarecka, D., Johnson, H., Burns, C., Manhães-Savio, A., Hamalainen, C., Yvernault, B., Salo, T., Jordan, K., Goncalves, M., Waskom, M., Clark, D., Wong, J., Loney, F., and Ghosh, S. (2018). Nipype. *Software*. doi: 10.5281/zenodo.596855.

Greve, D. and Fischl, B. (2009). Accurate and robust brain image alignment using boundary-based registration. *NeuroImage*, 48(1):63–72. doi: 10.1016/j.neuroimage.2009.06.060.

Hudetz, A., Liu, X., and Pillay, S. (2015). Dynamic repertoire of intrinsic brain states is reduced in propofol-induced unconsciousness. *Brain Connectivity*, 5(1):10. doi: 10.1089/brain.2014.0230.

Ito, T., Brincat, S., Siegel, M., Mill, R., He, B., Miller, E., Rotstein, H., and Cole, M. (2020). Task-evoked activity quenches neural correlations and variability across cortical areas. *PLOS Computational Biology*, 16(8):1007983. doi: 10.1371/journal.pcbi.1007983.

Jenkinson, M. and Smith, S. (2001). A global optimisation method for robust affine registration of brain images. *Medical Image Analysis*, 5(2):143–156. doi: 10.1016/S1361-8415(01)00036-6.

Jenkinson, M., Bannister, P., Brady, M., and Smith, S. (2002). Improved optimization for the robust and accurate linear registration and motion correction of brain images. *NeuroImage*, 17(2):825–841. doi: 10.1006/nimg.2002.1132.

Kaufmann, A., Parmigiani, S., Kawagoe, T., Zabaroff, E., and Wells, B. (2024). Two models of mind blanking. *European Journal of Neuroscience*, 59(5):786–795. doi: 10.1111/ejn.16164.

Kawagoe, T., Onoda, K., and Yamaguchi, S. (2019). The neural correlates of "mind blanking": When the mind goes away. *Human Brain Mapping*, 40(17):4934–4940. doi: 10.1002/hbm.24748.

Kim, B., Andrews-Hanna, J., Han, J., Lee, E., and Woo, C.-W. (2022). When self comes to a wandering mind: Brain representations and dynamics of self-generated concepts in spontaneous thought. *Science Advances*, 8(35):8616. doi: 10.1126/sciadv.abn8616.

Koch, C., Massimini, M., Boly, M., and Tononi, G. (2016). Neural correlates of consciousness: Progress and problems. *Nature Reviews Neuroscience*, 17(5):307–321. doi: 10.1038/nrn.2016.22.

Langner, O., Dotsch, R., Bijlstra, G., Wigboldus, D., Hawk, S., and Knippenberg, A. (2010). Presentation and validation of the radboud faces database. *Cognition and Emotion*, 24(8):1377–1388. doi: 10.1080/02699930903485076.

Li, C., Fronczek-Poncelet, J., Lange, D., Hennecke, E., Kroll, T., Matusch, A., Aeschbach, D., Bauer, A., Elmenhorst, E.-M., and Elmenhorst, D. (2020). Impact of acute sleep deprivation on dynamic functional connectivity states. *Human Brain Mapping*, 41(4):994–1005. doi: 10.1002/hbm.24855.

Massimini, M., Huber, R., Ferrarelli, F., Hill, S., and Tononi, G. (2004). The sleep slow oscillation as a traveling wave. *The Journal of Neuroscience*, 24(31):6862–6870. doi: 10.1523/JNEUROSCI.1318-04.2004.

Menicucci, D., Piarulli, A., Debarnot, U., d'Ascanio, P., Landi, A., and Gemignani, A. (2009). Functional structure of spontaneous sleep slow oscillation activity in humans. *PLOS ONE*, 4(10):7601. doi: 10.1371/journal.pone.0007601.

Mortaheb, S., Calster, L., Raimondo, F., Klados, M., Boulakis, P., Georgoula, K., Majerus, S., Ville, D., and Demertzi, A. (2022). Mind blanking is a distinct mental state linked to a recurrent brain profile of globally positive connectivity during ongoing mentation. *Proceedings of the National Academy of Sciences of the United States of America*, 119(41):2200511119. doi: 10.1073/pnas.2200511119.

Mortaheb, S., Fort, L., Mason, N., Mallaroni, P., Ramaekers, J., and Demertzi, A. (2024). Dynamic functional hyperconnectivity after psilocybin intake is primarily associated with oceanic boundlessness. *Biological Psychiatry. Cognitive Neuroscience and Neuroimaging*, 9(7):681–692. doi: 10.1016/j.bpsc.2024.04.001.

Munoz-Musat, E., Le Coz, A., Corcoran, A., Belloli, L., Naccache, L., and Andrillon, T. (2025). Mind the blank: Behavioral, experiential, and physiological signatures of absent-mindedness. *bioRxiv*. doi: 10.1101/2024.02.11.579845.

Patriat, R., Reynolds, R., and Birn, R. (2017). An improved model of motion-related signal changes in fmri. *NeuroImage*, 144, Part A:74–82. doi: 10.1016/j.neuroimage.2016.08.051.

Philip, P., Sagaspe, P., Taillard, J., Moore, N., Guilleminault, C., Sanchez-Ortuno, M., Åkerstedt, T., and Bioulac, B. (2003). Fatigue, sleep restriction, and performance in automobile drivers: A controlled study in a natural environment. *Sleep*, 26(3):277–280. doi: 10.1093/sleep/26.3.277.

Power, J., Mitra, A., Laumann, T., Snyder, A., Schlaggar, B., and Petersen, S. (2014). Methods to detect, characterize, and remove motion artifact in resting state fmri. *NeuroImage*, 84(Supplement C):320–341. doi: 10.1016/j.neuroimage.2013.08.048.

Power, J., Plitt, M., Laumann, T., and Martin, A. (2017). Sources and implications of whole-brain fmri signals in humans. *NeuroImage*, 146:609–625. doi: 10.1016/j.neuroimage.2016.09.038.

Power, J., Plitt, M., Gotts, S., Kundu, P., Voon, V., Bandettini, P., and Martin, A. (2018). Ridding fmri data of motion-related influences: Removal of signals with distinct spatial and physical bases in multiecho data. *Proceedings of the National Academy of Sciences*, 115(9):2105– 2114. doi: 10.1073/pnas.1720985115.

Robertson, I., Manly, T., Andrade, J., Baddeley, B., and Yiend, J. (1997). Oops!": Performance correlates of everyday attentional failures in traumatic brain injured and normal subjects. *Neuropsychologia*, 35(6):747–758. doi: 10.1016/s0028-3932(97)00015-8.

Robison, M., Miller, A., and Unsworth, N. (2019). Examining the effects of probe frequency, response options, and framing within the thought-probe method. *Behavior Research Methods*, 51(1):398–408. doi: 10.3758/s13428-019-01212-6.

Satterthwaite, T., Elliott, M., Gerraty, R., Ruparel, K., Loughead, J., Calkins, M., Eickhoff, S., Hakonarson, H., Gur, R., Gur, R., and Wolf, D. (2013). An improved framework for confound regression and filtering for control of motion artifact in the preprocessing of resting-state functional connectivity data. *NeuroImage*, 64(1):240–256. doi: 10.1016/j.neuroimage.2012.08.052.

Schaefer, A., Kong, R., Gordon, E. M., Laumann, T. O., Zuo, X.-N., Holmes, A. J., Eickhoff, S. B., and Yeo, B. T. T. (2018). Local-Global Parcellation of the Human Cerebral Cortex from Intrinsic Functional Connectivity MRI. *Cerebral Cortex*, 28(9):3095–3114. doi: 10.1093/cercor/bhx179.

Schwalm, M., Schmid, F., Wachsmuth, L., Backhaus, H., Kronfeld, A., Aedo Jury, F., Prouvot, P.-H., Fois, C., Albers, F., Alst, T., Faber, C., and Stroh, A. (2017). Cortex-wide bold fmri activity reflects locally-recorded slow oscillation-associated calcium waves. *eLife*, 6:27602. doi: 10.7554/eLife.27602.

Schölvinck, M., Maier, A., Ye, F., Duyn, J., and Leopold, D. (2010). Neural basis of global resting-state fmri activity. *Proceedings of the National Academy of Sciences*, 107(22):10238–10243. doi: 10.1073/pnas.0913110107.

Sheybani, L., Vivekananda, U., Rodionov, R., Diehl, B., Chowdhury, F., McEvoy, A., Miserocchi, A., Bisby, J., Bush, D., Burgess, N., and Walker, M. (2023). Wake slow waves in focal human epilepsy impact network activity and cognition. *Nature Communications*, 14(1):7397. doi: 10.1038/s41467-023-42971-3.

Shine, J., Bissett, P., Bell, P., Koyejo, O., Balsters, J., Gorgolewski, K., Moodie, C., and Poldrack, R. (2016). The dynamics of functional brain networks: Integrated network states during cognitive task performance. *Neuron*, 92(2):544–554. doi: 10.1016/j.neuron.2016.09.018.

Smallwood, J., Turnbull, A., Wang, H., Ho, N., Poerio, G., Karapanagiotidis, T., Konu, D., Mckeown, B., Zhang, M., Murphy, C., Vatansever, D., Bzdok, D., Konishi, M., Leech, R., Seli, P., Schooler, J., Bernhardt, B., Margulies, D., and Jefferies, E. (2021). The neural correlates of ongoing conscious thought. *iScience*, 24(3):102132. doi: 10.1016/j.isci.2021.102132.

Spadone, S., Della Penna, S., Sestieri, C., Betti, V., Tosoni, A., Perrucci, M., Romani, G., and Corbetta, M. (2015). Dynamic reorganization of human resting-state networks during visuospatial attention. *Proceedings of the National Academy of Sciences of the United States of America*, 112(26):8112–8117. doi: 10.1073/pnas.1415439112.

Stawarczyk, D. and D'Argembeau, A. (2016). Conjoint influence of mind-wandering and sleepiness on task performance. *Journal of Experimental Psychology. Human Perception and Performance*, 42(10):1587–1600.

Stawarczyk, D., Majerus, S., Maj, M., Linden, M., and D'Argembeau, A. (2011). Mind-wandering: Phenomenology and function as assessed with a novel experience sampling method. *Acta Psychologica*, 136(3):370–381. doi: 10.1016/j.actpsy.2011.01.002.

Stawarczyk, D., François, C., Wertz, J., and D'Argembeau, A. (2020). Drowsiness or mind-wandering? fluctuations in ocular parameters during attentional lapses. *Biological Psychology*, 156:107950. doi: 10.1016/j.biopsycho.2020.107950.

Steriade, M., Nunez, A., and Amzica, F. (1993). Intracellular analysis of relations between the slow ($>$ 1 hz) neocortical oscillation and other sleep rhythms of the electroencephalogram. *Journal of Neuroscience*, 13(8):3266–3283. doi: 10.1523/JNEUROSCI.13-08-03266.1993.

Tononi, G. and Cirelli, C. (2014). Sleep and the price of plasticity: From synaptic and cellular homeostasis to memory consolidation and integration. *Neuron*, 81(1):12–34. doi: 10.1016/j.neuron.2013.12.025.

Turchi, J., Chang, C., Ye, F., Russ, B., Yu, D., Cortes, C., Monosov, I., Duyn, J., and Leopold, D. (2018). The basal forebrain regulates global resting-state fmri fluctuations. *Neuron*, 97(4):940–952 4. doi: 10.1016/j.neuron.2018.01.032.

Tustison, N., Avants, B., Cook, P., Zheng, Y., Egan, A., Yushkevich, P., and Gee, J. (2010). N4itk: Improved n3 bias correction. *IEEE Transactions on Medical Imaging*, 29(6):1310–1320. doi: 10.1109/TMI.2010.2046908.

Türker, B., Belloli, L., Owen, A., Naci, L., and Sitt, J. (2023). Processing of the same narrative stimuli elicits common functional connectivity dynamics between individuals. *Scientific Reports*, 13(1):21260. doi: 10.1038/s41598-023-48656-7.

Türker, B., Manasova, D., Béranger, B., Naccache, L., Sergent, C., and Sitt, J. (2024). Distinct dynamic connectivity profiles promote enhanced conscious perception of auditory stimuli. *Communications Biology*, 7(1):856–859.

Uddin, L. (2017). Mixed signals: On separating brain signal from noise. *Trends in Cognitive Sciences*, 21(6):405–406. doi: 10.1016/j.tics.2017.04.002.

Uhrig, L., Sitt, J., Jacob, A., Tasserie, J., Barttfeld, P., Dupont, M., Dehaene, S., and Jarraya, B. (2018). Resting-state dynamics as a cortical signature of anesthesia in monkeys. *Anesthesiology*, 129(5):942–958. doi: 10.1097/ALN.0000000000002336.

Vyazovskiy, V. and Harris, K. (2013). Sleep and the single neuron: The role of global slow oscillations in individual cell rest. *Nature Reviews. Neuroscience*, 14(6):443–451. doi: 10.1038/nrn3494.

Vyazovskiy, V., Olcese, U., Hanlon, E., Nir, Y., Cirelli, C., and Tononi, G. (2011). Local sleep in awake rats. *Nature*, 472(7344):443–447. doi: 10.1038/nature10009.

Wang, H.-T., Smallwood, J., Mourao-Miranda, J., Xia, C., Satterthwaite, T., Bassett, D., and Bzdok, D. (2020). Finding the needle in a high-dimensional haystack: Canonical correlation analysis for neuroscientists. *NeuroImage*, 216:116745. doi: 10.1016/j.

neuroimage.2020.116745.

Ward, A. and Wegner, D. (2013). Mind-blanking: When the mind goes away. *Frontiers in Psychology*, 4:650. doi: 10.3389/fpsyg.2013.00650.

Wong, C., Olafsson, V., Tal, O., and Liu, T. (2013). The amplitude of the resting-state fmri global signal is related to eeg vigilance measures. *NeuroImage*, 83:983–990. doi: 10.1016/j.neuroimage.2013.07.057.

Włodarczyk, D., Jaśkowski, P., and Nowik, A. (2002). Influence of sleep deprivation and auditory intensity on reaction time and response force. *Perceptual and Motor Skills*, 94 (3_suppl):1101–1112. doi: 10.2466/pms.2002.94.3c.1101.

Zhang, J. and Northoff, G. (2022). Beyond noise to function: Reframing the global brain activity and its dynamic topography. *Communications Biology*, 5(1). doi: 10.1038/s42003-022-04297-6.

Zhang, Y., Brady, M., and Smith, S. (2001). Segmentation of brain mr images through a hidden markov random field model and the expectation-maximization algorithm. *IEEE Transactions on Medical Imaging*, 20(1):45–57. doi: 10.1109/42.906424.

Zhuang, X., Yang, Z., and Cordes, D. (2020). A technical review of canonical correlation analysis for neuroscience applications. *Human Brain Mapping*, 41(13):3807–3833. doi: 10.1002/hbm.25090.

Özbay, P., Chang, C., Picchioni, D., Mandelkow, H., Chappel-Farley, M., Gelderen, P., Zwart, J., and Duyn, J. (2019). Sympathetic activity contributes to the fmri signal. *Communications Biology*, 2(1):1–9. doi: 10.1038/s42003-019-0659-0.

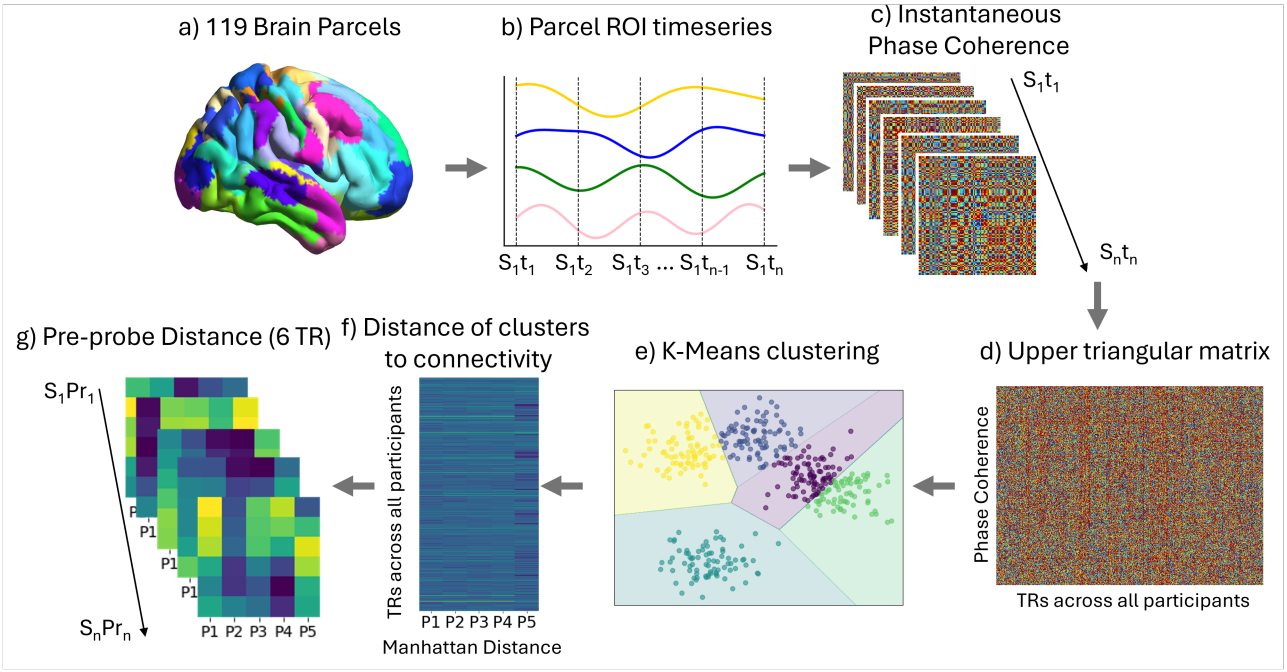

Figure S1. Schematic representation of time-varying functional connectivity clustering. a) Nineteen subcortical parcels were appended to the Schaefer 100 cortical regions of interest (ROIs), yielding a combined cortical–subcortical parcellation. **b)** For each subject S, the mean BOLD timeseries was extracted from every ROI, resulting in an $N_T R$ x 119 matrix, where each row corresponds to the mean BOLD signal per ROI. **c)** The Hilbert transform was applied to obtain an analytic representation of each ROI timeseries, from which instantaneous phase coherence was computed between all ROI pairs at every BOLD acquisition. **d)** Given that phase coherence matrices are symmetric, only the upper triangular elements were retained for each subject and time-point. These matrices were concatenated across subjects and time to generate a comprehensive dataset representation of phase coherence. **e)** To identify representative connectivity patterns that capture the temporal organization of functional connectivity, we applied K-means clustering using the Manhattan distance metric. This procedure yielded five recurring connectivity patterns that describe the observed functional connectivity across time. **f)** For each timepoint, we quantified the similarity to each of the five connectivity patterns by computing the Manhattan distance. Effectively, this informed us as to how similar the brain looks to each of the connectivity patterns at every TR. **g)** Finally, to investigate probe-specific functional connectivity, we extracted the last six TRs (approximately 10 s) preceding each probe P, capturing their distances to the identified connectivity patterns. The y-axis of each heatmap represents distances from $t_n - 6$ up to $t_n - 1$ BOLD scans before each probe. Each participant had approximately 40 probes.

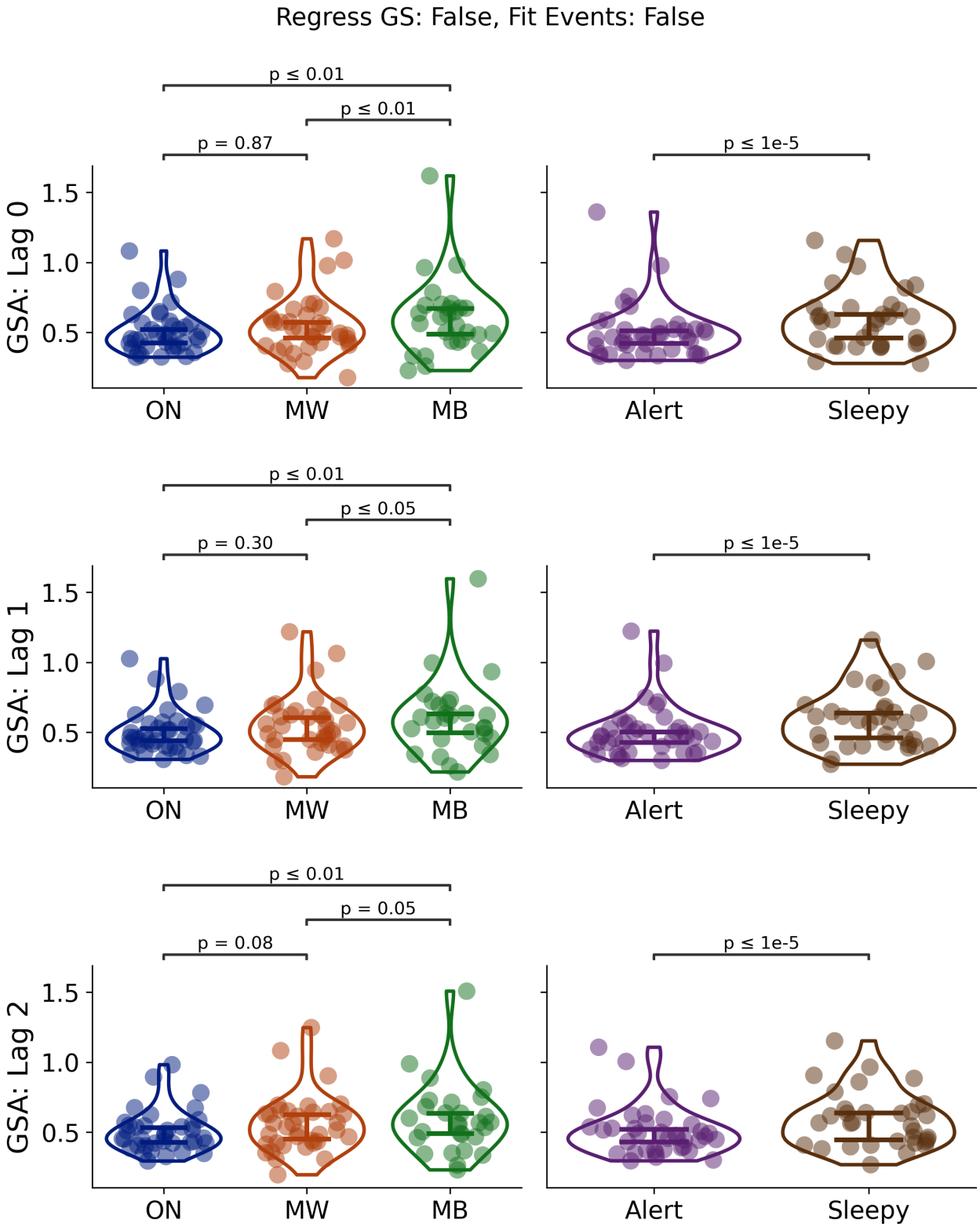

Figure S2. Replication analysis of the relationship between global signal amplitude, mental states and alertness levels. Analysis parameters: task regression = False, Global signal regression = False. Across 3 different lags (shifting the analysis windows by 1 TR relative to the auditory probe to report content and alertness), participant consistently indicate higher global signal amplitude during MB and sleepiness. GSA = global signal amplitude

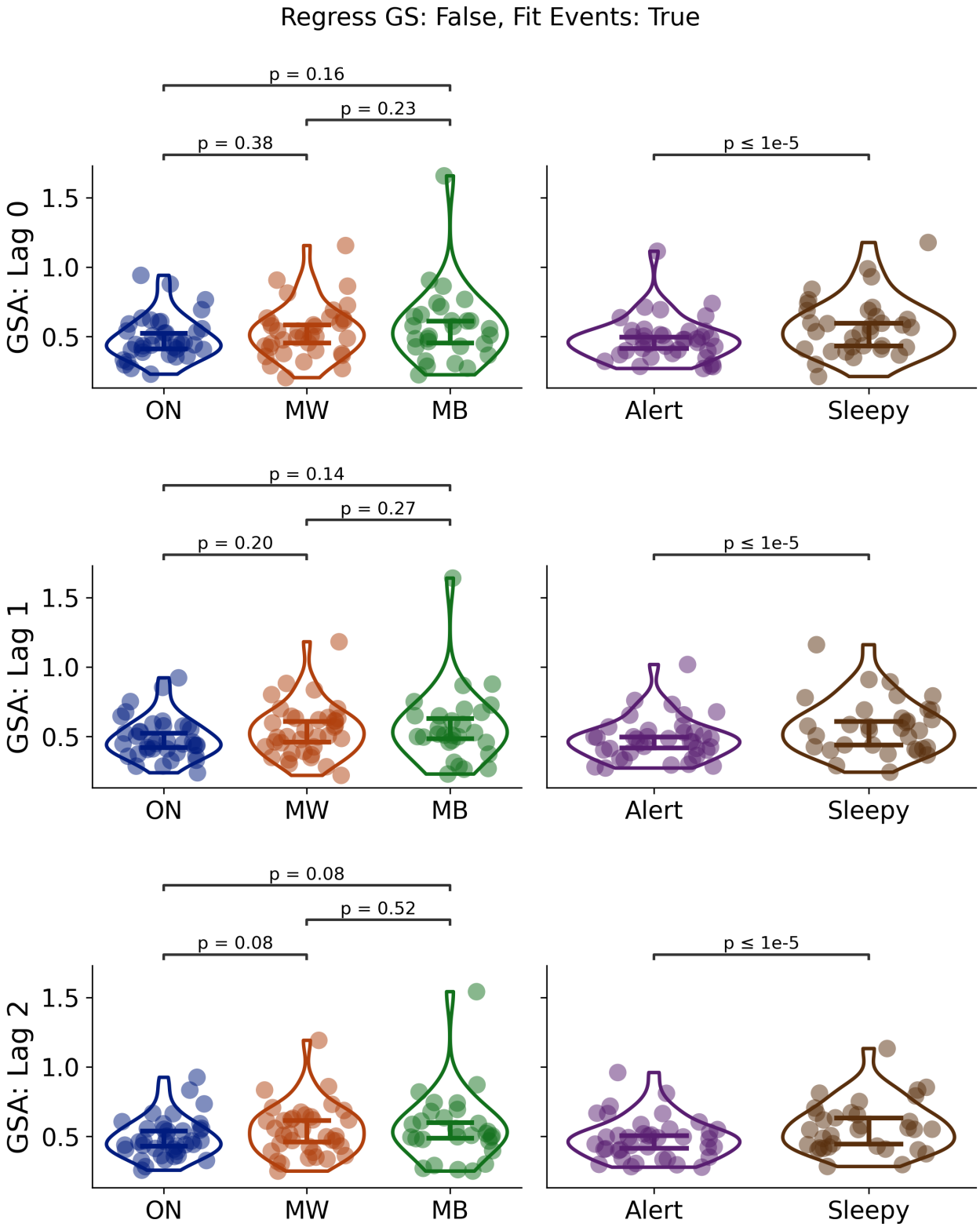

Figure S3. Replication analysis of the relationship between global signal amplitude, mental states and alertness levels. Analysis parameters: task regression = True, Global signal regression = False. Across 3 different lags (shifting the analysis windows by 1 TR relative to the auditory probe to report content and alertness), participant consistently indicate higher global signal amplitude during MB and sleepiness. GSA = global signal amplitude

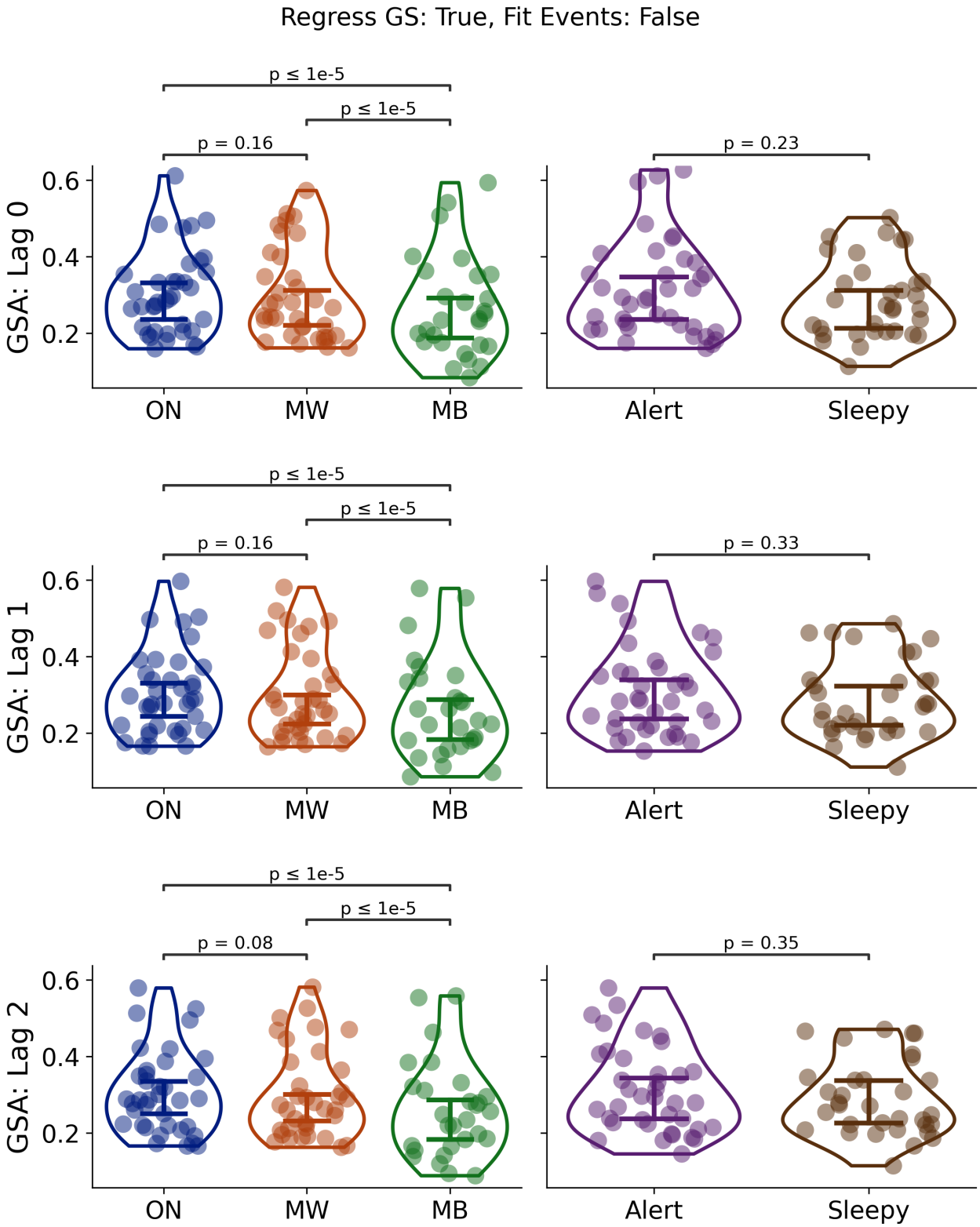

Figure S4. Replication analysis of the relationship between global signal amplitude, mental states and alertness levels. Analysis parameters: task regression = True, Global signal regression = False. Across 3 different lags (shifting the analysis windows by 1 TR relative to the auditory probe to report content and alertness), participant consistently indicate higher global signal amplitude during MB and sleepiness. GSA = global signal amplitude

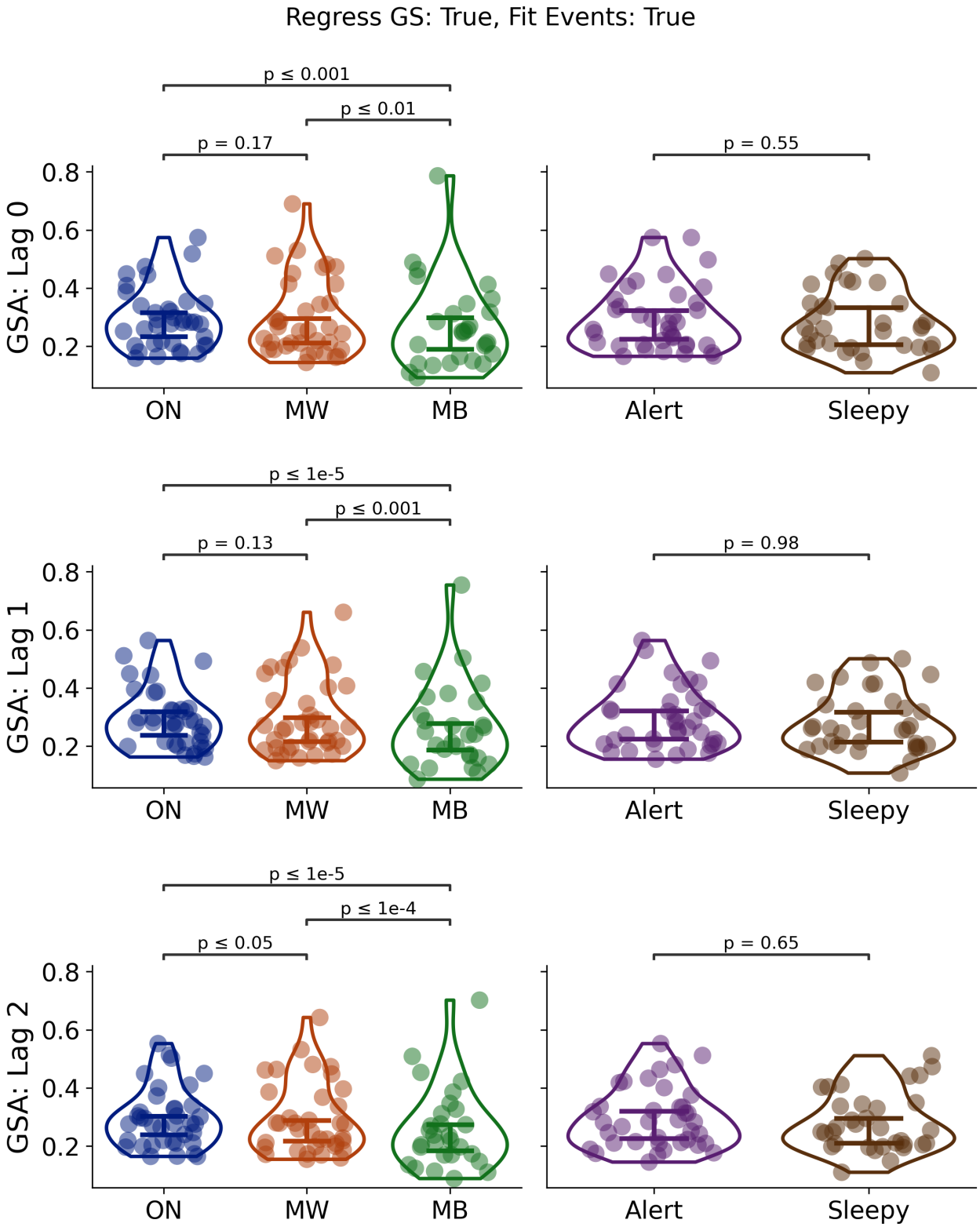

Figure S5. Replication analysis of the relationship between global signal amplitude, mental states and alertness levels. Analysis parameters: task regression = True, Global signal regression = True. Across 3 different lags (shifting the analysis windows by 1 TR relative to the auditory probe to report content and alertness), participant consistently indicate higher global signal amplitude during MB and sleepiness. GSA = global signal amplitude

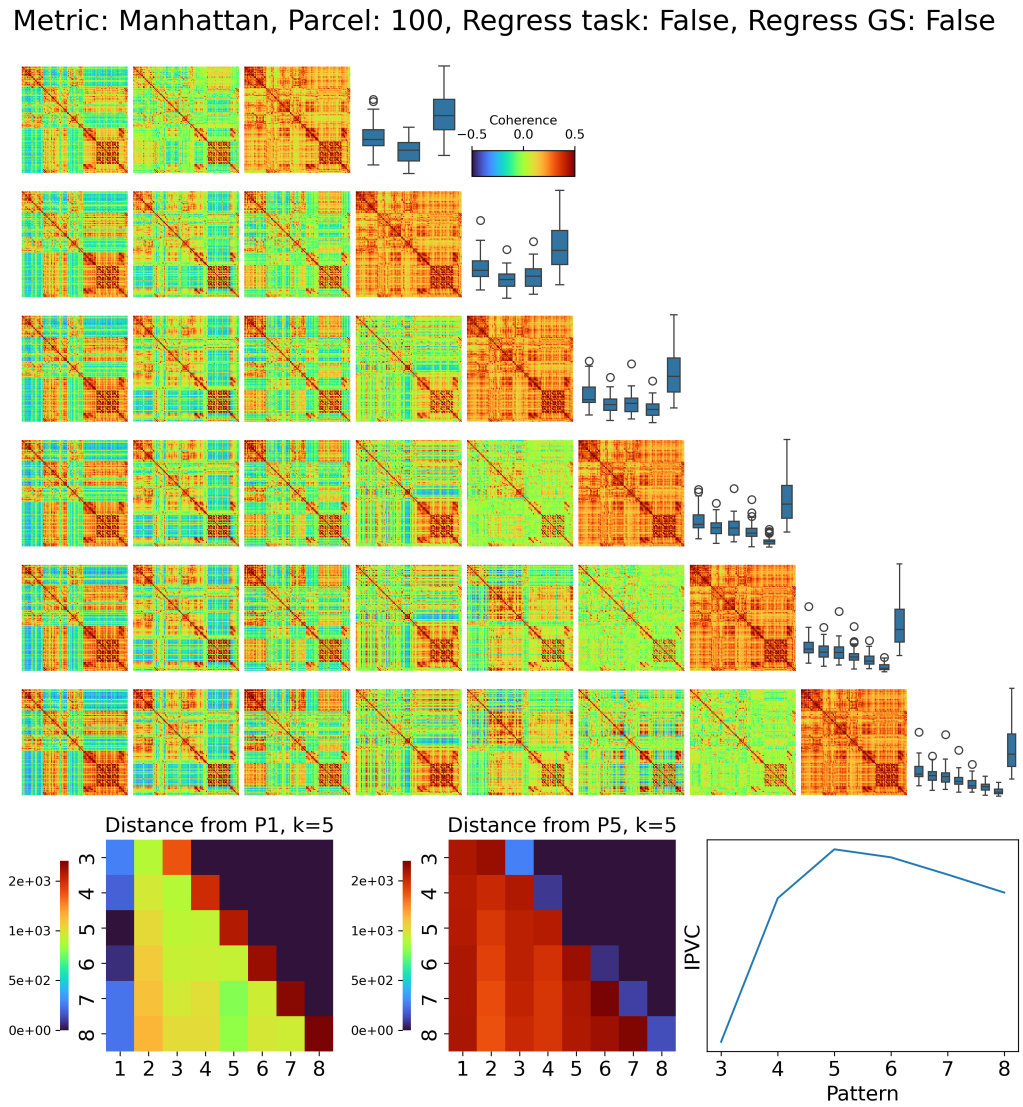

Figure S6. Supplementary Figure S6. Recurrent and consistent brain configurations emerge under different clustering dimensionalities during task engagement. Clustering parameters: Metric = Manhattan distance, Global Signal Regression: False, Event Regression: False. Heatmaps: For each value of k , patterns are ordered based on the standard deviation of their connectome, from the most variant (left) to the least (right). Bottom row – Left: To examine whether patterns produced across different values of k presented correspondence, we estimated the distance of pattern 1 for $k = 5$ with respect to all patterns obtained for $k = 3$ to $k = 8$. Similarly, we estimated the distance of pattern 5 for $k = 5$ with respect to all patterns obtained for $k = 3$ to $k = 8$. Bottom row – Right: For each selection of the number of clusters in the K-means algorithm, we computed the inter-pattern correlation variability (IPVC) between all the upper triangular parts of the resulting centroids. The variability of dynamic coordination patterns found by the clustering procedure is maximal with $k = 5$ clusters.

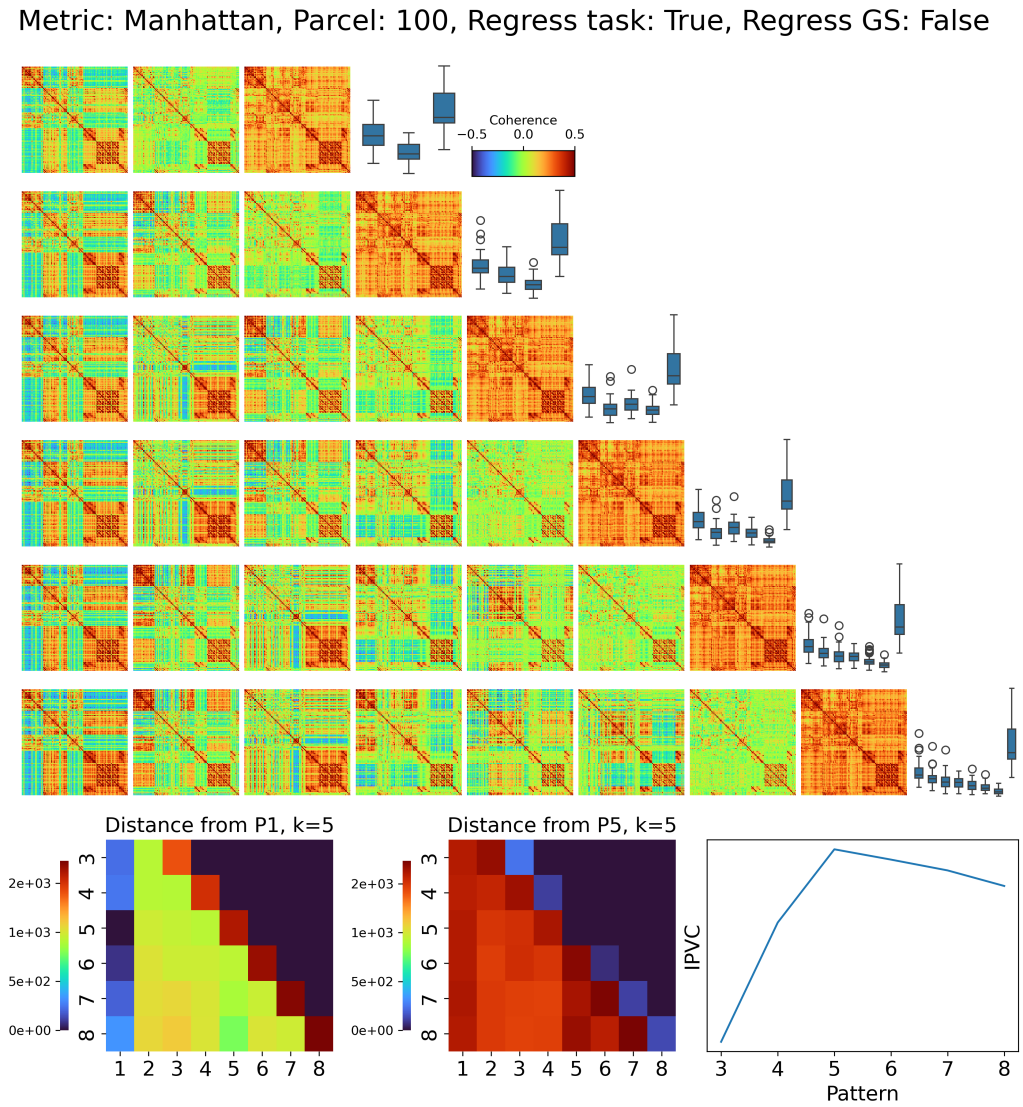

Figure S7. Recurrent and consistent brain configurations emerge under different clustering dimensionalities during task engagement. Clustering parameters: Metric = Manhattan distance, Global Signal Regression: False, Event Regression: True. Heatmaps: For each value of k , patterns are ordered based on the standard deviation of their connectome, from the most variant (left) to the least (right). Bottom row – Left: To examine whether patterns produced across different values of k presented correspondence, we estimated the distance of pattern 1 for $k = 5$ with respect to all patterns obtained for $k = 3$ to $k = 8$. Similarly, we estimated the distance of pattern 5 for $k = 5$ with respect to all patterns obtained for $k = 3$ to $k = 8$. Bottom row – Right: For each selection of the number of clusters in the K-means algorithm, we computed the inter-pattern correlation variability (IPVC) between all the upper triangular parts of the resulting centroids. The variability of dynamic coordination patterns found by the clustering procedure is maximal with $k = 5$ clusters.

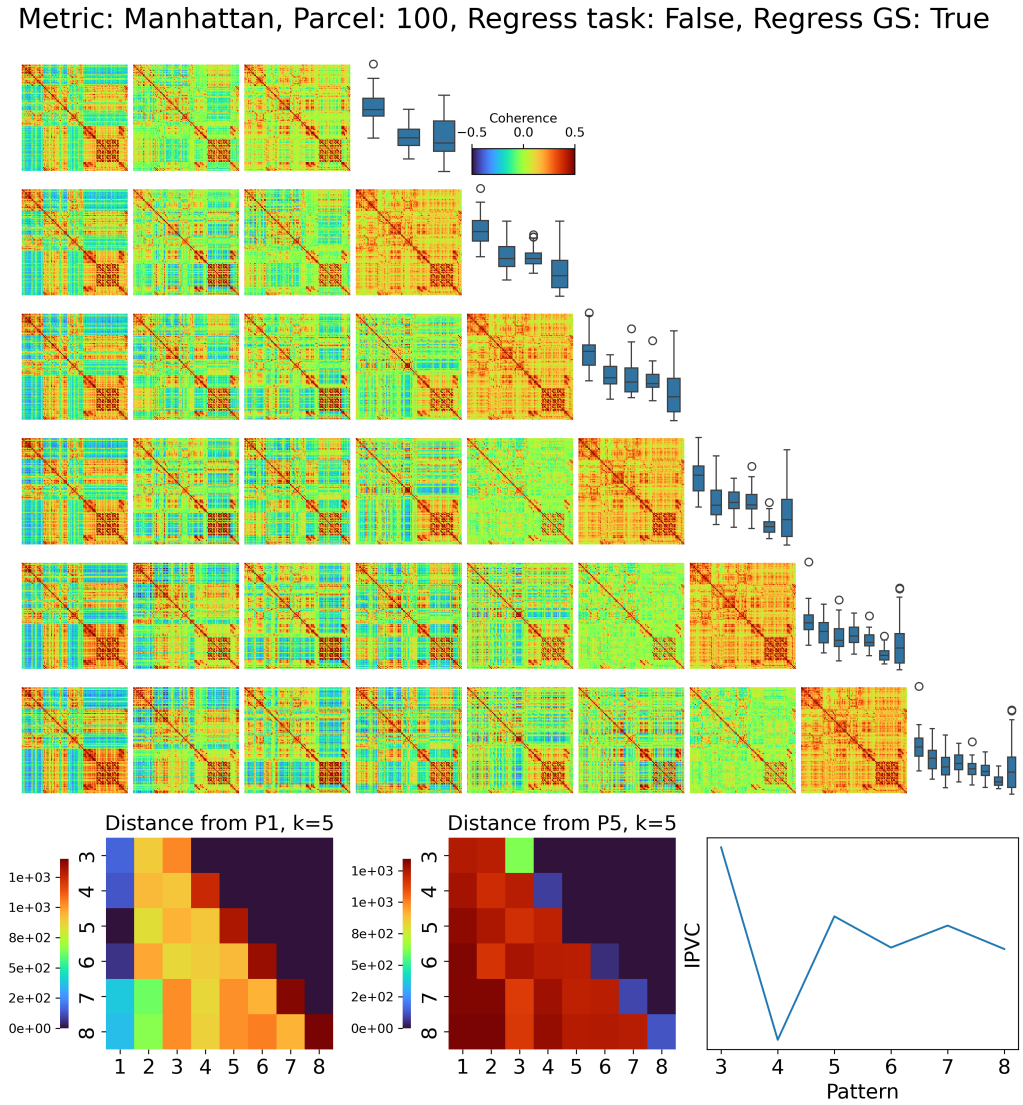

Figure S8. Recurrent and consistent brain configurations emerge under different clustering dimensionalities during task engagement. Clustering parameters: Metric = Manhattan distance, Global Signal Regression: True, Event Regression: False. Heatmaps: For each value of k , patterns are ordered based on the standard deviation of their connectome, from the most variant (left) to the least (right). Bottom row – Left: To examine whether patterns produced across different values of k presented correspondence, we estimated the distance of pattern 1 for $k = 5$ with respect to all patterns obtained for $k = 3$ to $k = 8$. Similarly, we estimated the distance of pattern 5 for $k = 5$ with respect to all patterns obtained for $k = 3$ to $k = 8$. Bottom row – Right: For each selection of the number of clusters in the K-means algorithm, we computed the inter-pattern correlation variability (IPVC) between all the upper triangular parts of the resulting centroids. The variability of dynamic coordination patterns found by the clustering procedure is maximal with $k = 5$ clusters.

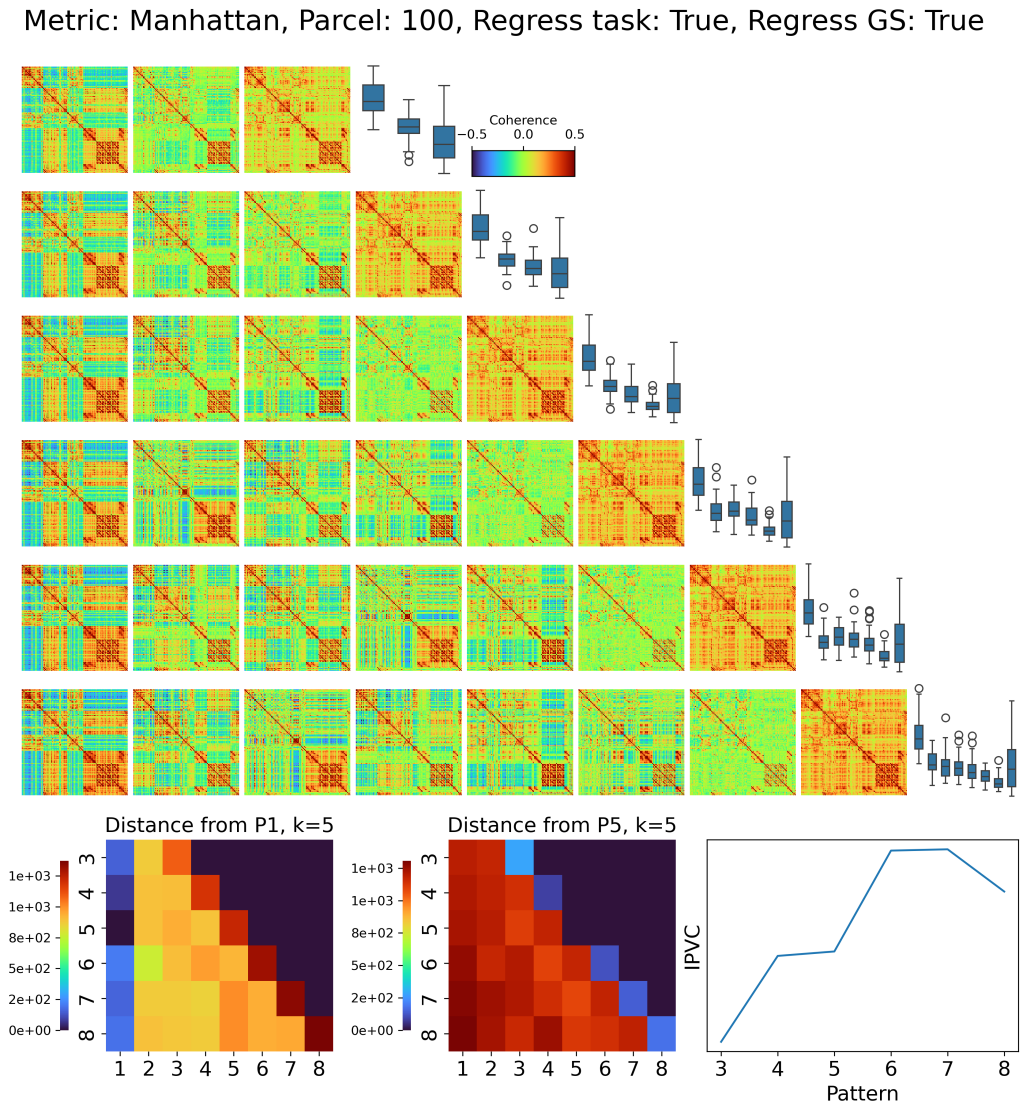

Figure S9. Recurrent and consistent brain configurations emerge under different clustering dimensionalities during task engagement. Clustering parameters: Metric = Manhattan distance, Global Signal Regression: True, Event Regression: True. Heatmaps: For each value of k , patterns are ordered based on the standard deviation of their connectome, from the most variant (left) to the least (right). Bottom row – Left: To examine whether patterns produced across different values of k presented correspondence, we estimated the distance of pattern 1 for $k = 5$ with respect to all patterns obtained for $k = 3$ to $k = 8$. Similarly, we estimated the distance of pattern 5 for $k = 5$ with respect to all patterns obtained for $k = 3$ to $k = 8$. Bottom row – Right: For each selection of the number of clusters in the K-means algorithm, we computed the inter-pattern correlation variability (IPVC) between all the upper triangular parts of the resulting centroids. The variability of dynamic coordination patterns found by the clustering procedure is maximal with $k = 5$ clusters.

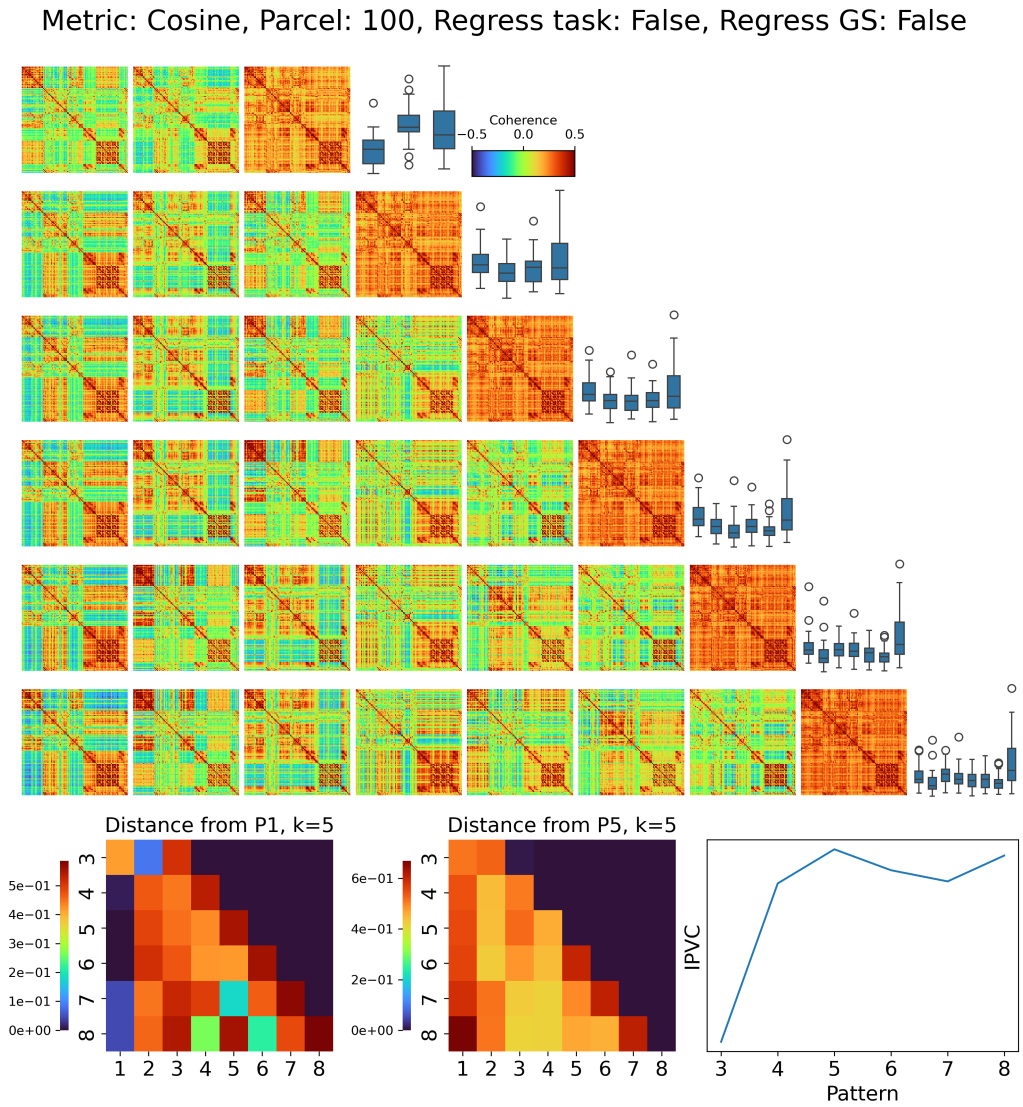

Figure S10. Recurrent and consistent brain configurations emerge under different clustering dimensionalities during task engagement. Clustering parameters: Metric = cosine distance, Global Signal Regression: False, Event Regression: False. Heatmaps: For each value of k , patterns are ordered based on the standard deviation of their connectome, from the most variant (left) to the least (right). Bottom row – Left: To examine whether patterns produced across different values of k presented correspondence, we estimated the distance of pattern 1 for $k = 5$ with respect to all patterns obtained for $k = 3$ to $k = 8$. Similarly, we estimated the distance of pattern 5 for $k = 5$ with respect to all patterns obtained for $k = 3$ to $k = 8$. Bottom row – Right: For each selection of the number of clusters in the K-means algorithm, we computed the inter-pattern correlation variability (IPVC) between all the upper triangular parts of the resulting centroids. The variability of dynamic coordination patterns found by the clustering procedure is maximal with $k = 5$ clusters.

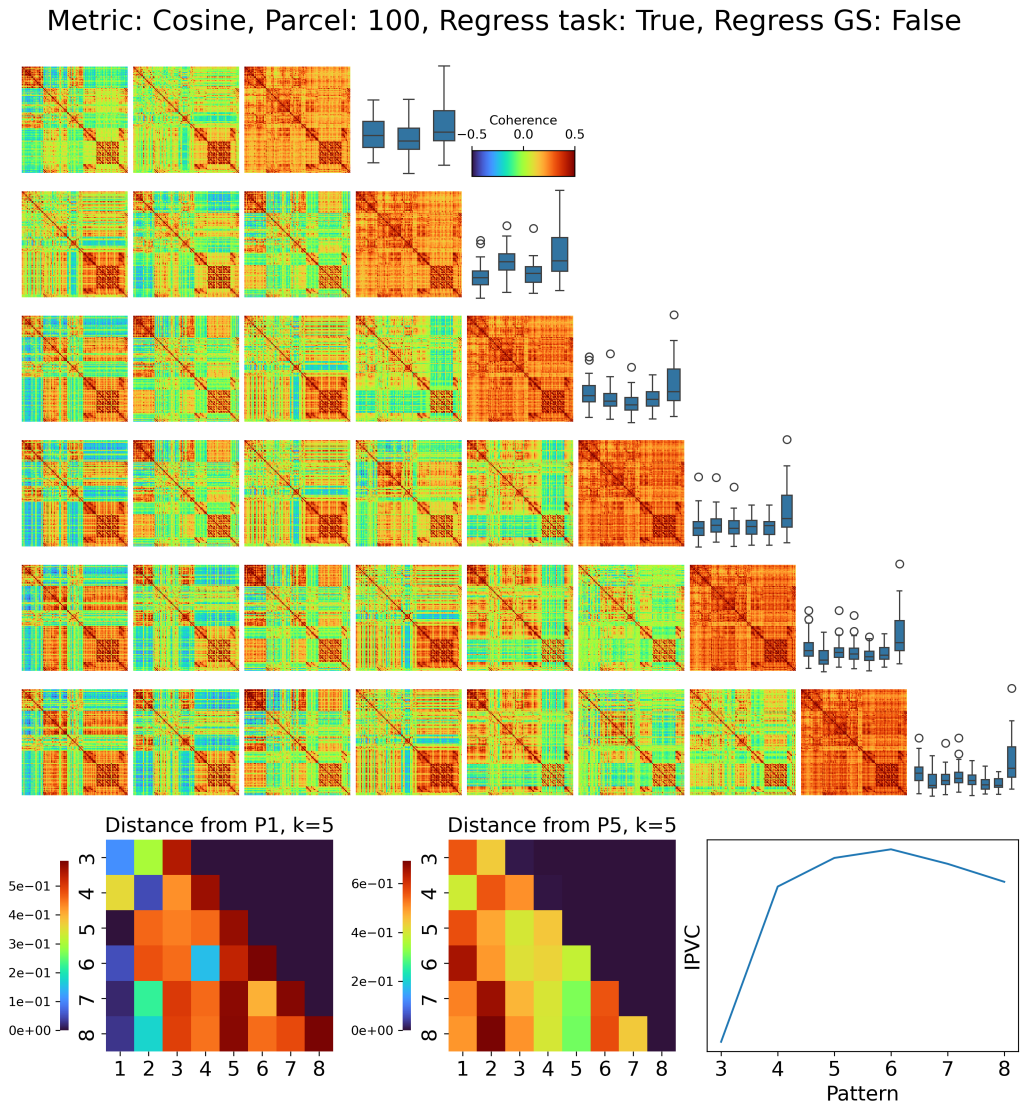

Figure S11. Recurrent and consistent brain configurations emerge under different clustering dimensionalities during task engagement. Clustering parameters: Metric = cosine distance, Global Signal Regression: False, Event Regression: True. Heatmaps: For each value of k , patterns are ordered based on the standard deviation of their connectome, from the most variant (left) to the least (right). Bottom row – Left: To examine whether patterns produced across different values of k presented correspondence, we estimated the distance of pattern 1 for $k = 5$ with respect to all patterns obtained for $k = 3$ to $k = 8$. Similarly, we estimated the distance of pattern 5 for $k = 5$ with respect to all patterns obtained for $k = 3$ to $k = 8$. Bottom row – Right: For each selection of the number of clusters in the K-means algorithm, we computed the inter-pattern correlation variability (IPVC) between all the upper triangular parts of the resulting centroids. The variability of dynamic coordination patterns found by the clustering procedure is maximal with $k = 5$ clusters.

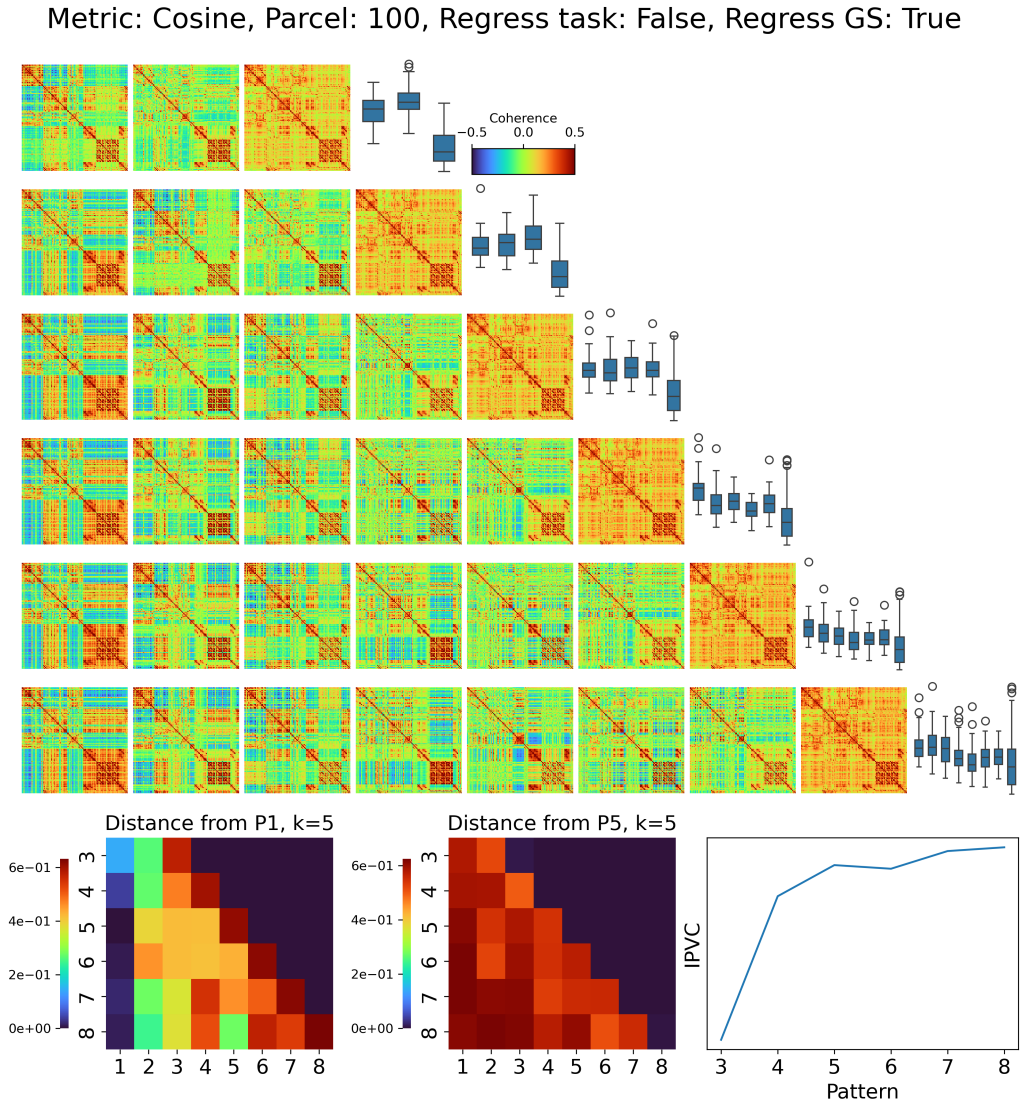

Figure S12. Recurrent and consistent brain configurations emerge under different clustering dimensionalities during task engagement. Clustering parameters: Metric = cosine distance, Global Signal Regression: True, Event Regression: False. Heatmaps: For each value of k , patterns are ordered based on the standard deviation of their connectome, from the most variant (left) to the least (right). Bottom row – Left: To examine whether patterns produced across different values of k presented correspondence, we estimated the distance of pattern 1 for $k = 5$ with respect to all patterns obtained for $k = 3$ to $k = 8$. Similarly, we estimated the distance of pattern 5 for $k = 5$ with respect to all patterns obtained for $k = 3$ to $k = 8$. Bottom row – Right: For each selection of the number of clusters in the K-means algorithm, we computed the inter-pattern correlation variability (IPVC) between all the upper triangular parts of the resulting centroids. The variability of dynamic coordination patterns found by the clustering procedure is maximal with $k = 5$ clusters.

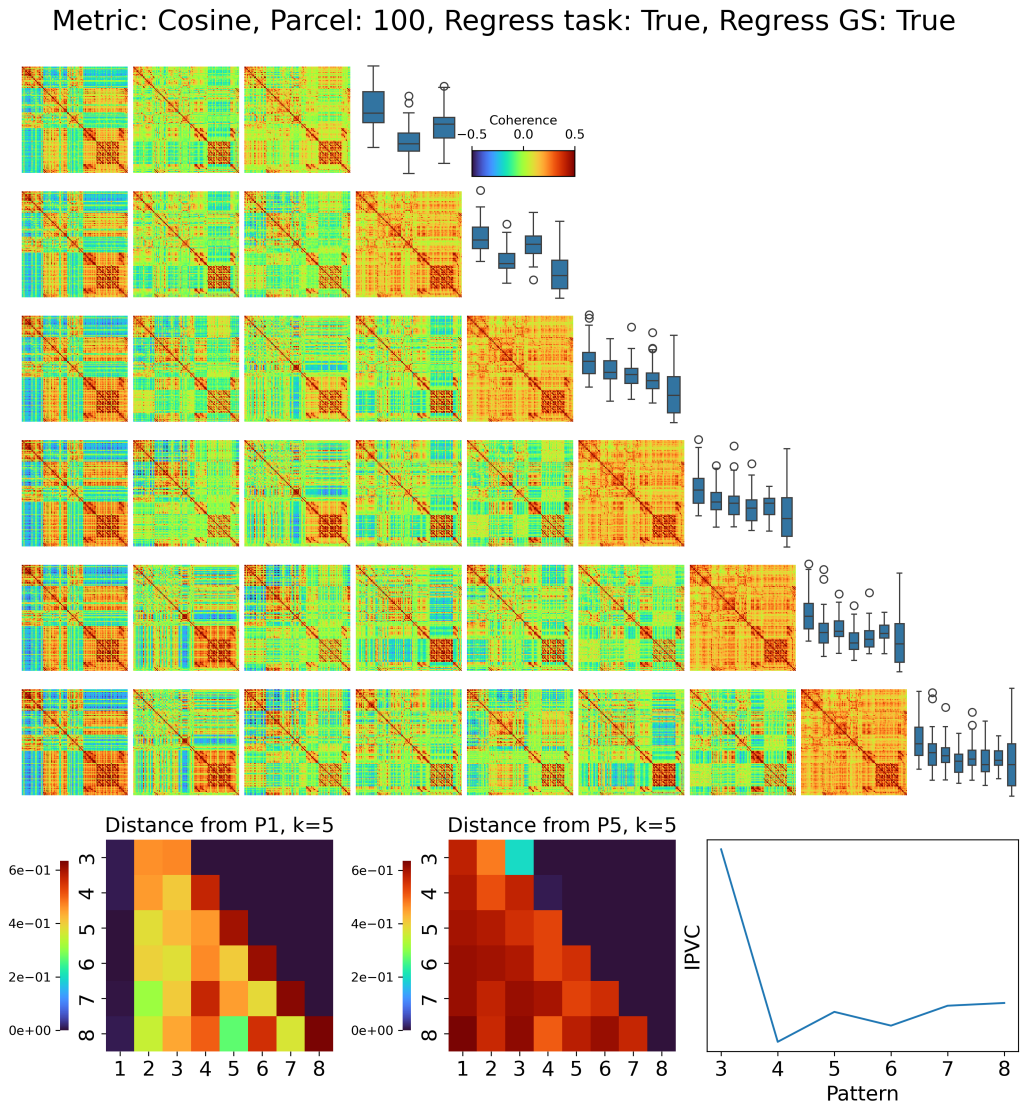

Figure S13. Recurrent and consistent brain configurations emerge under different clustering dimensionalities during task engagement. Clustering parameters: Metric = cosine distance, Global Signal Regression: True, Event Regression: True. Heatmaps: For each value of k , patterns are ordered based on the standard deviation of their connectome, from the most variant (left) to the least (right). Bottom row – Left: To examine whether patterns produced across different values of k presented correspondence, we estimated the distance of pattern 1 for $k = 5$ with respect to all patterns obtained for $k = 3$ to $k = 8$. Similarly, we estimated the distance of pattern 5 for $k = 5$ with respect to all patterns obtained for $k = 3$ to $k = 8$. Bottom row – Right: For each selection of the number of clusters in the K-means algorithm, we computed the inter-pattern correlation variability (IPVC) between all the upper triangular parts of the resulting centroids. The variability of dynamic coordination patterns found by the clustering procedure is maximal with $k = 5$ clusters.

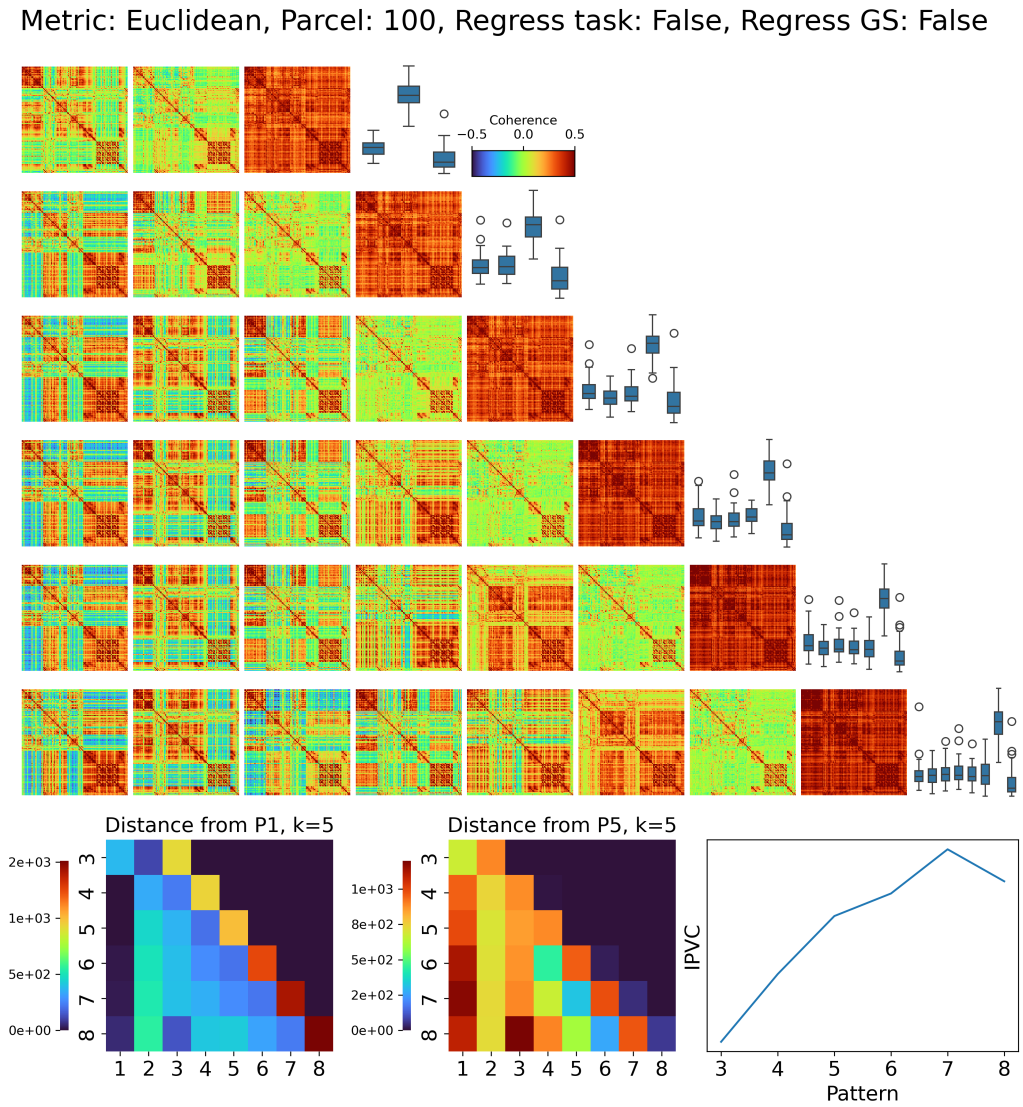

Figure S14. Recurrent and consistent brain configurations emerge under different clustering dimensionalities during task engagement. Clustering parameters: Metric = Euclidean distance, Global Signal Regression: False, Event Regression: False. Heatmaps: For each value of k , patterns are ordered based on the standard deviation of their connectome, from the most variant (left) to the least (right). Bottom row – Left: To examine whether patterns produced across different values of k presented correspondence, we estimated the distance of pattern 1 for $k = 5$ with respect to all patterns obtained for $k = 3$ to $k = 8$. Similarly, we estimated the distance of pattern 5 for $k = 5$ with respect to all patterns obtained for $k = 3$ to $k = 8$. Bottom row – Right: For each selection of the number of clusters in the K-means algorithm, we computed the inter-pattern correlation variability (IPVC) between all the upper triangular parts of the resulting centroids. The variability of dynamic coordination patterns found by the clustering procedure is maximal with $k = 5$ clusters.

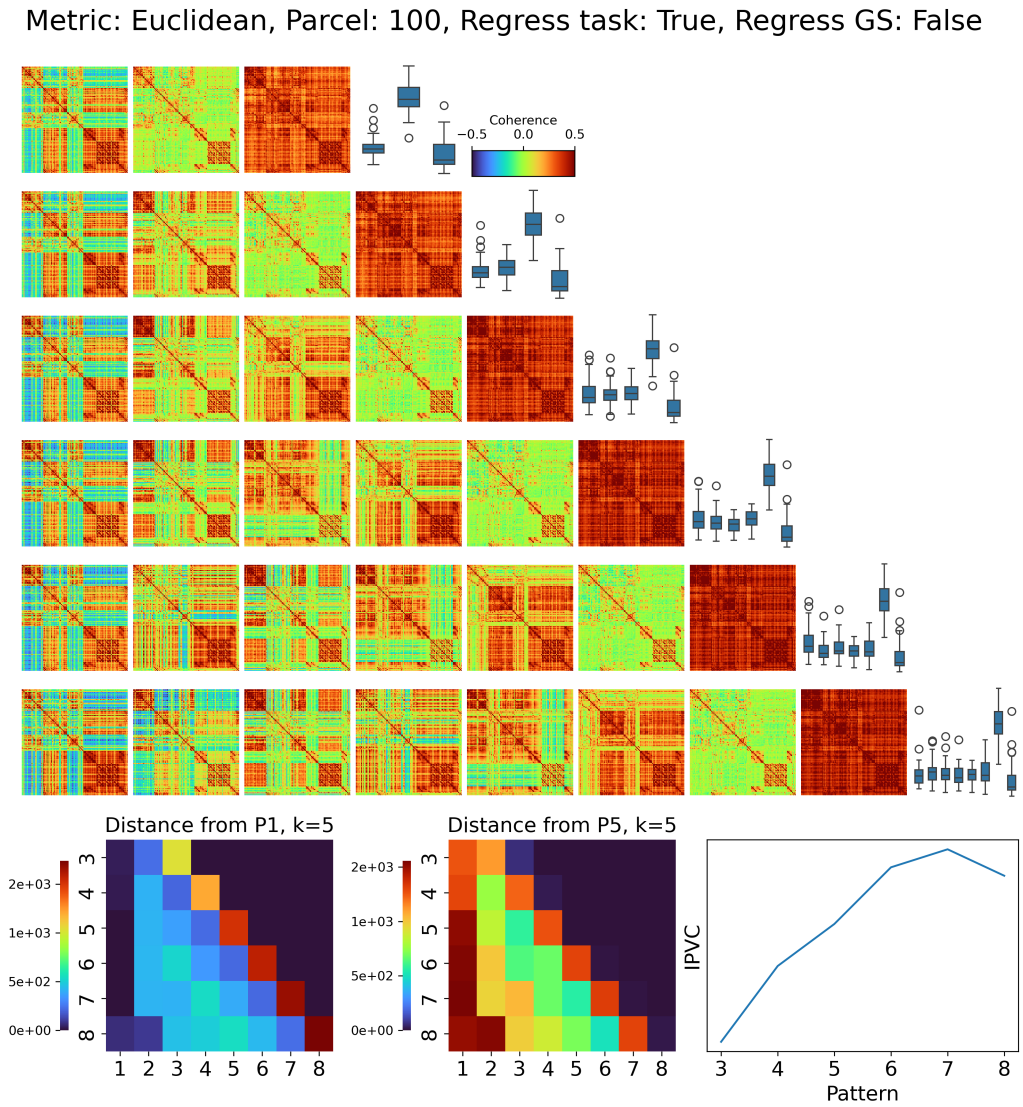

Figure S15. Recurrent and consistent brain configurations emerge under different clustering dimensionalities during task engagement. Clustering parameters: Metric = Euclidean distance, Global Signal Regression: False, Event Regression: True. Heatmaps: For each value of k , patterns are ordered based on the standard deviation of their connectome, from the most variant (left) to the least (right). Bottom row – Left: To examine whether patterns produced across different values of k presented correspondence, we estimated the distance of pattern 1 for $k = 5$ with respect to all patterns obtained for $k = 3$ to $k = 8$. Similarly, we estimated the distance of pattern 5 for $k = 5$ with respect to all patterns obtained for $k = 3$ to $k = 8$. Bottom row – Right: For each selection of the number of clusters in the K-means algorithm, we computed the inter-pattern correlation variability (IPVC) between all the upper triangular parts of the resulting centroids. The variability of dynamic coordination patterns found by the clustering procedure is maximal with $k = 5$ clusters.

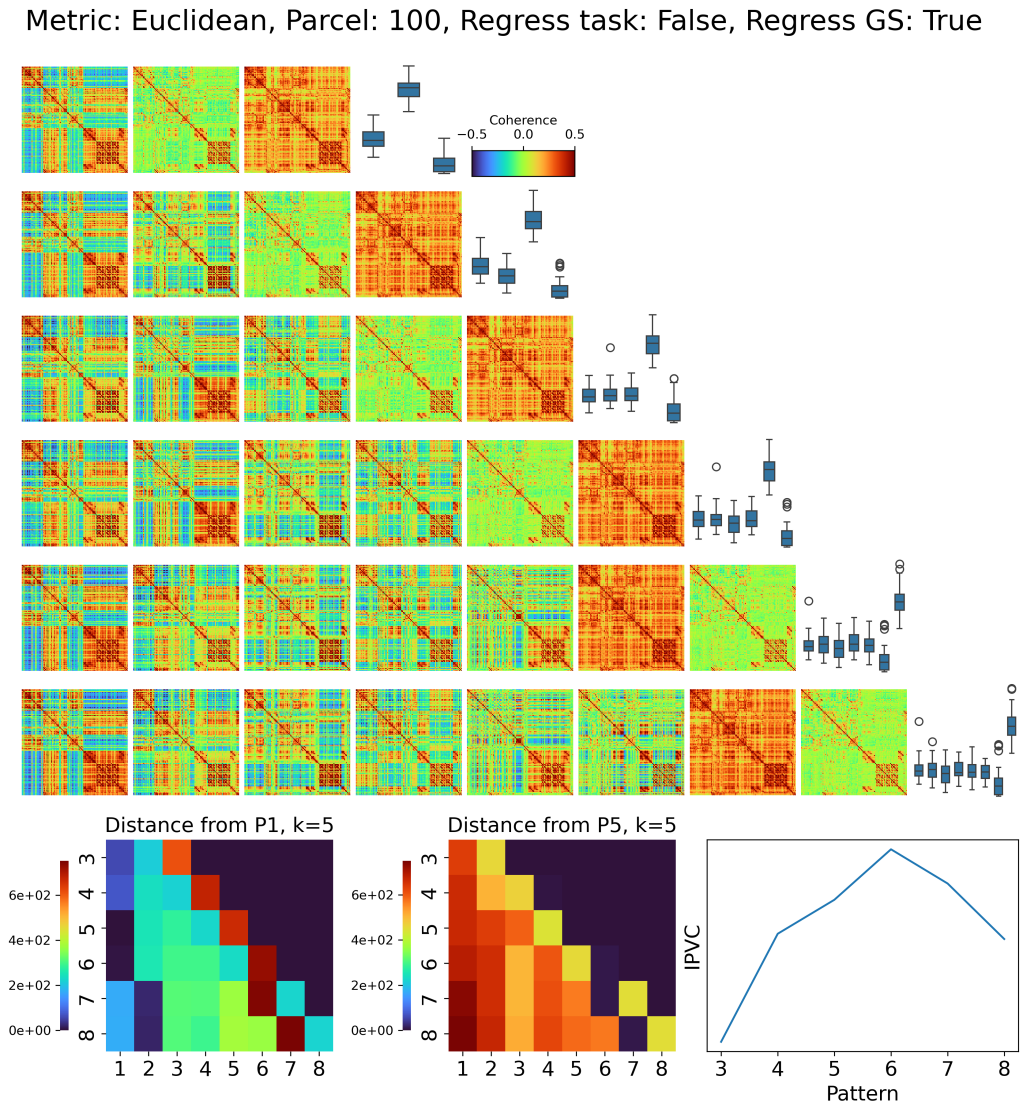

Figure S16. Recurrent and consistent brain configurations emerge under different clustering dimensionalities during task engagement. Clustering parameters: Metric = Euclidean distance, Global Signal Regression: True, Event Regression: False. Heatmaps: For each value of k , patterns are ordered based on the standard deviation of their connectome, from the most variant (left) to the least (right). Bottom row – Left: To examine whether patterns produced across different values of k presented correspondence, we estimated the distance of pattern 1 for $k = 5$ with respect to all patterns obtained for $k = 3$ to $k = 8$. Similarly, we estimated the distance of pattern 5 for $k = 5$ with respect to all patterns obtained for $k = 3$ to $k = 8$. Bottom row – Right: For each selection of the number of clusters in the K-means algorithm, we computed the inter-pattern correlation variability (IPVC) between all the upper triangular parts of the resulting centroids. The variability of dynamic coordination patterns found by the clustering procedure is maximal with $k = 5$ clusters.

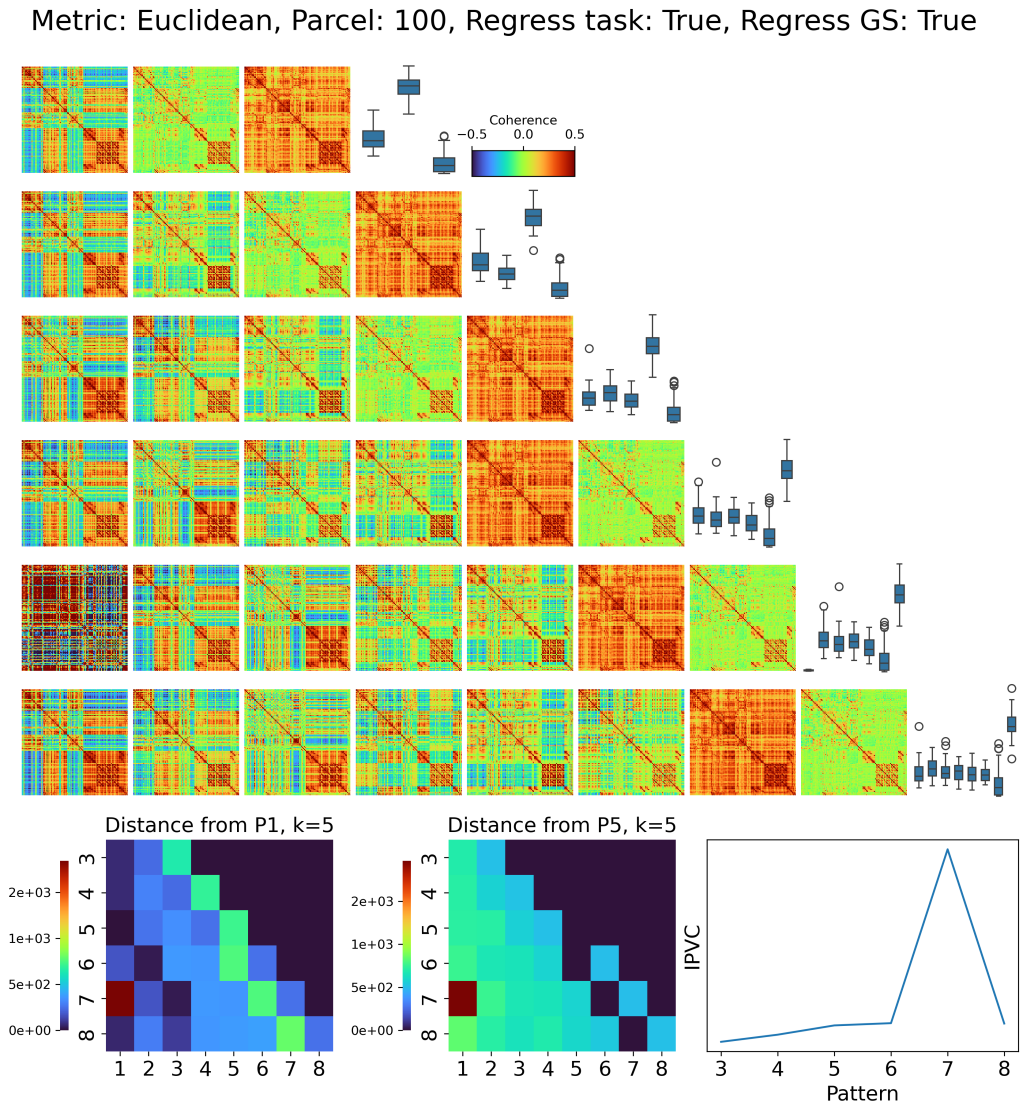

Figure S17. Recurrent and consistent brain configurations emerge under different clustering dimensionalities during task engagement. Clustering parameters: Metric = Euclidean distance, Global Signal Regression: True, Event Regression: True. Heatmaps: For each value of k , patterns are ordered based on the standard deviation of their connectome, from the most variant (left) to the least (right). Bottom row – Left: To examine whether patterns produced across different values of k presented correspondence, we estimated the distance of pattern 1 for $k = 5$ with respect to all patterns obtained for $k = 3$ to $k = 8$. Similarly, we estimated the distance of pattern 5 for $k = 5$ with respect to all patterns obtained for $k = 3$ to $k = 8$. Bottom row – Right: For each selection of the number of clusters in the K-means algorithm, we computed the inter-pattern correlation variability (IPVC) between all the upper triangular parts of the resulting centroids. The variability of dynamic coordination patterns found by the clustering procedure is maximal with $k = 5$ clusters.

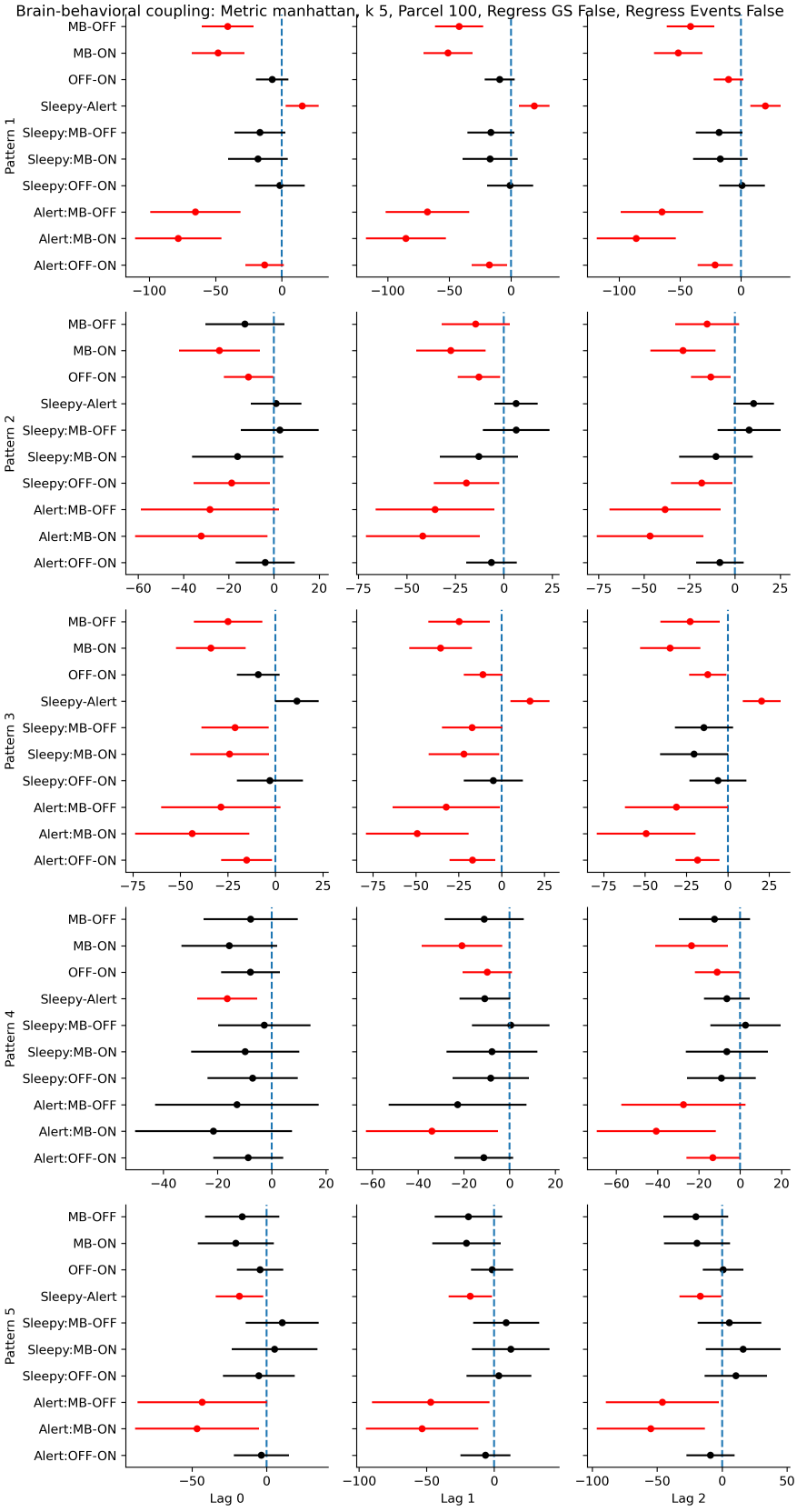

Figure S18. Replication analysis of the relationship between brain patterns, mental states and alertness. Analysis parameters: distance=Manhattan, k clusters = 5, task regression = False, Global signal regression = False, N ROI = 100.

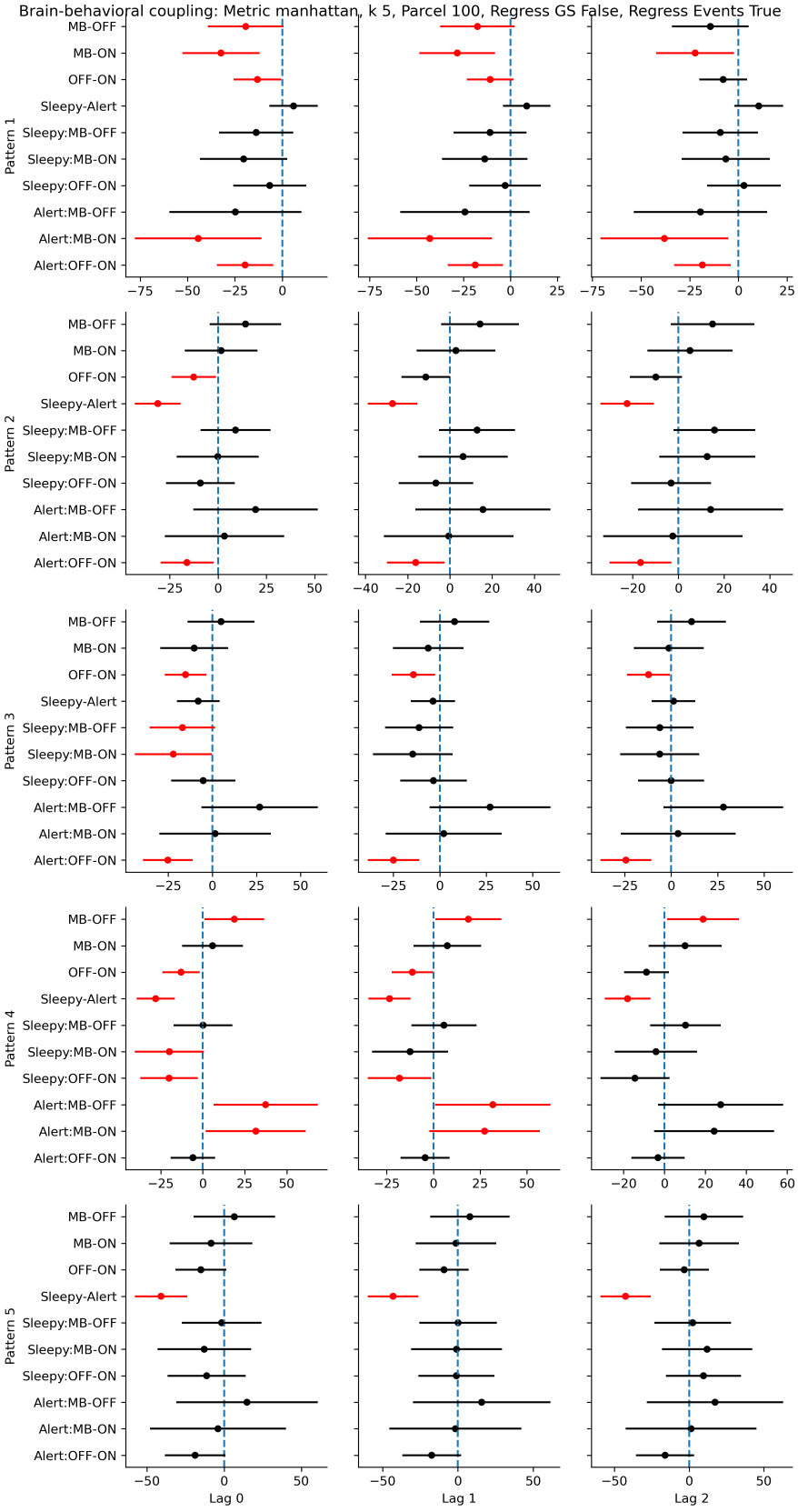

Figure S19. Replication analysis of the relationship between brain patterns, mental states and alertness. Analysis parameters: distance=Manhattan, k clusters = 5, task regression = False, Global signal regression = True, N ROI = 100.

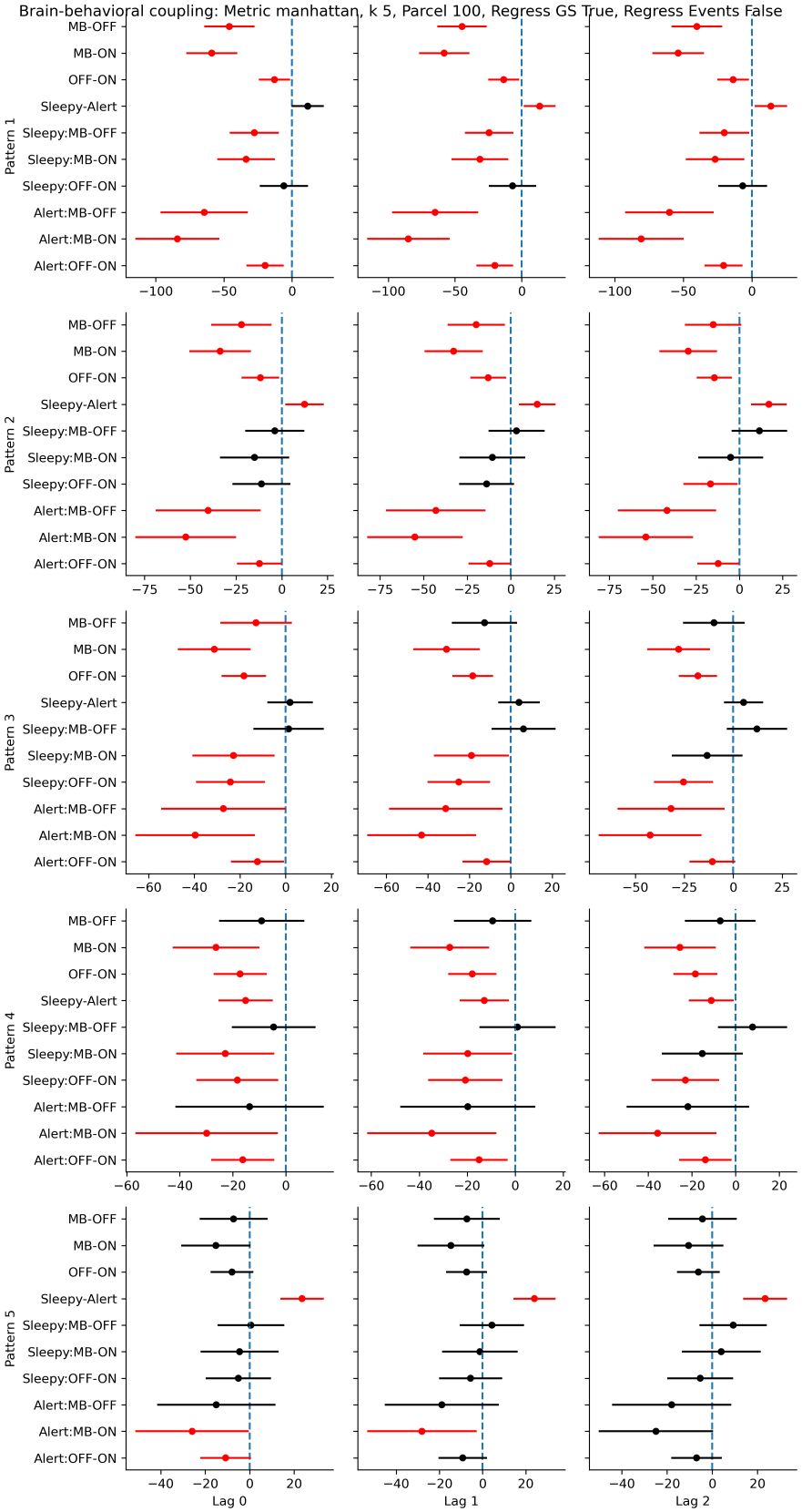

Figure S20. Replication analysis of the relationship between brain patterns, mental states and alertness. Analysis parameters: distance=Manhattan, k clusters = 5, task regression = True, Global signal regression = False, N ROI = 100.

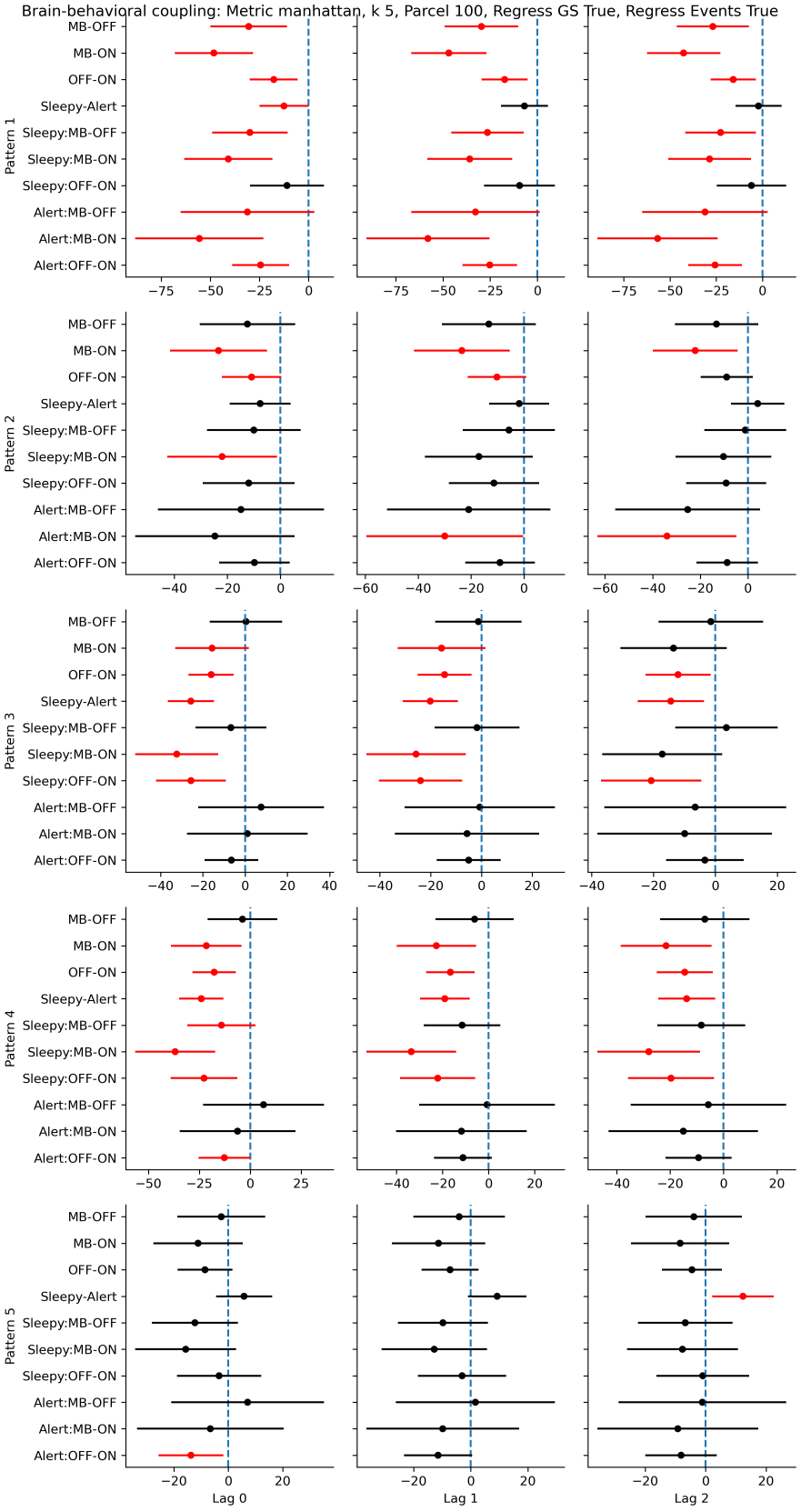

Figure S21. Replication analysis of the relationship between brain patterns, mental states and alertness. Analysis parameters: distance=Manhattan, k clusters = 5, task regression = True, Global signal regression = True, N ROI = 100.

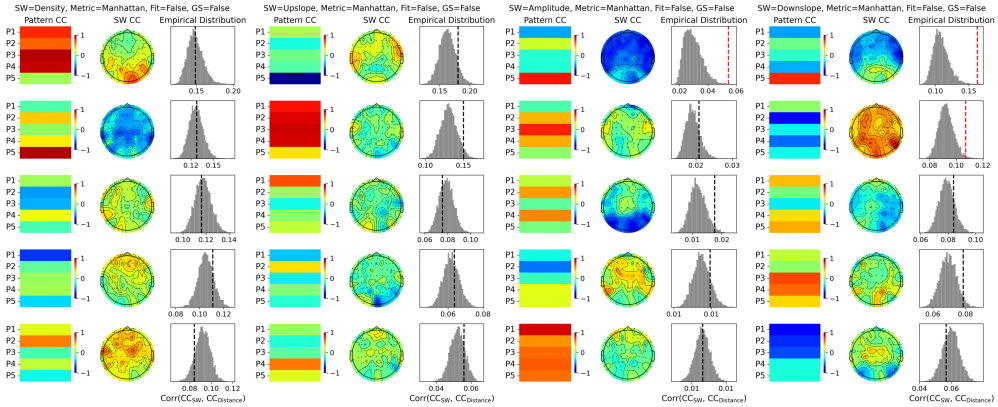

Figure S22. Replication analysis of the relationship between brain patterns and SW-like activity. Analysis parameters: distance=Manhattan, k clusters = 5, task regression = False, Global signal regression = False, N ROI = 100.

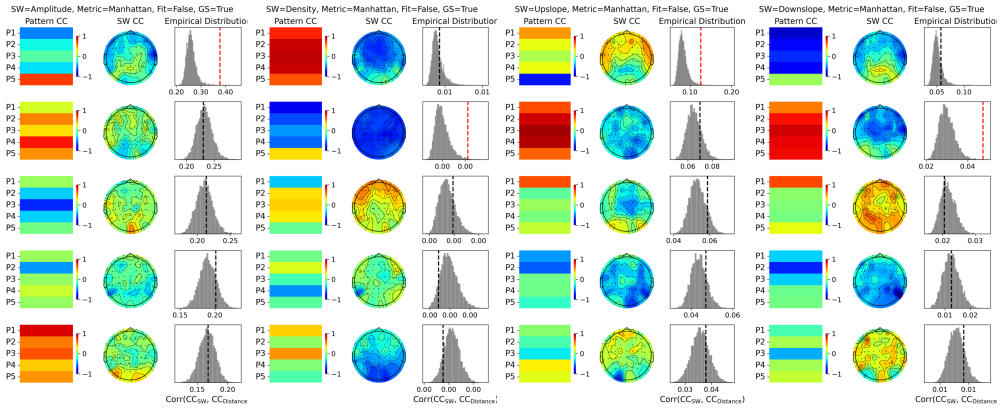

Figure S23. Replication analysis of the relationship between brain patterns and SW-like activity. Analysis parameters: distance=Manhattan, k clusters = 5, task regression = False, Global signal regression = True, N ROI = 100.

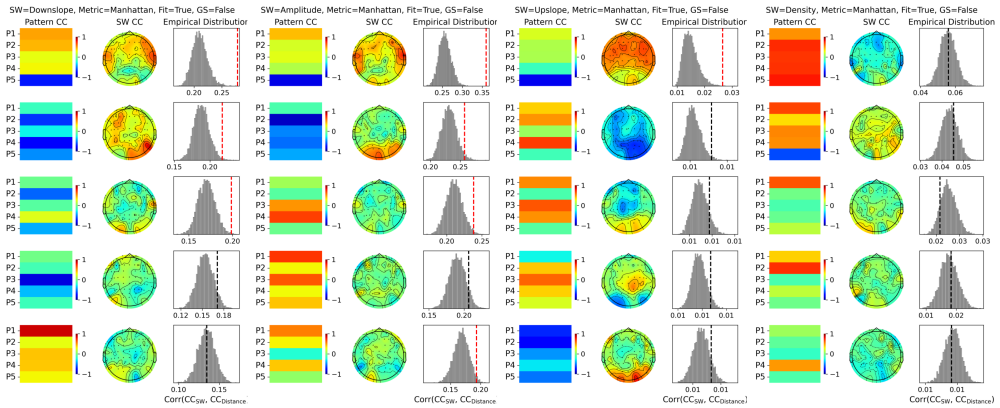

Figure S24. Replication analysis of the relationship between brain patterns, mental states and alertness. Analysis parameters: distance=Manhattan, k clusters = 5, task regression = True, Global signal regression = False, N ROI = 100.

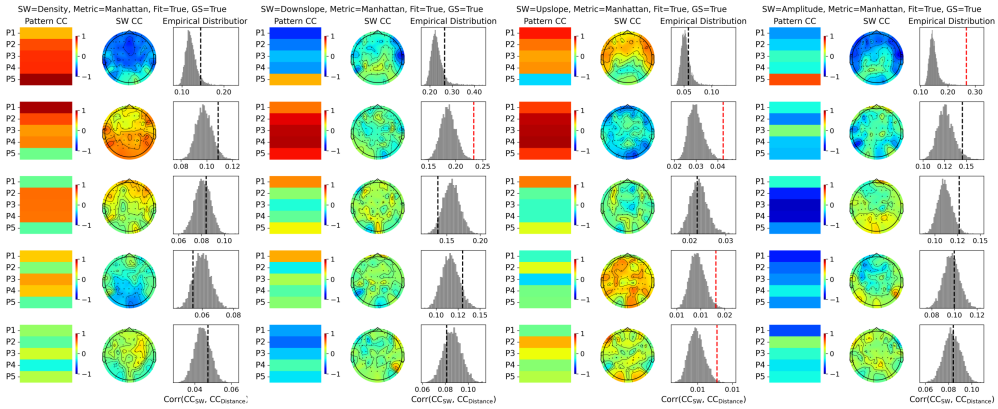

Figure S25. Replication analysis of the relationship between brain patterns, mental states and alertness. Analysis parameters: distance=Manhattan, k clusters = 5, task regression = True, Global signal regression = True, N ROI = 100.

Supplementary Tables

Table S1. Descriptive statistics of mental state and alertness level report frequencies

Report	Mean	Median	Min	Max	SD	IQR1	IQR3	Skewness	Kurtosis
ONTASK	0.486	0.462	0	1.000	0.253	0.288	0.644	0.294	-0.694
MW	0.389	0.404	0	0.800	0.217	0.229	0.534	0.082	-0.781
BLANK	0.100	0.065	0	0.444	0.115	0.000	0.135	1.235	0.682
NO RECALL	0.025	0.000	0	0.176	0.043	0.000	0.032	2.281	5.1
EXSLEEPY	0.133	0.046	0.000	0.675	0.181	0.000	0.199	1.306	0.605
SLEEPY	0.295	0.275	0.000	0.639	0.186	0.175	0.425	-0.051	-1.152
ALERT	0.484	0.478	0.075	1.000	0.261	0.283	0.628	0.411	-0.791
EXALERT	0.088	0.050	0.000	0.350	0.104	0.000	0.138	1.134	0.005

SD = standard deviation; IQR1 = interquartile range – 25% percentile; IQR3 = interquartile range – 75% percentile

Table S2. MB and Sleepiness were reported less frequently compared to other reports

Contrast	Statistic	pFDR	Rank-biserial r	CI
ONTASK-OFFTASK	-1.34	1.8e-01	0.21	[-0.05,0.44]
ONTASK-BLANK	-6.28	9.9e-10	0.8	[0.69-0.88]
OFFTASK-BLANK	-4.94	1.1e-06	0.69	[0.53-0.8]
SLEEPY-ALERT	2.02	4.2e-02	-0.27	[-0.49,-0.02]

CI = confidence intervals 95%; FDR = false discovery rate

Table S3. MB and OFFTASK reports increase during sleepiness, while ONTASK reports increase during alertness

Contrast	Odds Ratio	SE	Z ratio	CL	pFDR
ONTASK: SLEEPY / ALERT	0.15	0.02	-11.67	[0.11,0.21]	5.7e-31
OFFTASK: SLEEPY/ALERT	2.64	0.4	6.5	[1.7-3.53]	7.9e-11
BLANK: SLEEPY / ALERT	8.03	2.1	7.96	[4.8-13.4]	1.7e-15

SE = standard error; CL = confidence limits 95 %; FDR = false discovery rate

Table S4. Descriptive statistics of mental state and alertness level reaction times to probes

Report	Mean	Median	Min	Max	SD	IQR1	IQR3	Skewness	Kurtosis
ONTASK	1.649	1.143	0.272	7.690	1.397	0.687	2.053	1.732	2.759
OFFTASK	1.980	1.614	0.295	7.826	1.322	1.035	2.583	1.491	2.436
BLANK	2.793	2.330	0.325	7.886	1.760	1.501	3.567	1.087	0.676
SLEEPY	2.202	1.837	0.295	7.886	1.468	1.133	2.876	1.338	1.772
ALERT	1.713	1.213	0.272	7.690	1.424	0.723	2.201	1.762	3.039

SD = standard deviation; IQR1 = interquartile range – 25% percentile; IQR3 = interquartile range – 75% percentile

Table S5. Main effects and interaction contrasts describing the relationship between reaction times, mental states, and alertness levels

Contrast	Estimate	SE	Z ratio	CL	p-value
ONTASK - OFFTASK	0.03	0.02	1.25	[-0.03, 0.08]	2.13e-01
ONTASK - BLANK	**0.18**	**0.03**	**7.11**	**[0.12, 0.25]**	**3.55e-12**
OFFTASK - BLANK	**0.16**	**0.02**	**6.35**	**[0.10, 0.22]**	**3.21e-10**
SLEEPY - ALERT	0.03	0.02	1.51	[-0.01, 0.07]	1.31e-01
SLEEPY: ONTASK - OFFTASK	0.00	0.03	0.03	[-0.08, 0.08]	9.79e-01
SLEEPY: ONTASK - BLANK	**0.09**	**0.04**	**2.59**	**[0.01, 0.18]**	**1.45e-02**
SLEEPY: OFFTASK - BLANK	**0.09**	**0.03**	**3.27**	**[0.02, 0.16]**	**3.22e-03**
ALERT: ONTASK - OFFTASK	0.05	0.03	1.92	[-0.01, 0.12]	5.47e-02
ALERT: ONTASK - BLANK	**0.28**	**0.04**	**7.24**	**[0.18, 0.37]**	**1.38e-12**
ALERT: OFFTASK - BLANK	**0.22**	**0.04**	**5.44**	**[0.12, 0.32]**	**8.18e-08**

SE = standard error; CL = confidence limits 95 %; FDR = false discovery rate

Table S6. Descriptive statistics of global signal amplitude across mental states and alertness levels

Report	Mean	Median	Min	Max	SD	IQR1	IQR3	Skewness	Kurtosis
ONTASK	0.514	0.441	0.003	4.030	0.363	0.264	0.661	1.981	7.237
OFFTASK	0.538	0.465	0.005	3.468	0.370	0.278	0.709	1.888	6.988
BLANK	0.599	0.509	0.030	2.369	0.398	0.327	0.781	1.347	2.224
Sleepy	0.597	0.512	0.005	3.468	0.421	0.299	0.781	1.695	4.734
Alert	0.488	0.421	0.003	4.030	0.323	0.262	0.638	1.830	7.268

SD = standard deviation; IQR1 = interquartile range – 25% percentile; IQR3 = interquartile range – 75% percentile

Table S7. Main effect and interaction contrasts describing the relationship between global signal amplitude, mental states and alertness levels

Contrast	Estimate	SE	Z ratio	CL	p-value
ONTASK - OFFTASK	-0.00	0.02	-0.17	[-0.04, 0.04]	8.68e-01
ONTASK - BLANK	**-0.09**	**0.03**	**-3.02**	**[-0.15, -0.02]**	**4.43e-03**
OFFTASK - BLANK	**-0.08**	**0.03**	**-2.97**	**[-0.15, -0.02]**	**4.43e-03**
SLEEPY - ALERT	**0.12**	**0.02**	**5.71**	**[0.08, 0.17]**	**1.13e-08**
SLEEPY: ONTASK - OFFTASK	0.04	0.03	1.66	[-0.02, 0.11]	1.46e-01
SLEEPY: ONTASK - BLANK	-0.04	0.03	-1.31	[-0.12, 0.03]	1.91e-01
SLEEPY: OFFTASK - BLANK	**-0.09**	**0.03**	**-3.13**	**[-0.15, -0.02]**	**5.29e-03**
ALERT: ONTASK - OFFTASK	**-0.05**	**0.02**	**-2.40**	**[-0.10, 0.00]**	**2.49e-02**
ALERT: ONTASK - BLANK	**-0.13**	**0.05**	**-2.78**	**[-0.24, -0.02]**	**1.61e-02**
ALERT: OFFTASK - BLANK	-0.08	0.05	-1.64	[-0.19, 0.04]	1.01e-01

SE = standard error; CL = confidence limits 95 %; FDR = false discovery rate

Table S8. Descriptive statistics of brain pattern occurrence frequency

Brain Pattern	Mean	Median	Min	Max	SD	IQR1	IQR3	Skewness	Kurtosis
Pattern 1	0.209	0.184	0.094	0.410	0.071	0.167	0.256	0.961	0.679
Pattern 2	0.162	0.155	0.061	0.313	0.055	0.120	0.188	0.489	0.012
Pattern 3	0.166	0.161	0.071	0.392	0.062	0.114	0.192	1.190	2.539
Pattern 4	0.132	0.126	0.049	0.293	0.051	0.091	0.158	0.798	0.772
Pattern 5	0.331	0.320	0.134	0.679	0.132	0.228	0.427	0.532	-0.409

SD = standard deviation; IQR1 = interquartile range – 25% percentile; IQR3 = interquartile range – 75% percentile

Table S9. Contrast analysis of the differences in brain pattern occurrence frequencies

Contrast	Estimate	SE	Z ratio	CL	p-value
Pattern 1 - Pattern 2	**0.05**	**0.02**	**2.54**	**[-0.01, 0.10]**	**2.05e-02**
Pattern 1 - Pattern 3	**0.04**	**0.02**	**2.33**	**[-0.01, 0.09]**	**3.05e-02**
Pattern 1 - Pattern 4	**0.08**	**0.02**	**4.18**	**[0.02, 0.13]**	**9.96e-05**
Pattern 1 - Pattern 5	**-0.12**	**0.02**	**-6.71**	**[-0.17, -0.07]**	**9.69e-10**
Pattern 2 - Pattern 3	-0.00	0.02	-0.21	[-0.06, 0.05]	8.36e-01
Pattern 2 - Pattern 4	0.03	0.02	1.64	[-0.02, 0.08]	1.14e-01
Pattern 2 - Pattern 5	**-0.17**	**0.02**	**-9.24**	**[-0.22, -0.12]**	**1.20e-15**
Pattern 3 – Pattern 4	0.03	0.02	1.85	[-0.02, 0.09]	8.25e-02
Pattern 3 - Pattern 5	**-0.17**	**0.02**	**-9.04**	**[-0.22, -0.11]**	**2.74e-15**
Pattern 4 – Pattern 5	**-0.20**	**0.02**	**-10.89**	**[-0.25, -0.15]**	**1.20e-19**

SE = standard error; CL = confidence limits 95 %; FDR = false discovery rate

Table S10. Descriptive statistics of distances of time-varying FC during mental states and alertness levels from the brain patterns

Pattern	Report	Mean	Median	Min	Max	SD	IQR1	IQR3	Skewness	Kurtosis
P1	ONTASK	4440.301	4430.541	3910.006	6244.807	190.954	4333.560	4519.712	1.568	7.870
P1	OFFTASK	4432.874	4425.496	3960.780	5655.372	176.840	4335.004	4509.746	1.184	5.047
P1	BLANK	4424.426	4417.706	3893.356	5190.178	176.026	4321.109	4516.312	0.492	1.428
P1	Sleepy	4438.984	4427.483	3981.135	5401.561	174.620	4337.988	4519.839	0.946	2.860
P1	Alert	4433.034	4426.717	3893.356	6244.807	190.201	4328.146	4512.897	1.543	8.131
P2	ONTASK	4473.548	4453.604	3934.488	6072.208	174.012	4379.748	4536.416	1.949	9.536
P2	OFFTASK	4463.692	4449.971	3959.624	5601.975	156.508	4376.045	4530.844	1.180	4.998
P2	BLANK	4463.822	4445.065	4129.599	5156.260	139.840	4377.811	4533.040	0.866	1.870
P2	Sleepy	4464.524	4448.148	3959.624	5312.159	154.505	4373.013	4534.082	0.934	2.488
P2	Alert	4471.441	4453.587	3934.488	6072.208	169.743	4382.107	4534.557	1.991	10.330
P3	ONTASK	4460.675	4435.260	4045.824	6133.537	178.734	4362.456	4520.920	2.075	9.415
P3	OFFTASK	4456.744	4437.679	4033.137	5587.687	159.734	4365.919	4523.906	1.436	5.230
P3	BLANK	4445.873	4429.600	4057.406	5195.973	155.860	4349.987	4522.042	0.890	2.293
P3	Sleepy	4464.324	4442.391	4052.211	5387.385	163.552	4368.209	4535.896	1.176	3.071
P3	Alert	4452.404	4430.101	4033.137	6133.537	172.568	4359.073	4512.238	2.141	10.519
P4	ONTASK	4472.174	4441.831	4051.184	6232.415	169.202	4380.343	4528.024	2.470	12.697
P4	OFFTASK	4461.935	4436.054	4077.725	5640.300	157.344	4371.709	4521.159	1.952	7.975
P4	BLANK	4460.362	4438.273	4127.010	5278.435	149.941	4375.651	4527.183	1.130	3.347
P4	Sleepy	4460.565	4434.407	4051.184	5456.137	159.473	4369.433	4522.228	1.536	4.883
P4	Alert	4471.223	4443.381	4110.607	6232.415	164.525	4381.617	4527.515	2.585	13.847
P5	ONTASK	4414.449	4462.178	3455.978	5676.460	243.877	4296.275	4566.336	-0.610	1.626
P5	OFFTASK	4416.752	4465.423	3529.340	5583.751	239.234	4292.084	4571.685	-0.617	0.978
P5	BLANK	4425.492	4468.797	3587.530	5212.208	226.461	4315.341	4565.511	-0.680	1.397
P5	Sleepy	4407.826	4462.825	3455.978	5290.038	247.382	4277.344	4566.728	-0.699	0.859
P5	Alert	4422.983	4465.291	3477.422	5676.460	234.479	4308.900	4570.062	-0.549	1.769

SD = standard deviation; IQR1 = interquartile range – 25% percentile; IQR3 = interquartile range – 75% percentile

Table S11. Main effect and interaction contrasts describing the relationship between patterns, mental states and alertness levels

Pattern	Contrast	Estimate	SE	D.F.	CL	T-statistic	P-value
P1	ONTASK - OFFTASK	7.24	5.1	8122.91	[-4.97, 19.46]	1.42	1.56e-01
P1	**ONTASK - BLANK**	**48.1**	**8.31**	**8370.65**	**[28.19, 68.00]**	**5.79**	**2.24e-08**
P1	**OFFTASK - BLANK**	**40.85**	**8.17**	**8402.03**	**[21.30, 60.41]**	**5**	**8.70e-07**
P1	**Sleepy - Alert**	**15.38**	**6.37**	**7630.23**	**[2.89, 27.88]**	**2.41**	**1.58e-02**
P1	Sleepy:ONTASK - OFFTASK	1.5	7.86	8337.07	[-17.31, 20.31]	0.19	8.48e-01
P1	Sleepy:ONTASK - BLANK	18.02	9.39	8258.42	[-4.47, 40.50]	1.92	8.26e-02
P1	Sleepy:OFFTASK - BLANK	16.51	8.02	8380.86	[-2.68, 35.71]	2.06	8.26e-02
P1	**Alert:ONTASK - OFFTASK**	**12.98**	**6.06**	**8332.72**	**[-1.53, 27.49]**	**2.14**	**3.22e-02**
P1	**Alert:ONTASK - BLANK**	**78.18**	**13.64**	**8432.54**	**[45.53, 110.83]**	**5.73**	**3.05e-08**
P1	**Alert:OFFTASK - BLANK**	**65.19**	**14.21**	**8412.95**	**[31.16, 99.23]**	**4.59**	**6.84e-06**
P2	ONTASK - OFFTASK	11.27	4.56	7474.49	[0.35, 22.20]	2.47	2.03e-02
P2	**ONTASK - BLANK**	**24.1**	**7.45**	**8102.02**	**[6.27, 41.94]**	**3.24**	**3.65e-03**
P2	OFFTASK - BLANK	12.83	7.32	8190.08	[-4.70, 30.36]	1.75	7.97e-02
P2	Sleepy - Alert	0.96	5.69	6474.61	[-10.19, 12.11]	0.17	8.66e-01
P2	**Sleepy:ONTASK - OFFTASK**	**18.69**	**7.04**	**8017.14**	**[1.84, 35.53]**	**2.66**	**2.38e-02**
P2	Sleepy:ONTASK - BLANK	16.07	8.41	7810.65	[-4.06, 36.20]	1.91	8.39e-02
P2	Sleepy:OFFTASK - BLANK	-2.61	7.18	8131.38	[-19.81, 14.58]	-0.36	7.16e-01
P2	Alert:ONTASK - OFFTASK	3.86	5.43	7996.57	[-9.14, 16.85]	0.71	4.78e-01
P2	**Alert:ONTASK - BLANK**	**32.14**	**12.23**	**8286.69**	**[2.86, 61.41]**	**2.63**	**2.58e-02**
P2	**Alert:OFFTASK - BLANK**	**28.28**	**12.74**	**8223.13**	**[-2.23, 58.79]**	**2.22**	**3.97e-02**
P3	ONTASK - OFFTASK	9.01	4.7	7900.14	[-2.24, 20.27]	1.92	5.53e-02
P3	ONTASK - BLANK	33.95	7.67	8284.66	[15.59, 52.30]	4.43	2.89e-05
P3	OFFTASK - BLANK	24.94	7.53	8335.84	[6.90, 42.97]	3.31	1.40e-03
P3	Sleepy - Alert	11.33	5.87	7201.78	[-0.17, 22.83]	1.93	5.35e-02
P3	Sleepy:ONTASK - OFFTASK	2.9	7.24	8232.28	[-14.44, 20.24]	0.4	6.89e-01
P3	**Sleepy:ONTASK - BLANK**	**24.12**	**8.65**	**8108.38**	**[3.39, 44.84]**	**2.79**	**8.01e-03**
P3	**Sleepy:OFFTASK - BLANK**	**21.22**	**7.39**	**8301.42**	**[3.52, 38.92]**	**2.87**	**8.01e-03**
P3	**Alert:ONTASK - OFFTASK**	**15.12**	**5.59**	**8223.29**	**[1.74, 28.50]**	**2.71**	**1.02e-02**
P3	**Alert:ObNTASK - BLANK**	**43.78**	**12.58**	**8388.43**	**[13.66, 73.89]**	**3.48**	**1.51e-03**
P3	**Alert:OFFTASK - BLANK**	**28.65**	**13.11**	**8354.27**	**[-2.73, 60.04]**	**2.19**	**2.89e-02**
P4	ONTASK - OFFTASK	7.87	4.52	8006.77	[-2.95, 18.69]	1.74	1.23e-01
P4	ONTASK - BLANK	15.66	7.37	8326.79	[-1.98, 33.31]	2.13	1.01e-01
P4	OFFTASK - BLANK	7.79	7.24	8368.55	[-9.55, 25.13]	1.08	2.82e-01
P4	**Sleepy - Alert**	**-16.42**	**5.65**	**7401.84**	**[-27.48, -5.35]**	**-2.91**	**3.64e-03**
P4	Sleepy:ONTASK - OFFTASK	7.05	6.96	8283.23	[-9.62, 23.72]	1.01	4.67e-01
P4	Sleepy:ONTASK - BLANK	9.81	8.32	8180.78	[-10.11, 29.74]	1.18	4.67e-01
P4	Sleepy:OFFTASK - BLANK	2.76	7.11	8340.42	[-14.25, 19.78]	0.39	6.97e-01
P4	Alert:ONTASK - OFFTASK	8.69	5.37	8276.6	[-4.17, 21.55]	1.62	1.59e-01
P4	Alert:ONTASK - BLANK	21.51	12.09	8410.49	[-7.44, 50.46]	1.78	1.59e-01
P4	Alert:OFFTASK - BLANK	12.82	12.6	8383.37	[-17.35, 42.99]	1.02	3.09e-01
P5	ONTASK - OFFTASK	4.3	6.52	8430.99	[-11.32, 19.91]	0.66	5.10e-01
P5	ONTASK - BLANK	20.57	10.61	8468.31	[-4.84, 45.98]	1.94	1.58e-01
P5	OFFTASK - BLANK	16.28	10.42	8470.95	[-8.68, 41.23]	1.56	1.78e-01
P5	**Sleepy - Alert**	**-18.17**	**8.16**	**8323.18**	**[-34.17, -2.17]**	**-2.23**	**2.60e-02**
P5	Sleepy:ONTASK - OFFTASK	5.15	10.03	8464.31	[-18.86, 29.17]	0.51	6.50e-01
P5	Sleepy:ONTASK - BLANK	-5.44	11.99	8453.41	[-34.16, 23.28]	-0.45	6.50e-01
P5	Sleepy:OFFTASK - BLANK	-10.59	10.23	8469.26	[-35.09, 13.90]	-1.04	6.50e-01
P5	Alert:ONTASK - OFFTASK	3.44	7.74	8464.12	[-15.08, 21.97]	0.45	6.56e-01
P5	**Alert:ONTASK - BLANK**	**46.59**	**17.39**	**8472**	**[4.94, 88.23]**	**2.68**	**2.22e-02**
P5	**Alert:OFFTASK - BLANK**	**43.14**	**18.13**	**8471.54**	**[-0.28, 86.56]**	**2.38**	**2.61e-02**

SE = standard error; CL = confidence limits 95 %; FDR = false discovery rate; D.F. = degrees of freedom